Analysis and Characterization of Ancillary Service Demand Response Strategies for Variable Air Volume HVAC Systems

by

David H. Blum

Bachelors of Architectural Engineering
Department of Architectural Engineering, The Pennsylvania State University, 2011

Submitted to the Department of Architecture
in Partial Fulfillment of the Requirements for the Degree of

Master of Science in Building Technology

at the

Massachusetts Institute of Technology

June, 2013

Signature of Author:

Department of Architecture
May 10th, 2013

Certified by:

Leslie K. Norford
Professor of Building Technology
Thesis Supervisor

Accepted by:

Takehiko Nagakura
Associate Professor of Design and Computation
Chair of the Department Committee on Graduate Students

Analysis and Characterization of
Ancillary Service Demand Response Strategies for
Variable Air Volume HVAC Systems

by

David H. Blum

Submitted to the Department of Architecture
on May 10, 2013 in partial fulfillment of the requirements for the
Degree of Master of Science in Building Technology

Abstract

Output variability and prediction difficulties with respect to solar and wind electricity resources increase the requirement of grid-scale reserve capacity and add strain to existing firm generators used for reserves and other ancillary services. Residential and commercial buildings account for a large portion of the electricity consumed in the U.S. and can play a significant role in smart grids to help meet challenges brought about by intermittent renewable generation. High resolution power consumption and HVAC performance data measured in a real building was used to identify real-world operational qualities of VAV systems to be considered by building researchers and building practitioners. This includes the relative magnitude of building power loads, the direct and indirect relationships between environmental conditions and HVAC power consumption, the discrete operation of staged or cycled power loads, and the presence of HVAC operational faults. Also, three static pressure adjustment tests were performed over a one day period. Results showed that fan and terminal unit controllers responded within two minutes and system air flowrate was strongly related to power consumption.

Dynamic models were created in order to simulate the performance of a VAV system providing spinning reserves by four different common demand response strategies: zone air dry bulb temperature setpoint adjustment (ZDBA), duct static pressure setpoint adjustment (SPA), supply air temperature adjustment (STA), and chilled water temperature adjustment (CWA). Simulations were run over ranges of implementation and cooling load intensities and the results were used to create characteristic curves for each strategy, which map performance in terms of system power consumption reduction, system airflow reduction, and zone temperature rise. Inflection points on the curves that delineate performance effectiveness are found to result from maximum or minimum terminal unit damper positions. In the future, the development of mathematical functional forms of these characterization curves could help predict and optimize the performance of VAV systems in providing ancillary services to electricity networks.

Thesis Supervisor: Leslie K. Norford
Title: Professor of Building Technology

Acknowledgments

This work has been supported by the National Science Foundation EFRI-SEED award 1038230.

I am grateful to have performed this work under the supervision of Dr. Leslie K. Norford. In both academics and research, he has allowed me to pursue my interests with motivating, yet patient, mentoring.

Research is not possible without helpful contributions and generous donations of time and energy from others. Thank you Dr. Michael Caramanis, Dr. John Baillieul, Dr. Michael Gevelber, Bowen Zhang, Paul Gallagher, and BU facilities for your efforts to collect and share data from our test building as well as provide feedback and guidance for my research. Thank you also to John Batteh and Magnus Gäfvert of Modelon and to Connor Blood of Trane, Inc. for your technical support of this work.

I have received invaluable guidance and education from the entire Building Technology faculty as well as faculty members from the Department of Mechanical Engineering. Life at MIT would not be the same without the humor and support from friends and colleagues from around the institute, including my colleagues in the Building Technology Lab, past and present, the Misfits, and the Mighty Ducts. An additional thank you to Kathleen Ross, whose commitment and spirit makes every day of work both easier and enjoyable.

A special thank you to Tea, Ale, Bruno, Jin, Brian, and Leon. Your advice, support, encouragement, and friendship from the start has helped me settle comfortably into life as a graduate student in BT, MIT, and Boston.

To my Mom and Dad, brothers Ethan and Jake, Grandpop Pete and all of my extended family, thank you for providing a foundation of love, support, encouragement, and excitement that inspires me to do my best in everything that I do every single day.

To Grandmom Jean, Grandpop Lloyd, and Grandmom Esther, always in your loving memory.

Table of Contents

List of Figures **9**

List of Tables **12**

1 Introduction **13**

1.1 Modern Electric Grids 13

1.2 Growth and Impact of Wind and Solar Generation 15

1.3 The Role of Building HVAC Systems 17

1.4 Thesis Objectives and Structure 20

2 Literature Review **22**

2.1 Electricity Market Operations 22

2.2 Demand Response vs. Energy Efficiency 29

2.3 Demand Response Research 29

2.4 Demand Response Implementation 33

2.5 Conclusion 38

3 Test Building Analysis **40**

3.1 Building Overview 40

3.2 Considerations from Summertime Operation 46

3.3 Considerations from a Duct Static Pressure Adjustment Test 50

3.4 Conclusion 58

4 VAV System Modeling For Ancillary Service Simulations **60**

4.1 Model Requirements 61

4.2 EnergyPlus 61
4.3 TRNSYS 64
4.4 Modelica 67
4.5 Conclusion 71

5 Simulations **72**
5.1 System Design and Modeling 72
5.2 Simulated System Performance 81
5.3 Curtailment Characterization Setup 91
5.4 Curtailment Characterization Results 92
5.5 Discussion 105
5.6 Conclusion 107

6 Conclusions and Future Work **110**

References **113**

Appendix A Simulation Models **121**
A.1 VAV System - Top Level 121
A.2 Supply Fan 121
A.3 Supply Fan Power Model 121
A.4 Supply Fan Controller 123
A.5 Cooling Coil 123
A.6 AHU Resistance 125
A.7 Supply Duct Splitter 125
A.8 Terminal Unit 125
A.9 Terminal Unit Controller 129
A.10 Diffuser Resistance 131
A.11 Thermal Zones 131
A.12 Return Duct Splitter 136
A.13 Chilled Water Ideal Flow Source and Sink 136

A.14 Chilled Water Flow Splitter 136
A.15 Chilled Water Modulating Valve 137
A.16 Chilled Water Valve Controller 137

Appendix B Equipment Specifications and Performance 139

List of Figures

1.1 Map of regional electricity network operators in the U.S. 14

1.2 Diagram of System Marginal Price (SMP) determination during day-ahead energy markets . 16

1.3 Distribution of projected renewable generating capacity in the U.S. in the year 2020 17

1.4 Distribution of U.S. electricity consumption in 2011 18

2.1 Time line of electricity market operation for ISO New England 28

3.1 Diagram of test building HVAC system 43

3.2 Diagram of electrical panel recording system for test building 45

3.3 Real power consumption of test building distribution panels for one week in July, 2012 . . . 46

3.4 Environment and HVAC performance measurements from test building for one week in July, 2012 48

3.5 Real power measurements from the chiller and GPNH2 distribution panels in the test building for July 17th, 2012 49

3.6 Environment and main distribution panel measurements from test building during static pressure adjustment test 52

3.7 HVAC performance measurements from test building during static pressure adjustment test . 53

3.8 Terminal unit measurements from test building during static pressure adjustment test 54

3.9 Comparison of power reduction to air flowrate reduction in the test building during static pressure adjustment tests 56

4.1 Single day simulation in EnergyPlus with zone air temperature setpoint adjustment 63

4.2 TRNSYS dynamic flow network trial setups 66

4.3 Results of the successful TRNSYS simulation of the two flow split network 67

4.4 Setup for the four flow split network trial in Dymola 69

4.5 Results of the successful Dymola simulation of the four flow split network 70

5.1 Representative VAV system used for demand response simulations 73

5.2 Thermal zone layout with assumed placement of round ceiling diffusers 75

5.3 Terminal unit control and operation 76

5.4 Simulated performance of the supply fan 83

5.5 Simulated response of a representative VAV system to a step change in cooling load 86

5.6 Simulated response of a representative VAV system to a step change in duct static pressure setpoint 87

5.7 Simulated response of a representative VAV system to a step change in zone air temperature setpoint 88

5.8 Simulated response of a representative VAV system to a step change in supply air temperature setpoint 89

5.9 Simulated response of a representative VAV system to a step change in chilled water temperature setpoint 90

5.10 Simulated response of a representative VAV system to a step change in zone air temperature setpoint from 22 °C to 26 °C at thermal zone cooling load intensities of 9300 W, 6300 W, and 3300 W 93

5.11 Reduction magnitude characterization curves for ZDBA 94

5.12 Normalized reduction characterization curves for ZDBA 95

5.13 Simulated response of a representative VAV system to a step change in duct static pressure setpoint from 373.2 Pa to 186.6 Pa at thermal zone cooling load intensities of 9300 W, 6300 W, and 3300 W 96

5.14 Reduction magnitude characterization curves for SPA 97

5.15 Normalized reduction characterization curves for SPA 98

5.16 Simulated response of a representative VAV system to a step change in supply air temperature setpoint from 12.78 °C to 16.78 °C at thermal zone cooling load intensities of 9300 W, 6300 W, and 3300 W 99

5.17 Reduction magnitude characterization curves for STA 100

5.18 Normalized reduction characterization curves for STA 101

5.19 Simulated response of a representative VAV system to a step change in chilled water temperature setpoint from 6 °C to 10 °C at thermal zone cooling load intensities of 9300 W, 6300 W, and 3300 W 102

5.20 Reduction magnitude characterization curves for CWA 103

5.21 Normalized reduction characterization curves for CWA 104

A.1 Graphical implementation of representative VAV system model in Dymola 122
A.2 Graphical implementation of supply fan controller model in Dymola 124
A.3 Graphical implementation of terminal unit model in Dymola 126
A.4 Graphical implementation of thermal zone models in Dymola 132
A.5 Graphical implementation of chilled water valve controller model in Dymola 137

List of Tables

2.1 Current demand response programs in U.S. regional electricity networks 34

2.2 Performance data for NYISO demand response programs in summer 2012 35

2.3 Performance data summary for ISO New England spinning reserve pilot program from 2006 to 2010 36

2.4 Performance data summary for PJM demand response programs in 2012 37

3.1 Equipment breakout for two HVAC electrical panels in the test building 44

3.2 Summary of test building AHU performance during static pressure adjustment tests . . . 55

3.3 Summary of test building HVAC electrical panel performance during static pressure adjustment tests 55

5.1 Comparison of design conditions as designed and as simulated using the implemented VAV system model 82

5.2 Curtailment strategy intensities implemented for simulated VAV system demand response curtailment characterization 91

Chapter 1

Introduction

Due to mounting concerns over CO_2 emissions, air quality, resource depletion, national security, and cost, a focus has shifted to how usable energy is generated, transmitted, and consumed. Central to this energy revolution is the proposed revitalization of electric grids around the world, considered in both the U.S. and EU as "smart grids" (U.S. House, 110th Congress, 2007; European Commission, 2011). The common definitions of these enhanced electric grids describe an electric generation, transmission, distribution, and consumption infrastructure that provides sustainable, low cost, and high quality electricity to consumers. Features include large-scale renewable generators, increased distributed generation, upgraded measurement and automation for efficient network control, management of plug-in-hybrid-electric-vehicles (PHEV), and participation of demand-side resources. While such features in future electric grids have the potential to mitigate the concerns stated above, many challenges stand in the way of their wide-spread penetration. These challenges stem from a diverse collection of technical, economic, regulatory, and behavioral processes. This thesis focuses on exploring technical processes related to how buildings may help meet some of the growing number of challenges associated with the development of future electric grids.

1.1 Modern Electric Grids

Delivery of electricity to consumers can be separated into three parts; generation, transmission, and retail distribution. Generation includes the production of electricity, transmission includes the transport of large amounts of electricity between network nodes at high voltages, and retail distribution includes the delivery of electricity to consumers through low voltage networks. Nodes refer to points on the transmission network of energy injection or energy consumption, typically comprised of grid-scale generators and distribution substations. Before widespread restructuring, also called liberalization, took place across regions of the U.S. in the late 1990s, these three operations were primarily owned and operated by single local regulated utilities, where consumers paid a price determined as fair return on utility investments. Though the origin of restructuring this landscape is outside the scope of this thesis, its effect is of great importance to understand in the present context.

In a restructured electricity network, generation, transmission, and retail distribution are operated by

separate entities, each of which participate in electricity markets that are designed to ensure delivery of high quality electricity to consumers at the lowest cost. High quality electricity in the U.S. refers to the delivery of electricity within standards set by the North American Electric Reliability Corporation (NERC, 2013b). For consumers, the important standards are with regard to power voltage and frequency. Due to physical constraints imposed by Kirchoff's voltage and current laws, the injection of electrical energy into the network must equal the consumption of electrical energy from the network at all times. While the system contains a certain amount of instantaneous inertia from the rotating masses that comprise most generators, significant imbalances of such energy flows reduce the stability of the network and negatively affect the quality of electricity delivery, specifically the frequency. This assertion requires the network operator to have knowledge and control of the output of each generator on the network in order to match the real-time demand and ensure system stability. Under vertically integrated utilities, this was made possible almost trivially, as generators were owned by entities that also owned the transmission and distribution networks. However, under restructured regimes, monopolized control of the transmission network is given to an independent system operator (ISO) or regional transmission organization (RTO), as they are known in the U.S. Figure 1.1 depicts a map of U.S. regions operating under such organizations, which constitute approximately two-thirds of the population (King et al., 2011). Similar organizations exist in the EU, called transmission system operators (TSO), with slight technical variations from their American counterparts. For simplicity, ISO, RTO, and TSO will all be grouped under the term "system operator."

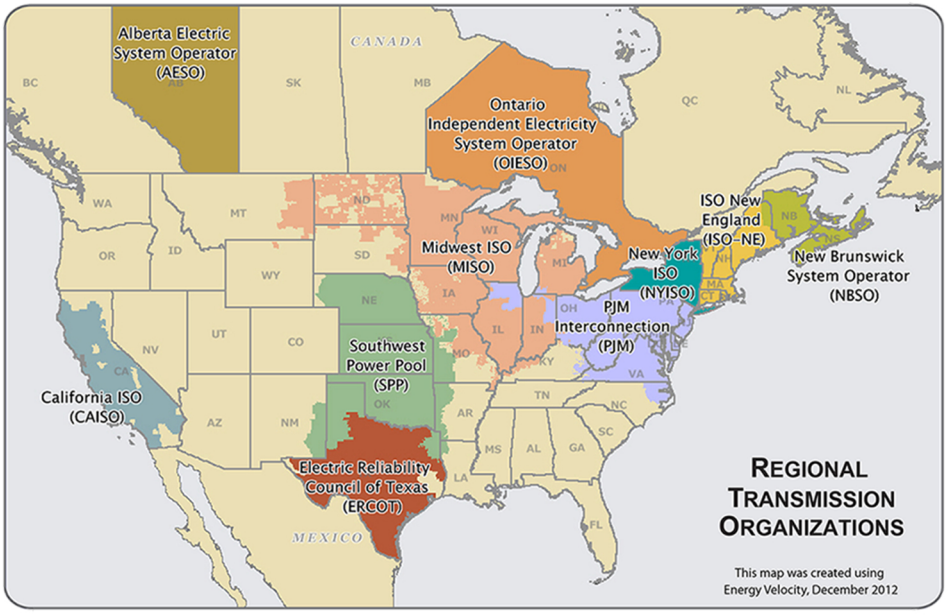

Figure 1.1 – Map of Regional Transmission Organizations operating in the U.S. (FERC, 2012)

System operators control the network by developing, directing, and overseeing a number of electricity wholesale markets that operate at varying time-scales and for different purposes. Through these markets, they are able to control generation such that network stability is maximized and cost of delivery is minimized for all nodes on their regional network for all time. Energy markets are used to ensure balance of the supply and demand of electricity and generally operate on day-ahead and hourly time-scales. Secondary markets procure balancing and stabilizing services from resources connected to the network and

operate from day-ahead to real-time, sub-hourly timescales. These services are called ancillary services and include contingency reserves and operating reserves. Contingency reserves represent extra capacity that can be dispatched in the event of a large contingency event, such as the sudden loss of a large generator or failure of a transmission substation. Operating reserves represent extra network capacity that can further be split into regulation, spinning reserves, and non-spinning reserves. Regulation refers to the second-by-second adjustment of generator output to follow the instantaneous variations in demand. Spinning reserves and non-spinning reserves are more intermediate reserves that generally account for forecasting errors or small contingency events. Spinning reserves refer to resources connected and synchronized with the grid, allowing them to respond within 10 minutes. Non-spinning reserves refer to resources that are not synchronized with the grid and generally have response times up to 30 minutes. Other markets, such as forward capacity or forward reserve markets, may exist to allow system operators and investors to strategically plan for future network expansion. It is important to note that the exact definition of ancillary service terms vary among regional markets. Their presentation here is generalized from the definitions given by NERC (2013a) to provide the reader with sufficient terminology definitions.

The buying and selling of energy is based on the economic concept of supply and demand. In the most commonly operated energy markets, independently owned generators bid their capacity and marginal cost of generation ($/MWh) for a given time period into the market. These marginal costs include both fixed costs and variable costs, such as fuel. Simultaneously, retail distributors submit their expected demand and corresponding marginal price to the same market. As shown in Figure 1.2, the cheapest generators are dispatched until the demand is satisfied, with the resulting price of electricity being the system marginal price (SMP), or clearing price. Base generators are marginally the cheapest and the most inflexible, causing them to be dispatched almost all of the time. Nuclear plants are an example of this type. Intermediate generators are marginally more expensive, but are also more flexible, allowing them to be dispatched somewhat periodically throughout a day. Coal power plants are an example of this type. Peak generators are marginally the most expensive but are also the most flexible. These generators are dispatched to meet peak demand throughout the day and participate heavily in ancillary service markets. Combined cycle gas turbines (CCGT) are examples of this type. After this economic dispatch scheduling takes place, adjustments are made to ensure spatial network stability based on transmission losses and congestion. These adjustments lead to slight modifications of the SMP at each network node. The new nodal prices are called Locational Marginal Prices (LMP), which are paid by retailers and to generators for the consumption or supply of electricity at that specific time and network location. Occurring during a day-ahead market, this process leads to the first hourly dispatch assignments and pricing schedules for the following operating day. Subsequent real-time energy markets and ancillary service markets refine the initial dispatching schedule to maintain instantaneous high quality delivery of electricity. Chapter 2 will present a more detailed description of the day-to-day operation of electricity markets for an example regional system operator in the U.S.

1.2 Growth and Impact of Wind and Solar Generation

A large part of the current energy revolution focuses on the integration of higher amounts of renewable energy sources on both the utility and distributed scale. These sources include hydro, wind, solar, biomass, municipal waste, and geothermal. In 2011 in the U.S., renewable generators accounted for approximately 50% of new electric-only generation capacity (EIA, 2012). In 2011 in the EU, renew-

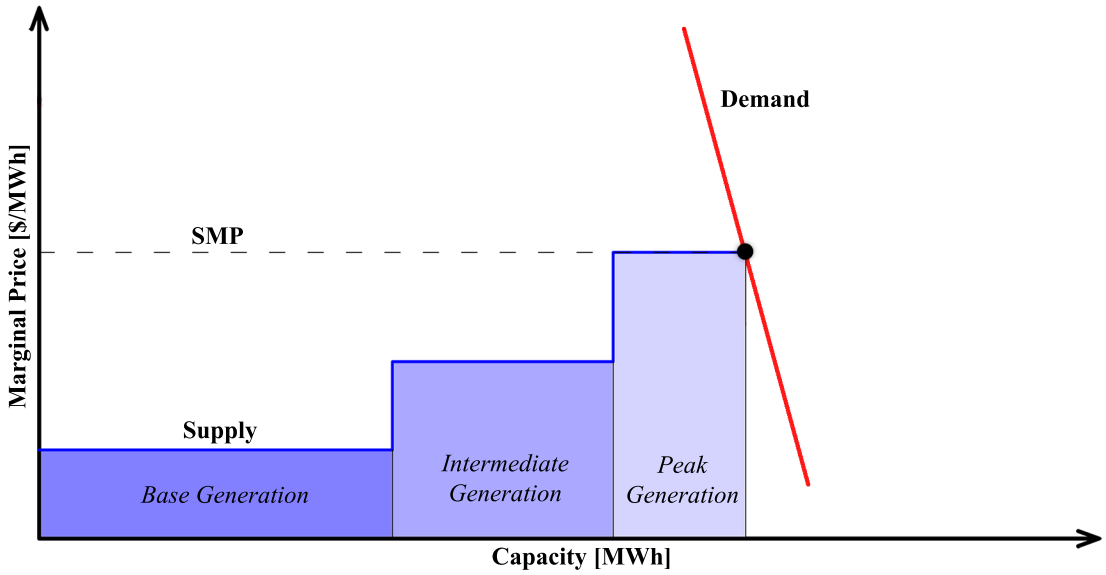

Figure 1.2 – Generalized determination of System Marginal Price (SMP) of electricity during day-ahead energy markets.

able generators accounted for approximately 71% of new capacity (EWEA, 2012). While the U.S. has no national target, 37 states have mandatory or voluntary renewable portfolio standards (RPS). Most of these standards target about 20% of state electricity generation to come from renewable sources by 2020 (DSIRE, 2013). The EU has mandated that by 2020, 20% of the energy supply be from renewable sources (Commission of the European Communities, 2008) and by 2050, the goal is to have electricity generation be zero-carbon (eurelectric, 2009). In addition to governmental portfolio targets, other drivers of increased renewable generation installment include net-metering programs, tax incentives, cash grants, feed in tariffs, and decreasing installation costs.

Of particular interest is the growth and penetration of wind and solar generation. By 2020, 34% of renewable electricity generating capacity in the U.S. is projected to come from wind and 13% is projected to come from solar (EIA, 2012), as depicted in Figure 1.3. Also by 2020, 43% of renewable generating capacity in the EU is projected to come from wind and 4% from solar (eurelectric, 2010). In each region, these two sources are expected to account for almost half of the renewable generating capacity, with the next highest coming from hydro. The primary advantages of using wind and solar resources include their virtually unlimited, free, and sustainable fuel supply, characteristics that help mitigate almost every energy-related concern. However, the natural variability in the real-time availability of wind and solar resources materialize into significant challenges for future electric grids that have implications for both network stability and cost.

Electricity grids are designed to meet variability introduced by loads or generators through the presence of ancillary service markets. However, the increased variability associated with wind and solar power requires larger capacities to be held in a number of these markets to counteract errors in forecasting and real-time generation fluctuations. Wind production forecasting uncertainties at the hour-ahead to day-ahead levels range approximately from 5 - 17% mean absolute error (eurelectric, 2010). eurelectric

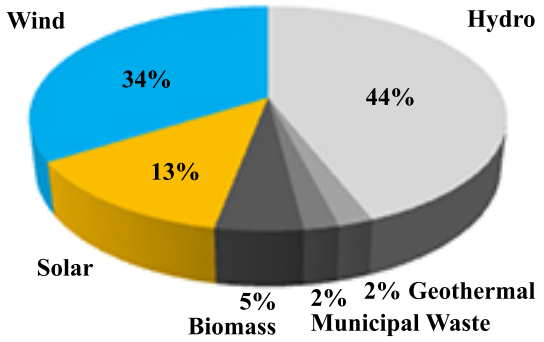

Figure 1.3 – Distribution of projected renewable generating capacity in the U.S. in the year 2020 (EIA, 2012).

(2010) also figures that every MW of wind capacity may require one MW of firm backup to ensure 90% availability. Similarly, King et al. (2011) reports that the capacity value, defined as the percentage of nameplate capacity that can be counted on to serve peak load, for wind can be as low as 20-30% . Additionally, King et al. (2011) suggests the average capacity requirement for spinning reserves (including regulation) could triple in the eastern region of the U.S. electric grid by 2024. Higher penetrations of wind require more expensive peaking plants to be online in order to provide a greater capacity of ancillary services, displacing the normal capacity otherwise supplied by intermediate generators. This, in addition to wind displacing base and intermediate generation from the bottom, can squeeze intermediate plants out of hourly dispatching schedules. The increased start and stop frequencies of these intermediate plants in addition to less remuneration from power sales will inevitably increase their marginal cost of generation, with the potential of ultimately increasing the SMP. Additionally, durability and reliability of these plants becomes a concern due to higher start and stop frequencies than anticipated during plant design.

Separate from energy balancing, a second major concern of grid-scale wind and solar is the decrease of system inertia (MIT, 2011). While thermal generators create electricity by spinning large masses with magnets through magnetic fields, wind and solar are often connected to the grid via power electronics to control their output; whether it be converting from DC to AC, in the case of solar photovoltaics, or minimizing the effect of turbine angular velocity changes on output quality, in the case of wind. Instantaneous energy imbalances in the grid network that cause frequency deviations can be absorbed by the large rotating inertia of thermal plants until plant-specific controls, called governors, regulate the rotational speed to the appropriate level. Therefore, the decrease in system inertia with increased penetration of wind and solar can also lead to increased capacity requirements for ancillary services.

1.3 The Role of Building HVAC Systems

The problems facing the electric grid as a result of the increasing penetration of variable renewable energy sources motivate a need for grid-scale technologies that can provide economic flexibility, namely storage potential. A number of promising storage technologies still face barriers to wide-spread adoption (MIT, 2011), including pumped hydroelectric storage plants (PHES), utility-scale batteries, and vehicle-to-grid

concepts. PHES require geographical areas with specific topography characteristics and require long lead-times for construction. Consequentially, there has been only one major PHES plant built in the U.S. in the last 15 years (Deane et al., 2010). Utility-scale batteries and flywheels have shown potential in pilot projects, however, are still considered to be too expensive for full implementation in today's electric grid (Rastler, 2008; Oldak, 2012). Vehicle-to-grid service (Kempton and Tomić, 2005a,b) relies on the wide-spread adoption of plug-in-electric vehicles, something that will take time to occur (MIT, 2011). Buildings consume 74% of the electricity in the U.S. (EIA, 2012) and contain inherent characteristics that can make their consumption flexible. The combination of these qualities can make the building stock an aid in providing grid-scale economic flexibility from the demand side.

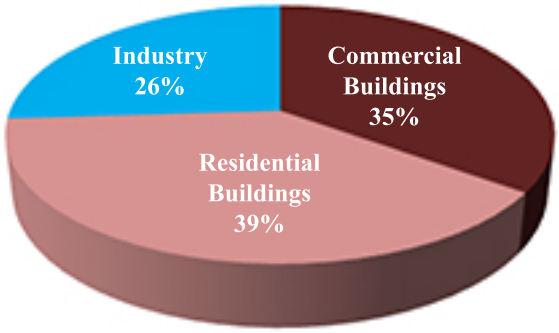

Figure 1.4 – Distribution of U.S. electricity consumption in 2011 (EIA, 2012).

Electricity consumption flexibility in buildings comes primarily through their HVAC systems, which directly couple a building's electricity use with its thermal storage potential and accounted for 27% of electricity consumption in commercial buildings in 2011 (EIA, 2012). It should be noted that potentials exist for lighting systems as well (Rubinstein and Kiliccote, 2007; Rubinstein et al., 2010), which accounted for 21% of commercial building electricity consumption (EIA, 2012), however this thesis does not concentrate on them. A simple example of HVAC flexibility considers a single room with a window air-conditioner supplying cooling such that the room air temperature is in the middle of thermal comfort limits. If the air-conditioner in the room is turned off, it will take a characteristic amount of time, dependent on the cooling load, construction, and contents of the room, for the air in the room to heat to an uncomfortable level. At this point, the room air-conditioner would have to be turned back on in order to restore proper service to its occupant. To a system operator, the electricity consumption of the air-conditioner is seen as flexible, as it may vary to a certain extent without significant loss of service. The keys to the potential of this flexibility lie in determining the extent of consumption alteration without subjecting occupants to a substantial loss in service. This service is composed of the provision of both thermal comfort and indoor air quality.

This concept of demand-side flexibility in electric grids is commonly known as *demand response* and can include both building and industrial loads. Demand response is different than energy efficiency in that demand response measures are enacted with a specific short-term operational goal in mind, while energy efficiency measures are implemented for long-term sustainability. This important distinction will be made more clear with examples in the literature review of the next chapter. The effectiveness of demand response activities are measured by the reduction in load compared to a baseline that represents "normal" operation during the same time period and conditions.

In the last decade, a number of research projects, demonstration projects, and system implementations have set out to explore the potential of demand response in buildings. In most cases, demand response is a considered resource when there is an anticipated imbalance between energy supply and demand on the network, and has been called *slow-DR* (Piette et al., 2008). This energy imbalance is typically brought about by demand spikes during hot summer afternoons and is represented by increases in hourly electricity prices at the wholesale level. A utility company or consumer with knowledge of such price volatility sheds or shifts electric loads during this time to save money and to prevent strains on the network. In a smaller number of cases, demand response is a considered resource to provide ancillary services, generally reserves, and has been called *fast-DR* (Piette et al., 2008). In these cases, a consumer or an organized group of consumers under a single utility company or Curtailment Service Provider (CSP) curtail load as dispatched by the system operator. Providing the expected magnitude and duration of service becomes more imperative to system operators as the window for planning reduces to real-time network operation. Therefore, fast-DR is inherently more challenging than slow-DR. More real-time instabilities are expected with the growing penetration of wind and solar generation, contributing to a similarly growing need to research how buildings may effectively provide the required ancillary services.

While building HVAC systems can provide solutions for economic grid-scale flexibility, a number of challenges exist with such implementations, particularly in the case of providing ancillary services where the importance of reliability is at its highest. These challenges stem from the dependence of HVAC electricity consumption on building type, building location, system type, and system loading, which is further a function of time-varying environmental conditions and occupant activities. This variability can make it difficult for system operators to rely on building HVAC systems for ancillary services unless the building can communicate reliable, predicted, and time-dependent service potentials to the system operator similar to the requirement of generators providing the same services.

Having buildings participate in the same ancillary service markets as generators and being able to provide reliable performance information allows system operators to produce the optimal plan to maintain a high quality of electricity delivery. However, providing such information requires not only new communications infrastructure for buildings, but the ability for a building's ancillary service potential to be predicted on market timescales. While a significant amount of work has resulted in a communication protocol for buildings to communicate with system operators (Piette et al., 2009; Ghatikar and Bienert, 2011), the work towards predicting and controlling a building's time-dependent ancillary service abilities has been less unified and comprehensive. This is particularly the case of commercial buildings, which constitute almost half of building electricity consumption in the U.S. (EIA, 2012). These buildings typically have multiple thermal zones and, as a result, utilize more complex HVAC systems than their residential counterparts, which have been the primary focus of study when considering building-provided ancillary services. Timescales associated with these services are in the seconds to minutes range, which correspond to the transient timescales of HVAC systems. Therefore, in order to predict the service potential of common commercial HVAC systems, the transient dynamics of the operation of these systems during demand response events must be fully considered and understood.

1.4 Thesis Objectives and Structure

In response to a growing need for economic grid-scale flexibility, the objective of this thesis is to explore the technical processes by which new and existing commercial building HVAC systems can provide ancillary services for the electric grid. The primary ancillary service considered is the provision of spinning reserves, where response times are expected to be within 10 to 30 minutes, depending on network requirements. Regulation service is discussed in the context of describing ancillary services, however, mechanical durability concerns associated with the necessary control of HVAC equipment leave this topic to be more fully developed elsewhere. The primary HVAC system considered is the variable air volume (VAV) system controlled by a building automation system (BAS) or energy management system (EMS). This system type is one of the most commonly implemented for new and existing multi-zone commercial buildings. Specifically, this thesis will:

- Identify real-world operational qualities of buildings with VAV systems which need to be considered for ancillary service provision.
- Identify the needs, requirements, and methods for dynamic simulation of HVAC systems for future study of ancillary service demand response.
- Develop characterization curves for a range of demand response strategies that can be used to map their performance for varying implementation and load intensities.
- Identify sources of performance variability within and among a range of common demand response strategies.
- Suggest advantages or disadvantages associated with a range of demand response strategies for providing ancillary services.

The objectives stated above are accomplished primarily through the analysis of high-resolution performance data from a test building and dynamic simulations of a representative VAV system. In conclusion, this work looks to lay a foundation for future development of ancillary service demand response in both new and existing commercial buildings, particularly that associated with developing algorithms to predict demand response potential for electricity market bidding.

This thesis is structured as follows:

Chapter 2 provides a literature review and background of the subject of research. This begins with a more detailed description of day-to-day electricity market operations so that the context of the research is more fully understood. A strict dichotomy is then emphasized between energy efficiency and demand response, which primarily separates design-based operational strategies from service-based operational strategies. This is followed by a literature review of demand response research and implementation activities in the last decade.

Chapter 3 details the analysis of a monitored test building. Electrical and HVAC performance data of both normal operation and a simple demand response test are presented, followed by a discussion of the real-world operational challenges and insights of building-provided ancillary services.

Chapter 4 develops the need and requirements for dynamic HVAC system simulation to further study ancillary service provision and discusses the challenges associated with such simulations. Multiple simulation programs are trialed in order to demonstrate the strengths and weaknesses of certain simulation programs to serve as the necessary tools for simulation and study.

Chapter 5 details the simulations of a representative VAV system performing ancillary service with different demand response strategies as well as varying implementation and load intensities. These simulations are used to identify sources of performance variability as well as advantages or disadvantages associated with each strategy in providing ancillary services.

Chapter 6 provides final conclusions and suggests future work.

Chapter 2

Literature Review

The goal of this chapter is to not only put the work of this thesis within the context of other building demand response research, but also to relate the work to real-world regional electric grid operation. To that end, Section 1 will provide a more detailed description of typical day-to-day electricity market operations than was presented in the previous chapter. The goal is to inform the reader of the complex, yet systematic approach to delivering high quality electricity to consumers, which emphasizes the need for predictability and reliability. Section 2 will express the differences between demand response and energy efficiency in order to clearly define the targeted services and outcomes of each. Section 3 provides an outline of important building demand response research activities so that it is better understood how the conclusions of this thesis progress the work in this area of research. Finally, Section 4 presents examples of building demand response operations and performance in regional electric grids today.

2.1 Electricity Market Operations

Building practitioners are often not aware of the complex, almost miraculous, processes performed by system operators, generators, and utilities to reliably deliver electricity to the buildings they design and operate. However, knowledge of grid operations is vital to the general understanding of where buildings currently fit into the larger scheme of energy use and foreseeing how this role can change in the future. More specifically, an awareness of the extensive planning efforts and execution precision gives reason to studying in more detail the demand response operations in multi-zone HVAC systems. In order for buildings to truly become an integral part of network operation, they need to be able to provide timely and accurate demand response information to the system operator.

The principles of operation are generally the same for each regional system operator, with only slight technical variations in timing and optimization. For this reason, and in the interest of scope, the operation of one regional grid will be described in this section; the Independent System Operator of New England (ISO New England). More specific references to individual system operators will be made in the later section on demand response implementations. The occurrence of both sequential and parallel time-sensitive processes can make understanding grid operation difficult. In order to relieve some of this difficulty, a graphic description of the daily operation time line is displayed in Figure 2.1 at the end of

this section. Unless otherwise noted, the information presented in this section is drawn from ISO New England (2013b).

2.1.1 Energy

Energy can be defined as the flow of electric power in the system from supply generators to demand consumers. It is an inherent property of regional electric systems that the amount of supply must meet the amount of demand at all instants in time. For this reason, two markets exist to procure enough energy (MWh) to meet both the anticipated and real-time demand. These two markets are the Day-Ahead Energy Market and the Real-Time Energy Market.

Day-Ahead Energy Market

The Day-Ahead Energy Market opens at 0000 the day before Operating Day, and closes at 1200 of the same day. During this time, market participants can submit supply offers and demand bids for the hourly production or consumption of energy the following day. Included in specific resource supply offers are items such as the magnitude and cost of supply, start-up or no-load fees, minimum run-time, economic maximum limits of supply, economic minimum limits of supply, and emergency minimum limits of supply. The offer is not to be below \$0/MWh or above \$1,000/MWh. Included in specific demand bids is the cost of demand, also in \$/MWh, which represents the price retailers are willing to pay for electricity. Note that units of capacity here are MWh, which denote the power in MW for the hour of interest. Upon market closure at 1200, ISO New England begins to create day-ahead hourly schedules of supply and demand for each market participant as well as hourly energy prices, called the system marginal price (SMP). Each of these pieces of information is developed based on a least-cost, security-constrained economic dispatch process, and is published on the ISO New England website at 1600. The specific energy prices that each market participant is responsible for are calculated at various locations throughout the system, called nodes, and take into account the system-wide cost of energy, node-specific transmission congestion, and node-specific transmission losses. The resulting Locational Marginal Prices (LMP) can, therefore, vary above and below the system-wide cost of energy by slight amounts. The results of the Day-Ahead Market are binding to the market participants. That is, suppliers are responsible for supplying their scheduled amount of energy for each hour during the Operating Day and will be compensated based on the Day-Ahead LMPs. Similarly, buyers are responsible for using their scheduled amount of energy for each hour during the Operating Day and must pay based on Day-Ahead LMPs. In general, the hourly day-ahead credit charged to each market participant can be expressed as Equations 2.1 and 2.2 on the following page (ISO New England, 2013a). Note that the day-ahead generation and demand obligations include energy contracted in bilateral agreements or other reported transactions that move the energy responsibility to or from the resource in question.

Real-Time Energy Market

The Real-Time Energy Market officially opens at 1600 the day before Operating Day. The time from 1600 to 1800 is considered the Re-Offer Period, whereupon after seeing the results of the Day-Ahead Market, and possibly better forecasts of supply and demand, market participants may edit and re-submit their supply offers and demand bids. Upon the close of the Re-Offer period at 1800, ISO New England performs a Reserve Adequacy Analyses (RAA), where it determines the adequacy of energy, reserves, and regulation scheduled for the Operating Day. Upon completion and publishing of the RAA at 2200

before the Operating Day, the ISO enacts the Current Operating Plan, to be used at the start of the Operating Day at 0000. The Real-Time Energy Market is re-evaluated every 5 minutes during the Operating Day. Upon each re-evaluation, the ISO sends new dispatch instructions to supply resources to maintain the stability and reliability of the system at all times. Additionally, 5-minute LMPs are calculated based on real-time system conditions. Market participants are responsible for payment or subject to compensation based on the net difference between the amount of energy supplied or purchased during real-time and the amount of energy that was scheduled as a result of the Day-Ahead market. Settlement of these differences is made based on Real-Time LMPs, which are calculated at the end of each hour as the time-weighted average of 5-minute LMPs during that hour. In general, the hourly real-time credit charged to each market participant can be expressed as Equations 2.3 and 2.4 below (ISO New England, 2013a). Note that the real-time generation and demand include energy contracted in bilateral agreements or other reported transactions that move the energy responsibility to or from the resource in question.

$$E_{DA} = G_{DA} - D_{DA} \tag{2.1}$$

$$C_{DA} = E_{DA} \times (LMP_{DA}^{Energy} + LMP_{DA}^{Congestion} + LMP_{DA}^{Loss}) \tag{2.2}$$

Where:

E_{DA}	=	Day-Ahead Net Energy Obligation	(MWh)
G_{DA}	=	Day-Ahead Generation Obligation	(MWh)
D_{DA}	=	Day-Ahead Demand Obligation	(MWh)
C_{DA}	=	Day-Ahead Charge(-) or Credit (+)	($)
LMP_{DA}^{Energy}	=	Day-Ahead Energy Component of LMP	($/MWh)
$LMP_{DA}^{Congestion}$	=	Day-Ahead Congestion Component of LMP	($/MWh)
LMP_{DA}^{Loss}	=	Day-Ahead Loss Component of LMP	($/MWh)

$$E_{RT} = G_{RT} - D_{RT} \tag{2.3}$$

$$C_{RT} = (E_{RT} - E_{DA}) \times (LMP_{RT}^{Energy} + LMP_{RT}^{Congestion} + LMP_{RT}^{Loss}) \tag{2.4}$$

Where:

E_{RT}	=	Real-Time Net Energy	(MWh)
G_{RT}	=	Real-Time Generation	(MWh)
D_{RT}	=	Real-Time Demand	(MWh)
C_{RT}	=	Real-Time Charge(-) or Credit (+)	($)
LMP_{DA}^{Energy}	=	Real-Time Energy Component of LMP	($/MWh)
$LMP_{DA}^{Congestion}$	=	Real-Time Congestion Component of LMP	($/MWh)
LMP_{DA}^{Loss}	=	Real-Time Loss Component of LMP	($/MWh)

2.1.2 Operating Reserves

Operating reserves are procured to handle the loss of generating equipment, loss of transmission equipment, errors in load forecasting, and regulation (ISO New England, 2011). Regulation will be discussed separately later in this section. There are three types of operating reserves, including Ten-Minute Spinning Reserves (TMSR), Ten-Minute Non-Spinning Reserves (TMNSR), and Thirty-Minute Operating Reserves (TMOR). TMSR and TMNSR are resources that are required to reach their dispatched energy output within 10 minutes of being called to do so, while TMOR resources are required to reach their designated energy output within 30 minutes. Spinning reserves are already synchronized to the system while non-spinning reserves are not. CLAIM10 and CLAIM30 values define the amount of megawatts a resource may output by the end of a 10 minute or 30 minute period respectively. These values are determined by periodic demonstration testing by the resource for the ISO.

The Forward Reserve Market procures TMNSR and TMOR to ensure the required amount of operating reserves is available. A forward reserve auction is held approximately two months before the reserve procurement period for that auction, where market participants submit reserve bids as TMNSR or TMOR with $ /MW-month amounts. The auction is held twice per year and is cleared, along with the Forward Reserve Clearing Price, to minimize the cost of providing the required amount of reserves for the reserve procurement period. The two procurement periods are from June 1 through September 30 (Summer Capability Period) and October 1 through May 31 (Winter Capability Period). Delivery of the Forward Reserve is only required on weekdays from hour ending 0800 through hour ending 2300, except those weekdays considered NERC holidays.

Market participants with resulting Forward Reserve Obligations must assign the megawatts of obligation to specific resources under their control for each hour of the Operating Day by the end of the Re-Offer period prior to each Operating Day during the same reserve procurement period as their obligations. Alternatively, the market participant may enter into a bilateral contract for fulfillment of the Forward Reserve Obligation, which must be processed by 2400 of the day prior to the Operating Day. Resources not obligated by the results of the Forward Reserve Market must also submit hourly supply offers for reserves into the Real-time Energy Market by the end of the Re-Offer period. The supply offer for a reserve resource must be at or above the Forward Reserve Threshold Price, a price that is calculated to ensure the offered resource has a low probability of being dispatched for energy and a high probability of being dispatched for reserves. If a resource is assigned a Forward Reserve Obligation and is not cleared in the Day-Ahead Energy Market, it is automatically offered into the Real-Time Energy Market. The ISO maintains an amount of Ten-Minute Reserve equal to the amount required to replace the capacity of the largest dispatched generator (first contingency loss) multiplied by an adjustment factor. A certain percentage of that must be TMSR, depending on the past performance of the ISO in handling contingencies (ISO New England, 2011). The ISO maintains an amount of TMOR equal to at least 50% of the capacity of the second largest operating generator (second contingency loss). An initial schedule for operating reserve designation is created as a result of requirements determined during the Day-Ahead Energy Market and is continually updated, every 5 minutes, through the Real-Time Energy Market based on system conditions and resulting reserve requirements.

As described by equations 2.5 to 2.8, market participants are compensated for their Final Forward Reserve Obligation Megawatts as well as their Real-Time Reserve Designation Megawatts (ISO New England, 2013a). Final Forward Reserve Obligation Megawatts are the minimum of Forward Reserve

Obligation Megawatts cleared from the Forward Reserve Market and the Forward Reserve Delivered Megawatts. The Forward Reserve Delivered Megawatts is the minimum of 1) CLAIM10 or CLAIM30 values as reported by the resource in the supply offer, 2) the Forward Reserve Assigned Megawatts, or 3) the Megawatts offered above the Forward Reserve Threshold Price. Final Forward Reserve Obligation Megawatts are compensated based on hourly Forward Reserve Market Clearing prices and Real-Time Reserve Designation Megawatts are compensated based on the Real-Time Reserve Clearing Price. This is calculated at the end of each hour as the time-weighted average of 5-minute Real-Time Reserve Clearing Prices throughout the same hour. A failure-to-reserve occurs when a market participant's Forward Reserve Delivered Megawatts is less than their Forward Reserve Obligation. This action results in forfeit of payment for any Forward Reserve Obligation not met plus a financial penalty. A failure-to-activate occurs when a market participant's resource fails to deliver the dispatched energy when called to do so by the ISO and results in financial penalty separate from the failure-to-reserve penalty. It is the responsibility of the market participant to communicate resource conditions that affect operating reserves to the ISO (ISO New England, 2011).

$$Cr_{FR} = P_{FR} \times R_{FR} \tag{2.5}$$

$$Cr_{RT} = P_{RT} \times R_{RT} \tag{2.6}$$

$$Ch_{FTR} = P_{FTR} \times (-1.5) R_{FR} \tag{2.7}$$

$$Ch_{FTA} = P_{FTA} \times max[-2.25 \times R_{FR}, -LMP_{RT}] \tag{2.8}$$

Where:

Cr_{FR}	=	Forward Reserve Credit	($)
P_{FR}	=	Forward Reserve Obligation	(MW)
R_{FR}	=	Forward Reserve Payment Rate	($/MW)
Cr_{RT}	=	Real-Time Reserve Credit	($)
P_{RT}	=	Real-Time Reserve Designation	(MW)
R_{RT}	=	Real-Time Reserve Clearing Price	($/MW)
Ch_{FTR}	=	Failure to Reserve Charge	($)
P_{FTR}	=	Failure to Reserve Megawatts	(MW)
Ch_{FTA}	=	Failure to Activate Charge	($)
P_{FTA}	=	Failure to Activate Megawatts	(MW)
LMP_{RT}	=	Applicable Real-Time LMP	($/MW)

2.1.3 Regulation

Regulation allows the ISO to stabilize the system on a moment-by-moment basis, as the process entails the adjustment of generation output by dispatching Automatic Generation Control (AGC) signals to

those generators providing regulation service every 4 seconds. Generators with the ability to supply regulation service can submit regulation offers along with their day-ahead energy bid in the Day-Ahead Energy Market. These offers include the hourly regulating unit status, regulation offer price ($/MWh), hourly regulation high and low limits, automatic response rate (minimum 1 MW/minute), and regulation capability (equal to the less of five times the automatic response rate or one-half of the regulation range defined by the high and low limits). Additionally, the Regulation Market is open during the Re-Offer period where generators can buy and sell regulation services.

Five minutes after every operating hour, and as needed throughout the hour, the ISO develops a Regulation Rank Price, used to rank the generators who have been scheduled for that hour in the most economical dispatch order to provide the determined regulation requirements for that hour. The Regulation Clearing Price is calculated at the end of each hour and is based on the time-weighted average of the highest Regulation Offer of all units scheduled to provide Regulation during the same hour. Also at the end of each hour, unit-specific Regulation Opportunity Costs are calculated that are based on the Real-Time LMPs. The Regulation Clearing Price and Regulation Opportunity Costs are used for determining regulation service settlement with each generator.

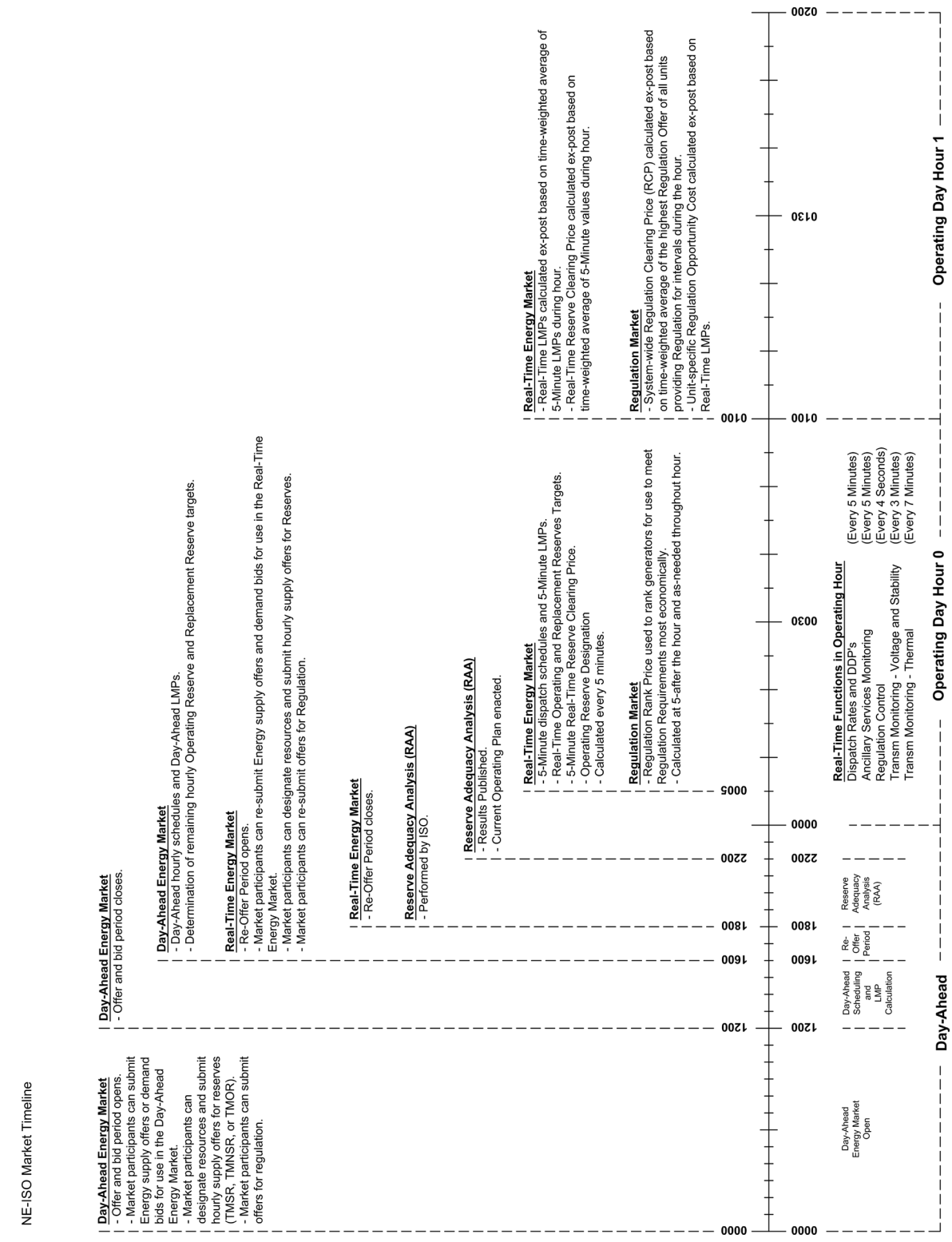

Figure 2.1 – Time line of electricity market operation for ISO New England.

2.2 Demand Response vs. Energy Efficiency

Demand response is action taken by a load resource to alter its electricity demand in response to a dispatch signal or trigger by the system operator or utility. While it can also include distributed demand-side generation, these reductions generally come from industrial processes or building HVAC and electrical systems. Order 745 of the Federal Energy Regulatory Commission (FERC, 2011a) identifies two types of demand response; I) price responsive and II) resource oriented. Type I is generally dispatched in the case of emergency situations when the network is strained on generating capacity or transmission congestion, indicated in real time by high real-time LMPs or forecasted by high day-ahead LMPs. Benefits for the load participant include either outright remuneration for taking action or general cost reductions resulting from using less energy during periods of high prices. The latter case is only applicable where wholesale prices are directly translated to retail rates, such as real-time pricing schemes. Mutually beneficial to system operators is the maintained stability of the network without the need for blackouts. Type II treats demand-side resources similarly to generators, giving them the ability to bid a variety of services into existing electricity markets. Here, demand response is in direct economic competition with generation for specific services, including the provision of capacity, energy, or ancillary services.

Energy efficiency is action taken by a demand-side resource that promotes the long-term reduction in energy usage. Energy efficiency strategies are not utilized for a specific service or during a specific time period, as demand response strategies are. A simple example is that of replacing incandescent light bulbs with compact fluorescent ones. Other HVAC-related examples range from design-oriented to control-oriented. Design-oriented measures include those found in ASHRAE Standard 189.1 (ASHRAE, 2011), such as improving the construction of facades or installing high efficiency equipment. Control-oriented examples include night-time zone temperature setbacks, VAV duct static pressure reset strategies (Englander and Norford, 1992b; Warren and Norford, 1993), advanced fault detection and diagnostics (Samouhos, 2010), or daily energy optimization using thermal mass (Armstrong et al., 2006b,a; Gayeski, 2010; Zakula, 2013). Seeing the need for a global reduction in energy usage in both space and time, some system operators are include energy efficiency measures as viable capacity bids in their future planning markets (PJM, 2010; ISO New England, 2012b).

2.3 Demand Response Research

The predominance of research on multi-zone commercial building demand response has been in the area of type I demand response, as defined in the previous section. One of the largest studies of demand response in commercial buildings was performed by the Demand Response Research Center (DRRC) at the Lawrence Berkeley National Laboratory (LBNL), which is a leader in many aspects of demand response research. A 2007 report (Motegi et al., 2007) summarized the findings of demand response tests performed on 28 non-residential buildings from California to New York from 2003 to 2006 and offered recommendations regarding the effectiveness of various demand response strategies. The majority of building types were offices, along with supermarkets, retail stores, public assemblies, a high school, laboratory, a museum, and a post office. Tests utilized three hours of afternoon high price signals to enact pre-programmed demand response strategies for each building. The strategies included both HVAC and lighting system alterations. The four most common HVAC strategies were global zone setpoint adjustment, duct static pressure decrease, supply air temperature increase, and chilled water temperature

increase. A fifth strategy often combined with supply air temperature increase and chilled water temperature increase was supply fan speed limiting. The dynamics associated with each of these strategies will be discussed in more detail in Chapter 4 of this thesis and form the basis of the simulations described in Chapter 5. In general, LBNL found a global zone setpoint temperature adjustment to be the most effective due to the combination of electricity curtailment with the relative control of occupant service loss. A dependence of load curtailment on outdoor air temperature and time of day is also noted, though the study suggests more research to better understand the performance potential of different buildings, with different systems, in different climates. Finally, the findings also point out the occurrence of rebound, where an electricity spike occurs after returning system operation to normal. Other studies (Mathieu et al., 2011) have defined additional characteristic parameters of demand response performance, including average shed (kW), intrashed variability (kW), and residual ramp time (min). These parameters are important for comparing demand response performance between among individual events and buildings. Mathieu et al. (2011) also introduce a 15-minute interval baseline load prediction model based on an ordinary least squares regression on past load, time, and outdoor temperature data. This model was then used to analyze variability in performance characteristics over different demand response events (Mathieu et al., 2011). This study, using 15-min demand response performance data from 38 commercial and industrial buildings, found that performance variability could be more related to baseline calculation variability then actual performance variability.

A second major study of type I demand response was performed by the Pacific Northwest National Laboratory (PNNL) as part of their Pacific Northwest GridWise Testbed Demonstration projects. The Olympic Peninsula Project (Hammerstrom et al., 2007) demonstrated that the use of real-time pricing can be used to limit distribution feeder congestion, by delivering real-time wholesale market energy prices to residential and commercial loads. Residential thermostats adjusted setpoint temperatures based on real-time market prices and commercial buildings controlled their energy use by using *transactive control*, a controls philosophy that uses the economics of efficient supply and demand to meet heating and cooling loads. Under this strategy, zone thermostats would bid for available cooling or heating energy (based on feeder conditions) with signals proportional to the amount of cooling or heating needed. The most needed zones were allotted more of the available cooling or heating energy. In addition to building load reduction, this study also utilized buildings' emergency diesel generators to effectively island their facilities from the grid.

Raustad and Basarkar (2011) performed over 32,000 building simulations to quantify the effect building type, HVAC system type, demand response strategy type and implementation method, and climate have on demand response performance. The simulations assumed a three hour demand response signal in the afternoon. Lighting power density reductions were found to be able to curtail approximately 10% of electric load, peak demand savings for thermostat setpoint adjustments were found to be 12%, peak demand savings for chilled water temperature reset were 16% with pump speed limiting, and peak demand savings for supply air temperature reset were 14% with supply fan speed limiting. Savings varied greatly, however, with respect to all of the varied input parameters from negative, to negligible, to the peak value. It was noted that without pump and fan speed limiting, adjustment of supply air and chilled water temperature could increase electric demand, as the supply fan and chilled water pump speed up to maintain the same level of cooling in these cases. EnergyPlus(v4) (U.S. Department of Energy, 2013a) was used as the simulation program, to which code modifications had to be made in order to simulate fan speed and pump speed limiting. While a large number of inputs were varied, meaningful correlations between performance and input are difficult to make with the data presented. Specifically, identifying

what is happening within the HVAC system to cause such performance variations.

Lee and Braun (2008) and Greensfelder et al. (2011) use optimal pre-cooling of thermal mass to minimize peak electricity demand in response to time-of-use and real-time pricing schemes respectively. Both identify zone temperature cooling setpoint trajectories for air-based HVAC systems throughout the day using either a model predictive control algorithm applied to an inverse model, in the case of Lee and Braun (2008), or simulation software, in the case of Greensfelder et al. (2011). Other research utilizes inverse models to optimize the schedule of chiller operation in radiant cooling applications to minimize daily energy use (Gayeski, 2010; Zakula, 2013). The study of optimal pre-cooling strategies and development of inverse modeling techniques to minimize peak demand or daily energy begins to transition our study of type I demand response to type II demand response. The use of these optimization and prediction schemes can conceivably serve as a basis for the formation of day-ahead or real-time electricity market bids, either for energy or ancillary service.

For type II demand response there has been a large amount of research on residential-type HVAC systems. Phase I of the Demand Response Spinning Reserve Demonstration by LBNL (Eto et al., 2007) demonstrated the ability for residential AC units on a single distribution feeder to be switched off for use as 10-minute spinning reserves in the CAISO operating area. Results showed demand response within 20 seconds of signaling, far less than the required 10 minutes for the reserve type. Additionally, statistical methods were used to develop correlations between ambient weather conditions and time of day with load curtailment amount. These correlations, however, require a wider range of weather conditions and more specific information about individual units for further development and increased accuracy. Phase 2 of this demonstration (Eto et al., 2009) expanded the project to include multiple distribution feeders spreading among multiple geographical regions. It also tested the ability for curtailment signals to be initiated via the CAISO Automated Dispatch System (ADS) every five minutes. While this report also found that demand-side curtailment can respond much faster than the required 10 minutes, there was difficulty in predicting the exact effect of the curtailment on two of the four distribution feeders. This was due to a limited number of participants, small loads per AC unit, or other technical difficulties in communication and feeder assignments. Another study demonstrated the ability for hotel room air-conditioners to provide spinning reserves (Kirby et al., 2008). A 162-room hotel in Tennessee was able to curtail 22% and 37% of its load during tests performed over two days. For each test, the load was curtailed within 12 to 60 seconds of dispatch of the curtailment signal. Curtailment lasted 15 minutes and an average room temperature rise of 1.7 °F was observed over that time. The study points out that HVAC systems may actually perform better as spinning reserves than as peak load reducers or energy providers. This is due to the time it takes zone temperature to rise compared to the characteristic time period of each service.

Other projects have explored the ability for residential-type loads to provide instantaneous frequency or power factor support. The first is the Grid Friendly Appliance Project (Hammerstrom et al., 2007), the second part of the Pacific Northwest GridWise Testbed Demonstration projects referenced earlier. This project demonstrated the use of frequency detection technology to control residential appliances for automatic response to grid underfrequency events. Specifically, grid friendly appliance (GFA) controllers were installed on 150 new residential clothes dryers and 50 retrofitted residential water heaters and were programmed to shed their load upon detection of 59.95 Hz or less. Though the number of participants and corresponding load amount was small compared to the system at large, the study demonstrated the successful operation of such controllers and, therefore, the possibility of automatic, fast acting (< 1 s), demand-side response to underfrequency events. Research at Virginia Tech explored other support-

related roles for residential buildings, including power factor correction services performed by a Plug-in Hybrid Electric Vehicle (PHEV) connection in combination with renewable generation and other common residential loads (Cvetkovic, 2010). It was proposed that a bidirectional power converter (BPC), in conjunction with the PHEV battery, can be used to control the power factor seen by the utility at the house feeder connection. A central control system to be located inside the house is developed that can receive power factor setpoints from the system operator, monitor the total house power factor, and send control signals to the BPC to modulate the power factor accordingly. Laboratory tests showed successful power factor adjustment by this system.

Callaway (2009) showed the ability for a collection of thermostatically controlled loads (TCL) to be controlled using small temperature setpoint adjustments by a central operator such that their aggregate power output follows a wind generator. The TCL dynamics are represented by a general first-order resistance capacitance model served by a discrete ON/OFF heater or cooler with constant heating power efficiency or cooling coefficient of performance (COP). Koch et al. (2011) generalized the method of control to a state space formulation in order to allow for system identification techniques to be used when the measured states of all or a group of TCL's are known. This method was used in a model predictive control scheme in which the collection of TCLs followed a desired power output trajectory. Callaway and Hiskens (2011) point out the difficulty in centralized load control due to the size of the data and communications infrastructure that would have to be established, past the current implementation of digital load meters and smart meters. Much for this reason, Mathieu and Callaway (2012) extended the direct TCL control work in the case of incomplete state knowledge for the collection of TCLs, showing that, to an extent, a Kalman filter may used for system identification and control with incomplete state knowledge. While this work pushes the boundary for the control of TCLs for load following, the assumptions of such discrete HVAC system control with constant efficiencies, in addition to a first-order resistance capacity model to represent load temperature evolution, may only go so far in real applications. Multi-zone commercial buildings often utilize VAV systems with variable speed drives (VSD) controlling fans, pumps, or compressors that do not have such discrete power consumption profiles. COP is also a function of operating conditions, particularly evaportating and condensing temperatures, which are set by chilled water and outdoor air temperatures respectively. Lastly, all of the zones do not experience the same daily heating or cooling load profiles, mainly due to building orientation, and a more rigorous approximation of individual zone temperature evolution is needed to maintain thermal comfort. Citing the requirements of this additional state information for multi-zone commercial buildings, a communications infrastructure where buildings are responsible for producing their own performance potential forecasts and bidding them into already existing ancillary service markets could be more practical, as described by the following study.

Three buildings, including an office building, a furniture store, and a bakery, were used in another project by the Pacific Gas and Electric Company (PG&E) called Participating Load Pilots (PLP) (Kiliccote et al., 2009). During this study, the buildings actively bid hourly load curtailment into the CAISO non-spinning reserve ancillary service market two days in advance. These bids were based on 5 minute load forecasts created by Itron/Metrix IDR (Itron, 2013), a company that develops retail consumption forecasts for electricity and gas utilities and customers. A second window to change bids occurred the following morning until 9 am. The day-ahead market closed at 10 am and dispatch results were awarded at 1 pm the day before real-time according to the CAISO economic dispatch schedule. An OpenADR infrastructure (Piette et al., 2009; Ghatikar and Bienert, 2011) was used to communicate the dispatch schedule from the CAISO automatic dispatch system to the building energy management systems. Additionally, metering

was installed to deliver 4-second telemetry information to CAISO system operators in order to verify load shed and maintain stability for the grid. Monetary settlement was made based on the 5 minute load data that indicated the difference between actual load and forecasted load (used as baseline). For the office building, the DR strategy used was global zone temperature setpoint adjustment. A feedback approach was attempted in which the zone temperature was scaled by 1 °F in an attempt to maintain load output. Conclusions from the project found that HVAC and global temperature adjustments meet the requirements for non-spinning reserve ancillary service participation (10 minute response and two-hour duration). However, better forecasting methods are required for the initial ramp dynamics of curtailment as well as highly variable loads.

2.4 Demand Response Implementation

Recently, two final rulings by the Federal Energy Regulatory Commission (FERC) have tried to encourage the adoption of demand side resources in all electricity markets. FERC Order 745 (FERC, 2011a) promoted the fair and non-discriminatory compensation of energy supplied by demand resources by mandating full payment of nodal LMP's for such services. FERC Order 755 (FERC, 2011b) promoted the fair compensation of ancillary services supplied by demand resources by trying to delineate frequency regulation compensation by the quality of service provided. This ruling differentiates between resources with small capacities with high ramp rates, such as storage, demand response, and distributed generation, from resources with high capacities but slower ramp rates, such as many traditional generating plants. This section presents opportunities that currently exist for demand resources to participate in wholesale electricity markets as well as example performance data from a few of these programs.

Table 2.1 summarizes the opportunities for demand response within each U.S. RTO or ISO. Every program listed operates under different market and dispatch rules specific to each regional operator. However, an effort was made to generalize the programs into broader classes of market types to promote a succinct depiction of existing opportunities. The market types are defined as:

- **Forward Capacity** - Resources may bid reduction capacity for energy balance on a timescale of years.
- **Price Responsive / Emergency** - Resources are capable of responding to high price signals or dispatch signals from the system operator during a time of high network stress or capacity deficiency.
- **Energy** - Resources may submit time-sensitive energy reduction bids into day-ahead or real-time energy markets. If cleared, the bids are binding and settlement is subject to the individual market rules.
- **Ancillary Services** - Resources may submit time-sensitive energy reduction bids into ancillary service markets such as those for operating reserves and/or regulation. If cleared, the bids are binding and settlement is subject to the individual market rules.

It can be seen that most of the system operators allow almost full participation in their electricity markets from demand response. In most cases, demand response resource bids have minimum capacity requirements that require the aggregation of individual load resources by curtailment service providers or load

ISO / RTO	Demand Resource Market Type			
	Forward Capacity	Price Responsive / Emergency	Energy	Ancillary Services
NE-ISO[1]	On-Peak, Seasonal Peak, and Real-Time Demand Response Resource	Real-Time Load Response Program	Day-Ahead Demand Response Program	Pilot Project
NYISO[2]	Installed Capacity-Special Case Resource Program	Emergency Demand Response Program	Day Ahead Demand Response Program	Demand Side Ancillary Services Program
PJM[3]	Reliability Pricing Model	Emergency Demand Response	Economic Demand Response	Economic Demand Response
MISO[4]	Load Modifying Resources	Emergency Demand Response	Demand Response Resource Type I & II	Demand Response Resource Type II
CAISO[5]	Resource Adequacy Plan	Reliability Demand Response Product	Proxy Demand Resource System	Proxy Demand Resource System
ERCOT[6]	None	Emergency Response Service & Voluntary Load Response	Day-Ahead Market Bidding	Load Resources

[1] (ISO New England, 2012a, 2013b)

[2] (NYISO, 2013)

[3] (PJM, 2013; McAnany, 2013)

[4] (MISO, 2010)

[5] (California ISO, 2011, 2013)

[6] (ERCOT, 2007)

Table 2.1 – Current demand response programs in U.S. regional electricity networks.

serving entities (e.g. utilities). For energy markets, there is a minimum LMP threshold above which the inclusion of demand response is determined to be economically beneficial for the network. This price is determined by the Net Benefits Test, to be performed by each system operator as outlined in FERC Order 745 (FERC, 2011a). For a detailed description of each program, the reader is referred to the references listed under each RTO or ISO name in Table 2.1. Note that the Southwest Power Pool (SPP) also contains opportunities for demand response in the form of a Dispatchable Demand Response Resource and a Block Demand Response Resource (SPP, 2013). However, specific details regarding how these demand response resources are procured and dispatched were unobtainable and a specific market type could not be defined.

Table 2.2 displays 2012 data from the NYISO Emergency Demand Response Program (EDRP) and Installed Capacity-Special Case Resource Program (ICAP/SCR), which together accounted for 5.8% of the 2012 Summer Capability Period peak demand of 32,439 MW (NYISO, 2013). EDRP pays demand response resources the greater of $500/MWh and the LMP to reduce load in response to ISO dispatch signals that occur from a deficiency in reserve capacity. All registered loads acted through an aggregator or Load Serving Entity (LSE). While they provide an available reduction capacity upon registration, the value is not binding upon dispatch. ICAP/SCR allows demand response resources to sell curtailment into the installed capacity market through Responsible Interface Parties (RIPs). Cleared curtailment capacity is binding for each resource. In the summer of 2012, ICAP/SCR represented 92.2% of the sum of EDRP and ICAP/SCR. Note that while the Day Ahead Demand Response Program (DADRP) and Demand Side Ancillary Service Program (DSASP) were available for participation in 2012, no offers were made in either program for the data analysis period of September 2011 to August 2012.

From the winter of 2006 to the summer of 2010, ISO New England performed the Demand Response

SCR			
Event Time	**Obligated SCR (MW)**	**Average Hourly Response (MW)**	**Response Performance (%)**
May 29, 2012	969.6	359.0	37.0%
June 20, 2012	426.4	312.0	73.2%
June 21, 2012	1361.6	944.0	69.3%
June 22, 2012	412.8	330.6	80.1%
July 17, 2012	59.1	20.6	34.9%
July 18, 2012	380.1	311.5	82.0%
Summer Total	**3609.6**	**2277.7**	**63.1%**

EDRP			
Event Time	**Available EDRP Capacity (MW)**	**Average Hourly Response (MW)**	**Response Performance (%)**
May 29, 2012	63.0	16.8	26.7%
June 20, 2012	63.5	1.1	1.7%
June 21, 2012	141.6	19.5	13.8%
June 22, 2012	71.6	12.7	17.7%
July 17, 2012	9.4	0.0	0.0%
July 18, 2012	71.9	12.9	17.9%
Summer Total	**421.0**	**63.0**	**15.0%**

Table 2.2 – Performance data for NYISO demand response programs in summer 2012 (NYISO, 2013).

Reserve Pilot Program in order to asses the capability of small demand resources to provide 30-minute operating reserves (KEMA, 2010) under varying system conditions. A total of 107 events occurred during the program, each lasted between 30 and 60 minutes, and the times varied from morning to afternoon. The load resources were separated into three categories, including Load Reduction Assets, Generation Assets, and Direct Load Control Assets. Load Reduction Assets participated by reducing their electricity consumption relative to a baseline and included mainly building HVAC and lighting systems. Generation Assets participated by starting behind-the-meter generators. Direct Load Control Assets consisted of groups of residential air-conditioners under direct control. Reduction compared to a baseline, therefore, was only used for the Load Reduction Assets. Each asset enrolled with a contracted amount of reduction capacity. Table 2.3 shows the average performance of Load Reduction Assets calculated by averaging the demand reduction (MW) over each event for each time period as well as for each resource. The Load Reduction Assets provided approximately half of their contract overall. Note that individual event performances averaged over all of the resources ranged from 30% to 70% with outliers at 20% and 130%. Load Reduction Asset performance was deemed less reliable than diesel and gas turbine generators performance the same service.

The PJM Interconnect has some of the most active demand response programs in the country. In the year 2012, over 8,800 MW of demand response were active in the PJM system, with 2,250 MW (25%) participating in economic demand response programs, which include participation in energy and ancillary service markets, and 6,577 MW (75%) participating in emergency demand response, which are only dispatched during network capacity deficiencies (McAnany, 2013). Of the emergency demand response capacity, 22% comes from HVAC load, 22.5% coming from manufacturing, 22.6% coming from backup

Load Reduction Asset			
Event Time	**Contracted Amount (MW)**	**Average Event Response (MW)**	**Response Performance (%)**
Winter 06/07	8.9	4.9	55.1%
Summer 07	14.7	8.4	57.1%
Winter 07/08	8.2	3.9	47.6%
Summer 08	13.6	6.8	50.0%
Winter 08/09	0.0	0.0	0.0%
Summer 09	24.5	13.5	55.1%
Winter 09/10	16.0	9.0	56.3%
Program Total	**85.9**	**46.5**	**54.1%**

Table 2.3 – Performance data summary for ISO New England spinning reserve pilot program from 2006 to 2010 (KEMA, 2010).

generation mainly diesel generators. Industrial and manufacturing facilities account for 46% of the emergency demand response capacity, while only 6% come from office buildings and 14% from residential buildings. Detailed statistics could not be found on the economic demand response sources, however, performance statistics are displayed in Table 2.4. This data summarizes the performance of economic demand response for each month of 2012 as well as the participation of demand in two types of ancillary services, synchronous (spinning) reserves and regulation. The portion of reserves served by demand response for a particular load zone is also given.

Day-Ahead Economic Demand Response			
Event Time	**Cleared (MWh)**	**Settled (MWh)**	**Response Performance (%)**
January	15.0	4.0	26.7%
February	0.0	0.0	0.0%
March	0.0	0.0	0.0%
April	4338.0	4839.0	111.5%
May	6220.0	6981.0	112.2%
June	11345.0	12100.0	106.7%
July	21581.0	22752.0	105.4%
August	6786.0	5906.0	87.0%
September	4419.0	4658.0	105.4%
October	1042.0	1169.0	112.2%
November	9185.0	306.0	3.3%
December	1154.0	1199.0	103.9%
Yearly Totals	**66085.0**	**59914.0**	**90.7%**

Real-Time Economic Demand Response			
Event Time	**Notified (MWh)**	**Settled (MWh)**	**Response Performance (%)**
January	66.0	34.0	51.5%
February	63.0	31.0	49.2%
March	0.0	0.0	0.0%
April	520.0	514.0	98.8%
May	2164.0	1735.0	80.2%
June	14208.0	11516.0	81.1%
July	26654.0	20779.0	78.0%
August	20337.0	20242.0	99.5%
September	9051.0	9292.0	102.7%
October	10661.0	11569.0	108.5%
November	5653.0	6016.0	106.4%
December	2390.0	2644.0	110.6%
Yearly Totals	**91767.0**	**84372.0**	**91.9%**

Ancillary Service Demand Response			
Event Time	**Synchronous Reserves (MW)**	**Average Synchronous Reserves Penetration in Mid-Atlantic Reserve Zone (% Total Reserves)**	**Regulation (MW)**
January	385.0	8.0%	0.2
February	408.0	7.5%	0.2
March	478.0	10.0%	0.5
April	393.0	7.6%	0.5
May	402.0	4.9%	0.5
June	386.0	9.9%	3.7
July	404.0	5.7%	3.7
August	409.0	5.0%	4.5
September	413.0	5.6%	4.5
October	414.0	1.8%	4.5
November	415.0	6.4%	4.5
December	419.0	3.0%	4.8
Monthly Average	**410.5**	**6.3%**	**2.7**

Table 2.4 – Performance data summary for PJM demand response programs in 2012 (McAnany, 2013).

2.5 Conclusion

A two-day workshop, organized in October 2011 in Washington D.C., brought together many of the leading minds in ancillary service demand response research and some of the most influential people in its industry adoption (Kirby et al., 2011). Representatives were present from both the system operator perspective in addition to the demand-side perspective. The findings of the workshop agree well with the general conclusions from this research review. In summary, these findings were:

- Load participation in ancillary services can increase system flexibility to help manage higher penetrations of sustainable variable energy resources.
- While demonstration projects have shown the capabilities of residential and small commercial customers to provide ancillary services, they do not typically participate in today's markets.
- While HVAC loads match well with the requirements of ancillary service provision, particularly spinning reserves, temporal and service constraints limit the amount of service HVAC systems can provide at any one time.
- Physical and operational limitations of HVAC systems in providing ancillary services must be better understood.
- Reliability of demand response for ancillary services is difficult for system operators; as is the forecasting of performance in terms of ramp rate (MW/min) and magnitude (MW).
- There is a need for better commercial HVAC system control systems, in association with decision support tools, to bid reliable services.

The results of the literature review suggest a need to better understand the dynamics associated with multi-zone commercial HVAC system demand response strategies, which are on the same time-scale as ancillary service operations (sub-hourly). A review of daily market operations revealed the extensive planning undertaken by system operators to ensure network stability and high-quality electricity delivery. Financial penalties ensure the reliability of generators to perform the dispatched service. For demand response to be economically viable in the long run for commercial building owners and system operators alike, reliability must be a priority. A review of demand response research indicates the lack of study of specific HVAC-provided ancillary service strategy dynamics for common multi-zone systems, such as VAV systems. This includes both the thermo-fluid and cascading control loop responses from thermostat to central plant, which ultimately drive both the change in electrical consumption as well as occupant services. Much of the baseline and curtailment load predictions use outdoor air temperature and time as independent variables, without considering the physical and engineering processes that underlie performance variability. These dynamics are important for understanding and ultimately forecasting the ancillary service potential for HVAC systems utilizing various curtailment strategies and operating under differing load conditions. Additionally, there is a lack of simulations aimed at better understanding these dynamics. Simulations can be valuable tools in the subject of building controls engineering, especially in the case of demand response, because there are no occupants to service and virtually any operating condition can be tested. Lastly, a review of the performance of some demand response programs implemented or piloted around the U.S. reveals the performance variability in some of today's demand

response markets as well as a hesitation for some load to participate in ancillary service markets. Overall, these topics motivate the need for the research presented in the the next three chapters of this thesis, which aim to improve the understanding of VAV HVAC demand response operation and serve as a basis for future forecasting of demand response potential in ancillary service markets.

Chapter 3

Test Building Analysis

A test building was equipped with monitoring devices to measure both electrical and HVAC system performance at high-resolution timescales. The data collected is used to gain insights into the operation of a VAV system on a normal basis as well as during an example demand response event. The goal of this chapter is to identify real-world operational qualities of multi-zone buildings with VAV systems which need to be considered for ancillary service provision. Section 1 will describe the test building architectural design, engineering systems, and data recording systems. Section 2 will use data collected during normal summertime operation to identify everyday operational and control characteristics that affect a building's ability to provide ancillary services. Section 3 will describe the setup and results of a simple demand response test, during which the duct supply static pressure setpoints for two air-handling units (AHU) were lowered for 30 minutes three times during a day. Data from these tests will be used to identify event-specific operational and control characteristics that affect ancillary service provision.

3.1 Building Overview

3.1.1 Architecture Design and Construction

The test building is used jointly between the Fraunhofer Center for Manufacturing Innovation (CMI) and the Boston University Department of Manufacturing Engineering. It is located on the Boston University Campus in Brookline, MA and is designed to serve as a leading R&D center for applied research in the U.S. (Fraunhofer USA, Inc, 2011). The exterior of the building was erected in 1992 to be used as a parking garage and a renovation in 1995 added the research facilities and offices that exist today.

The test building is approximately 4,069 m^2 total (3,251 m^2 usable) over two stories, with research laboratories and a few offices on the basement floor, and offices and conference rooms on the first floor. A carport is located on the basement floor in the west wing of the building and is unconditioned. The floor-to-floor height is 4.84 m for the basement floor and 3.1 m for the first floor. An average 1.78 m truss depth gives a plenum of the same average depth between the roof and first floor ceiling. Where large manufacturing machinery is located on the basement floor, the space extends two stories high. The building is attached on the north side to neighboring buildings whose entrances are oriented north on

Commonwealth Avenue. The entrance to the test building is on the first floor and is facing east onto St. Marys Street. The south facade and relatively insignificant western facade face directly onto the Massachusetts Turnpike.

The exterior walls are approximately 0.191 m (7.5 in) thick masonry connected via a 0.0254 m (1 in) expansion joint to a 0.0921 m (3-5/8 in) metal stud wall with 0.0889 m (3-1/2 in) fibrous insulation and 0.0159 (5/8 in) gypsum wallboard on the interior. Office partitions are 0.092 m (3-5/8 in) metal stud with 0.0159 (5/8 in) gypsum wallboard while research lab partitions and those around stairwell and elevator shafts are 0.203 m (8 in) concrete blocks with 0.0159 (5/8 in) gypsum wallboard attached by 0.0222 m (7/8 in) furring channels 0.406 m (16 in) oc. Corridor partitions with offices are 0.0921 m (3-5/8 in) metal stud with 0.0921 m (3-5/8 in) gypsum wallboard and a second layer of 0.0127 m (1/2 in) gypsum wallboard on the corridor side. The first floor corridor partition with the two-story section of the basement is 0.00635 m (1/4 in) laminated glass with an aluminum frame. The basement floor is a 0.152 m (6 in) slab-on-grade while the first level floor is primarily supported by a concrete t-beam system with floor thickness of 0.127 m (5 in). The building contains a shallowly sloped roof that is composed of a roofing membrane on top of polyisocyanurate insulation supported by a concrete substrate.

3.1.2 Mechanical Systems

The HVAC system, diagrammed in Figure 3.1, is composed of two VAV systems served by a central plant and is controlled by a Schneider Electric Andover Continuum control system (Schneider Electric, 2013b). AHU1 serves the ground floor lab and office areas with a design capacity of 11.5 m^3/s (24,400 cfm) and 4.365 m^3/s (9,250 cfm) of outdoor air. AHU2 serves the first level office areas with a capacity of 11.3 m^3/s (24,000 cfm) and 1.89 m^3/s (4,000 cfm) of outdoor air. AHU1 is located on a mezzanine above the first floor level and AHU2 is located on the basement floor. Each air handler is equipped with a pre-filter, preheat coil, cooling coil, final filter, humidifier, and supply fan. Each supply fan has a 0.768 m (30-1/4 in) wheel diameter and blows cooling supply air at 12.8 °C (55 °F) to terminal unit boxes at each zone. Each supply fan is served by a 29.8 kW (40 HP) motor with 480 V/3 phase/60 Hz electrical service and a variable frequency drive (VFD). Each AHU system also contains an in-line centrifugal return fan with a wheel diameter of 1.02 m (40-1/4 in) that moves air from a return plenum on each floor back to its respective AHU. Both return fans are served by a 11.2 kW (15 HP) motor with 480/3/60 electrical service and a VFD. In addition, a total of seven smaller roof exhaust or propeller fans exhaust air from toilet rooms, two electrical rooms, two mechanical rooms, and a fume hood. All of these fans contain motors of 0.186 or 0.248 kW (1/4 or 1/3 HP) and are served by 120/1/60 electrical service with no VFDs.

A total of 51 pressure-independent terminal unit (TU) boxes with hot water reheat deliver the appropriate amount and temperature of air to condition each zone. All perimeter zones on the south side of the building along with a few perimeter zones on the north side of the building also contain one of two types of fin-tube radiation. With few exceptions, the fin-tubes are located under the windows. Two cabinet unit heaters are located on the ground floor of two stairwells on the north side of the building and two unit headers are located in the loading area on the north side of the ground floor. Additionally, one cabinet unit heater is located above the main entrance vestibule on the first floor level.

Chilled water (CHW) is produced by a 615 kW (175 ton) air-cooled chiller. The chiller contains two refrigerant circuits with screw-type compressors, one rated at 281 kW (80 ton) and the other at 334 kW (95 ton). The rated load amperage (RLA) at 460 Volts of each compressor are 136 A and 155 A

respectively, corresponding to a total power draw of approximately 185 kW and a nominal COP of 3.3 if a power factor of 0.8 is assumed. The condenser is made up of a fin and tube heat exchanger and (14) 0.711 m (28 in) diameter fans, each with a 1.12 kW (1.5 HP) motor. The evaporator uses a shell and tube type heat exchanger and is designed to cool 0.0235 m^3/s (373 gpm) of water from 11.1 °C (52 °F) to 5.56 °C (42 °F) for service to the AHU cooling coils. The chiller is loaded at one of eight operating capacities from 0% to 100% by independently staging the two compressors at 0%, 50%, 75%, or 100% in a lead-lag arrangement. This staging is clearly seen in the presentation of recorded chiller power consumption data in the next section. Two CHW distribution pumps sized for 0.0240 m^3/s (380 gpm) at 20.9 kPa (70 ftwg) distribute chilled water from the chiller to the AHU cooling coils with 7.46 kW (10 HP) motors. The pumps operate with n+1 redundancy and no VFDs. The chiller is located on the roof of the western wing of the building and the chilled water distribution pumps are located in the ground level mechanical room on the north side of the building.

Hot water (HW) at 93.3 °C (200 °C) is produced through a heat exchanger with low pressure 50.3 kPa (7.3 psi) district steam. A summer time gas fired boiler also produces 63 kW (215,000 btuh) with a net efficiency of 0.70. A boiler circulation pump sized for 0.00126 m^3/s (20 gpm) at 35.8 kPa (12 ftwg) circulates hot water through the boiler when needed with a 0.248 kW (1/3 HP) motor. Two HW distribution pumps sized for 0.0158 m^3/s (250 gpm) at 179 kPa (60 ftwg) distribute hot water produced by the steam heat exchanger and/or boiler to the AHU pre-heat coils, terminal unit re-heat coils, fin-tube radiation, and unit heaters with 5.59 kW (7-1/2 HP) motors. The pumps operate with n+1 redundancy and no VFDs. The steam heat exchanger, boiler, boiler circulation pump, and the hot water distribution pumps are located in the mezzanine mechanical room above the first floor level on the north side of the building.

Equipment cooling water (ECW) is created by a closed circuit cooler (CCC) that is designed to cool 0.00568 m^3/s (90 gpm) of water from 35 °C (95 °F) to 29.4 °C (85 °F) at 24.4 $°C_{WB}$ (76 $°F_{WB}$). The spray basin is filled with domestic cold water and contains a 2 kW pan heater, assumed to keep the spray water from freezing. The closed circuit cooler fan is served by a 7.46 kW (10 HP) motor while the spray pump contains a 0.373 kW (1/2 HP) motor. Two ECW distribution pumps sized for 0.00568 m^3/s (90 gpm) at 164 kPa (55 ftwg) distribute cooled water from the closed circuit cooler to the laboratories or other equipment cooling water outlets with 2.24 kW (3 HP) motors. The pumps operate with n+1 redundancy and no VFDs. The closed circuit cooler and the equipment cooling water distribution pumps are located in the mezzanine mechanical room above the first floor level on the north side of the building.

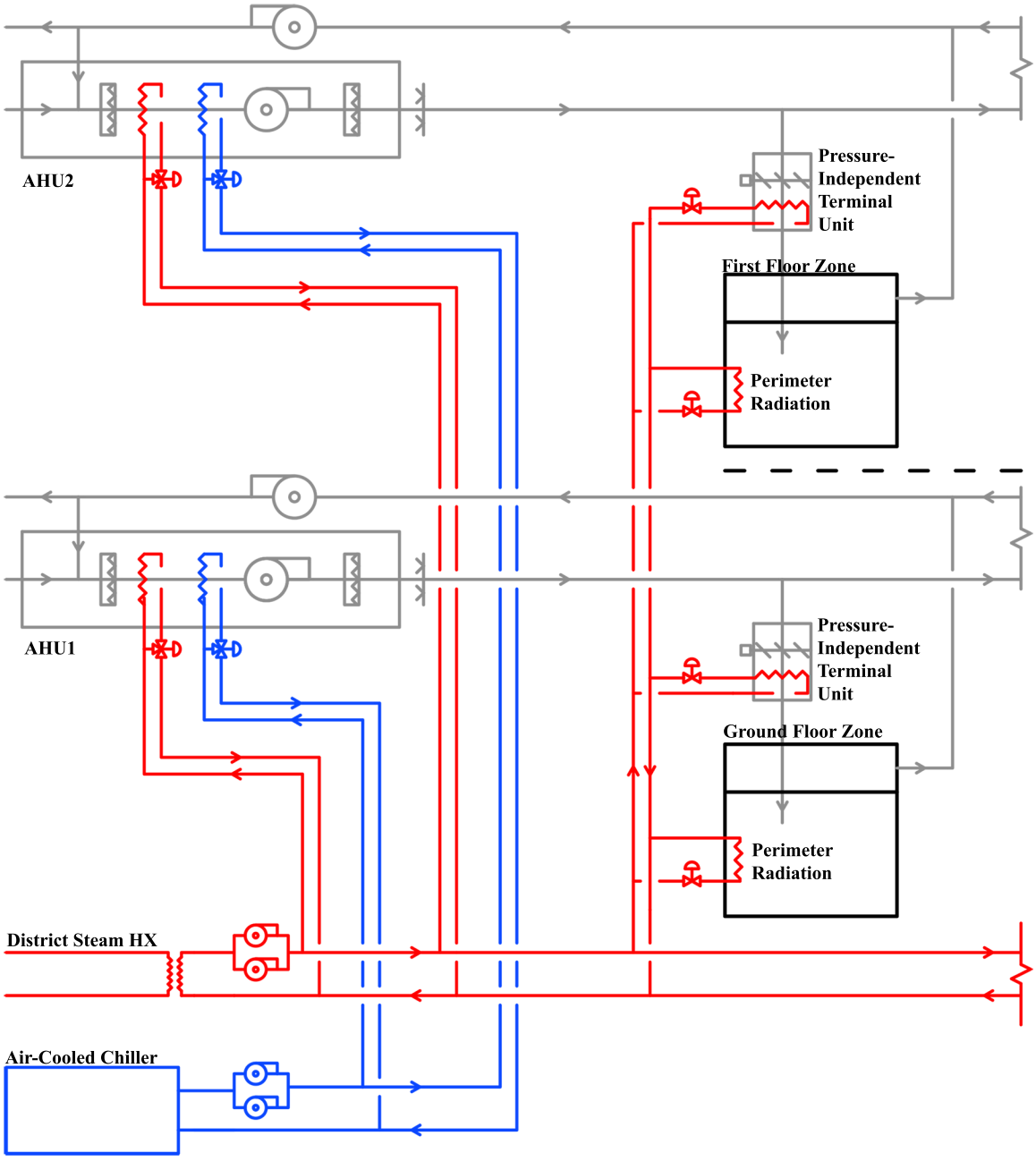

Figure 3.1 – Diagram of test building HVAC system.

3.1.3 Electrical Systems

A 1500 kVA transformer connects 13.8 kV utility service to the building's main 480/277 V, 2400 A switchboard. The main switchboard distributes power to seven main distribution panels through transformers as required:

1. ACC-1 (Air-cooled chiller, 450 A)
2. MPNH1 (HVAC 1, 225 A)
3. 480/277 Bus (400 A)
4. 208/120 Bus (600 A)
5. GLNH1 (Outdoor lighting and future, 150 A)
6. GPNH2 (HVAC 2, 225 A)
7. 1PNL1 (Main lighting and plug, 600 A).

Table 3.1 below displays the breakout of the two main HVAC panels, MPNH1 and GPNH2. Note that seven exhaust fans, serving mechanical rooms, electrical rooms, toilets, and a fume hood, are located on sub-panels served by 1PNL1.

Panel MPNH1 in Mezzanine Mech Room			
Equipment	**Description**	**Electrical Service**	**Motor HP**
SF-1	AHU1 Supply Fan (VFD)	480/3ϕ, 3 Wire Delta	40
RF-1	AHU1 Return Fan (VFD)	480/3ϕ, 3 Wire Delta	15
RF-2	AHU2 Return Fan (VFD)	480/3ϕ, 3 Wire Delta	15
P-1	HW Distr. Pump (Primary)	480/3ϕ, 3 Wire Delta	7.5
P-2	HW Distr. Pump (Secondary)	480/3ϕ, 3 Wire Delta	7.5
P-5	ECW Distr. Pump (Primary)	480/3ϕ, 3 Wire Delta	3
P-6	ECW Distr. Pump (Secondary)	480/3ϕ, 3 Wire Delta	3
F-1	ECW CCC Fan	480/3ϕ, 3 Wire Delta	10
FSP-1	ECW CCC Spray Pump	480/3ϕ, 3 Wire Delta	1.5
CP-1	Condensate Return Unit	480/3ϕ, 3 Wire Delta	2

Panel GPNH2 in Ground Floor Mech Room			
Equipment	**Description**	**Electrical Service**	**Motor HP**
SF-2	AHU2 Supply Fan (VFD)	480/3ϕ, 3 Wire Delta	40
P-3	CHW Distr. Pump (Primary)	480/3ϕ, 3 Wire Delta	10
P-4	CHW Distr. Pump (Secondary)	480/3ϕ, 3 Wire Delta	10
AP-1	Air Compressor	480/3ϕ, 3 Wire Delta	15
OD-1	Overhead Door	480/3ϕ, 3 Wire Delta	1

Table 3.1 – Equipment breakout for two HVAC electrical panels in the test building.

3.1.4 Recording Systems

Building electricity data is collected using one Veris Industries H8238 Multi-Circuit Monitor (Veris Industries, 2013b), one Veris Industries H8822 Data Acquisition System (Veris Industries, 2013c), and 21 Veris Industries Current Transducers (CT) (Veris Industries, 2013a), as diagrammed in Figure 3.2 below. Seven sets of CTs were installed on the A, B, and C phase feeders of the main panel and six of the distribution panels. The output signals from the CTs are terminated in panel-specific terminal blocks, which are connected to the H8238 Multi-Circuit Monitor. The H8822 Data Acquisition (DAQ) system collects and time stamps the data from the multi-circuit monitor. The data is then downloaded from the DAQ to a Boston University network hard drive via an ethernet connection. The DAQ is set to collect and time stamp data continuously at one-minute intervals while the data is downloaded to the Boston University network drive every one hour. All of the power data presented in this thesis for the test building was measured at one-minute intervals using this system.

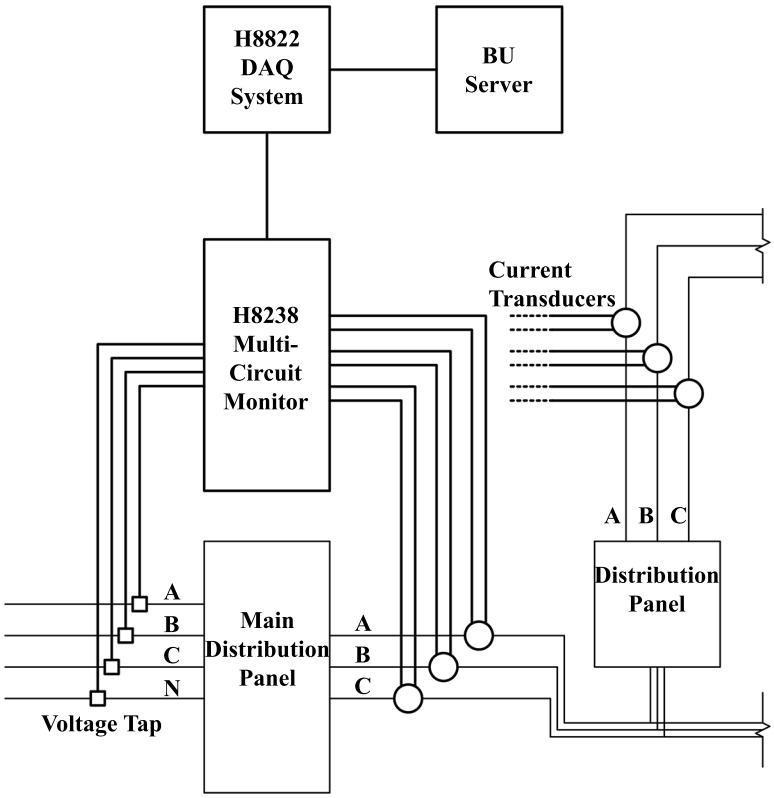

Figure 3.2 – Diagram of electrical panel recording system for test building.

Building HVAC system data is collected using a software product called Automatic Extended Log Archiver for Andover Continuum (Schneider Electric, 2013a). The software system is installed on a Boston University central server where points can be logged from multiple buildings around campus, one of which being the test building. The resolution of the collected data depended on the number of points recorded and the length of their recording. This was due to limitations set upon the amount of data that could be transferred to the central server at one time without disturbing its operation.

3.2 Considerations from Summertime Operation

3.2.1 Relative Magnitude of End-use Power Consumption

The first major consideration for the ability to provide ancillary services must be given to the relative magnitude of controllable loads to whole-building power consumption. In the case of demand response, these controllable loads primarily comprise of lighting and HVAC, though could also include non-essential plug loads or other equipment loads. Comparing the power demand of each load type tells building owners which could provide the most service. In addition, if sub-metering is possible, specific equipment could be targeted for use. While EIA (2012) reports HVAC electricity consumption accounted for an average of 27% of commercial whole-building power consumption in 2011, the true number for any particular building will vary based on system type, loading, and operation scheme. Figure 3.3 below presents the measured power demand of all of the electrical panels of the test building for a one-week period in July, 2012. The first two days on the figure are a Saturday and Sunday. Using a total usable floor space of 3,261 m^2, the max building power of 284 kW amounts to 87 W/m^2, the max HVAC power of 230 kW amounts to 71 W/m^2, and the max plug load of 30 kW amounts to 9 W/m^2. Notice that the chiller is responsible for approximately half of building power demand during occupied hours. Additionally, panels MPNH1, GPNH2, and 1PNL1 account for power consumption of similar order. Overall, it can be seen that on the most demanding day, July 17th, HVAC power accounts for approximately 80% of building power demand. While this value diminishes over the other days of the week, it is clear that HVAC power is the primary consumer of electricity in the test building, particularly the chiller. Therefore, providing ancillary services with HVAC loads over any other is a clear choice, with the target piece of equipment being the chiller.

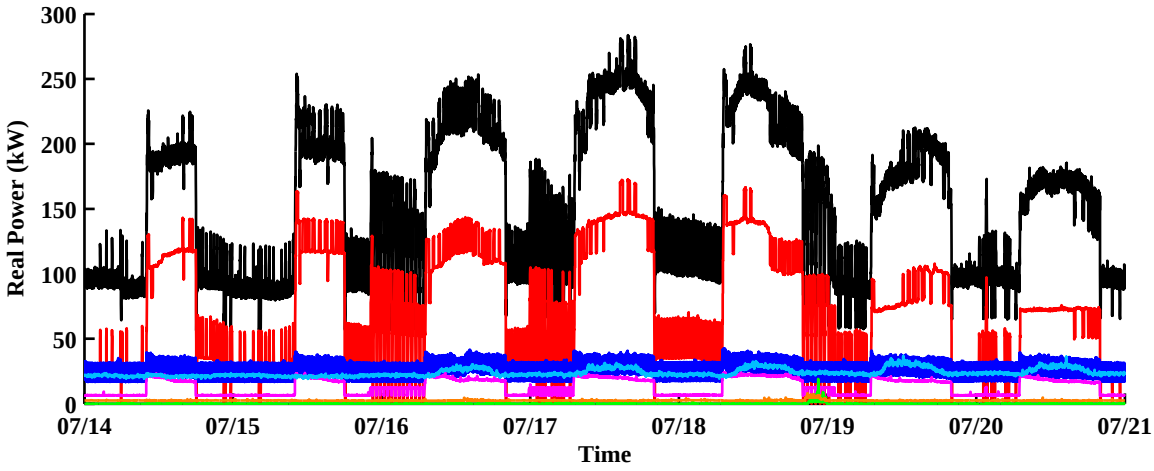

Figure 3.3 – Plot of Main (black), ACC-1 (red), MPNH1 (pink), 480/277 Bus (green), 208/120 Bus (orange), GPNH2 (dark blue), and 1PNL1 (light blue) electrical panels' real power demand for one week in July, 2012 for the test building. Data measured at a one-minute resolution.

3.2.2 Environmental Dependencies

One of the most implicit challenges of utilizing commercial buildings for ancillary service provision is their power consumption dependence on environmental factors, driven primarily by HVAC systems. This is most clearly seen by Figure 3.4, where outdoor air temperature and solar irradiation is plotted along with chiller, MPNH1, and GPNH2 power consumption and AHU supply air volumetric flowrates for a one-week period in July, 2012. The environmental data was collected with five-minute resolution from a weather station located in Cambridge, MA (Weather Underground, Inc, 2013), approximately two miles from the test building site. A relationship between outdoor air temperature and air-cooled chiller power consumption can clearly be seen both as a general trend throughout the week as well as throughout each day. While it is expected that air flowrate fan power may follow a similar suit, these values are dependent on the total space cooling load, which is not only a function of environment, but also occupancy, equipment operation, and building construction. As the test building is only exposed to the environment through two exterior walls and the roof, it is not surprising that space cooling load does not follow environmental conditions as closely as the air-cooled chiller for each hour during the day, though a general relationship is seen throughout the week. However, because the chiller accounts for the majority of HVAC power consumption, and in this test building case whole-building power consumption, the total building power consumption appears to follow outdoor air temperature. Note that outdoor air temperature-based regression models are common in predicting baseline building power, such as in Mathieu et al. (2011). While a model of a similar sort will not be developed in this thesis, it is important to consider why HVAC power can depend on the environment, and why it may not always be the case.

Both the COP and capacity of a chiller are strongly dependent on whats happening at the evaporator and condenser (Gayeski, 2010). An increase in the condensing temperature at the same condenser fluid mass flowrate requires the refrigerant to be compressed to a higher temperature and pressure for the same heat rejection, requiring more compressor work. In the case of an air-cooled chiller, this is directly related to outdoor air temperature. An increase in the evaporator inlet chilled water temperature at the same chilled water mass flowrate requires more heat to be rejected by the condenser, also increasing the compressor power. In the case of cooling supply air in a VAV system, a change in evaporator chilled water inlet temperature is directly related to the supply air mass flowrate through the cooling coil, which in turn is related to the amount of cooling load in the building and, subsequently, to the environmental conditions. Supply and return fan power consumption is also a function of air mass flowrate, as a higher flowrate requires more energy to be imparted to the air by the fan. These dependencies are important to consider when deciding on curtailment strategies and predicting performance during ancillary service provision. HVAC power consumption will vary heavily with outdoor air temperature if a chiller is air-cooled due to condensing temperatures and if the building is externally-load dominant due to inlet chilled water evaporator temperatures and required fan power. Alternatively, if a building is internally-load dominated or the chiller utilizes a cooling tower, the HVAC power consumption will be a stronger function of the occupant, plug, and equipment loads or outdoor air wet-bulb temperature respectively.

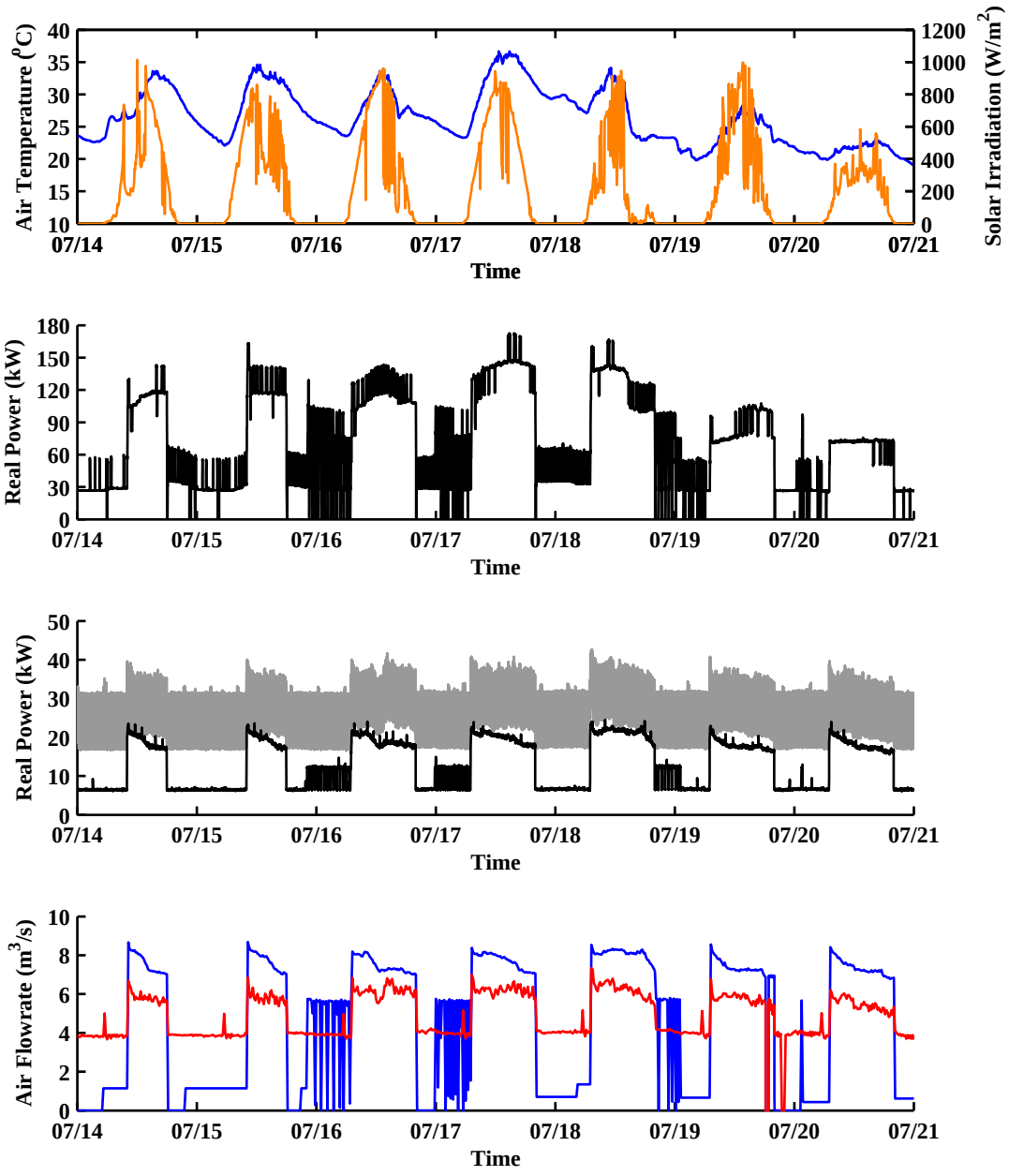

Figure 3.4 – Plots of outdoor air temperature (top, blue), solar irradiation (top, orange), ACC-1 (upper middle), MPNH1 (lower middle, black), GPNH2 (lower middle, gray), AHU1 supply air flowrate (lower, blue), and AHU2 supply air flowrate (lower, red) for one week in July, 2012 for the test building. Environmental data measured at a five-minute resolution, real power data measured at a one-minute resolution, and air flowrate data measured at a 15-minute resolution.

3.2.3 Discrete Operations

Consideration must also be given to the presence of electrical equipment with discrete operation. This operation may come in two forms, as represented in Figure 3.5 below, which presents chiller power and GPNH2 power for July 17th. The first form of discrete operation is staging and is represented by the chiller power consumption profile. As mentioned in the previous section, the chiller is staged through eight available capacities by a lead-lag arrangement on two compressors that operate at discrete part-load ratios; 0%, 50%, 75%, and 100%. This can present itself as a significant advantage or challenge to the provision of ancillary services. It presents an advantage if perfect knowledge of the required capacity is known for the duration of the service provision. In this case, ancillary services can be provided in known and discrete magnitudes by changing the operating stage of the chiller. However, if there is imperfect knowledge of the required capacity a slight miscalculation can result in a variation in actual performance from expected performance equal to the power differences between stages. A remedy for this could be the controlled prevention of staging during service provision, however, this is likely to have significant effects on mechanical durability if staging would otherwise be required.

The second form of discrete operation is on-off cycling of equipment, represented by the GPNH2 panel power consumption profile. The frequent oscillations displayed can be traced to the 15 Hp (11.2 kW) air compressor served by the panel cycling on and off once every 1-3 minutes. The exact cause of this cycling is unknown, though is likely due to the maintainability of air pressure in a storage tank that is subject to demand. In general, if the frequency of cycling is orders of magnitude faster than the time period of service provision, or if the magnitude of cycling is orders of magnitude smaller than the amount of service provided, than the oscillatory nature of the equipment could be considered just as noise that is present normally. If this this not the case, consideration must be given to shutting the equipment down during service provision, or taking its operation into consideration when providing a service bid.

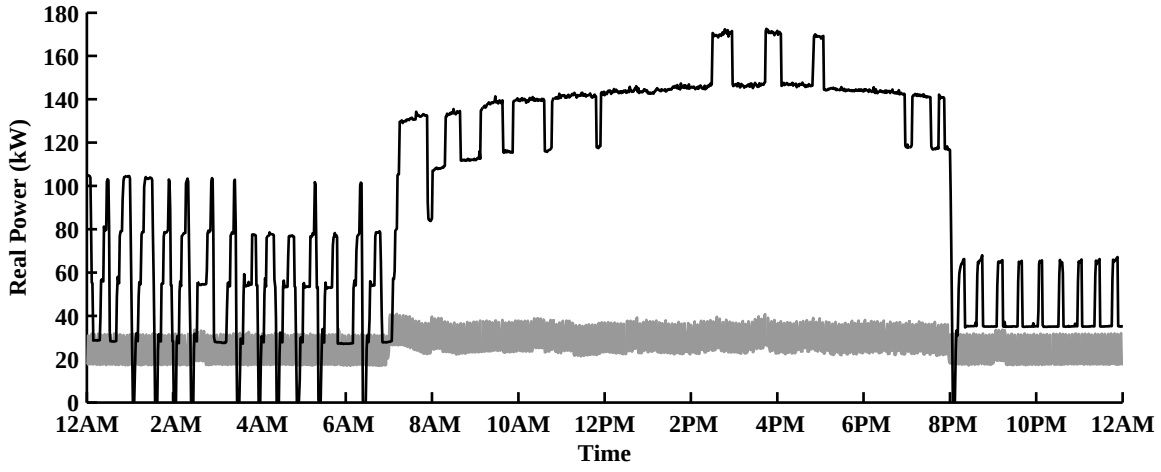

Figure 3.5 – Plot of ACC-1 (black) and GPNH2 (gray) real power for July 17th, 2012. Data measured at a one-minute resolution.

3.2.4 Operational Faults

Faults in HVAC systems are common sources of building energy inefficiency (Li, 2009; Samouhos, 2010). These can include mechanical faults, such as stuck valves or dampers, clogged coils or filters, and deteriorating equipment, or they can include control faults, such as improper controller tuning, simultaneous heating and cooling, or schedule deviations. If the fault occurs suddenly, the performance of ancillary service provision can be significantly different than the bid performance, specifically in the case of stuck actuators. If the fault is developed over a period of time, such as equipment degradation, it becomes necessary to update performance models with the most recent data available for the bidding of ancillary services.

3.3 Considerations from a Duct Static Pressure Adjustment Test

3.3.1 Test Setup

A simple test was performed on the test building in order to gain insight into the short term transient response of a real VAV system to a demand response strategy implementation. The strategy implemented was a duct static pressure setpoint reset in both AHUs, which was a popular strategy in Motegi et al. (2007) and was the easiest to implement in the test building BAS system. The test was implemented on Saturday, November 17th. Though this time represents a period of limited loading on the system, due to the reduced occupancy, cooler outdoor air temperatures, and weaker solar irradiation, valuable observations could still be made about the response of the air system. This system ultimately drives the thermo-fluid and electrical response of the HVAC system, as will be described in more detail in Chapter 4. The observations to be made during the test included how quickly pressure-independent terminal unit boxes respond to step changes in duct static pressure, how quickly supply fan speed changes in response to step changes in duct static pressure, the effect system load variations have on air system component responses, and how these responses ultimately effect electricity consumption.

The test consisted of lowering the static pressure of both AHUs for 30 minutes at three times during the test day; 10:30 AM, 1:30 PM, and 4:30 PM. The duration of each test was chosen to simulate the delivery of reserve services as described in Chapter 2. The generally accepted spinning reserve time period of 10 minutes was not chosen in order to allow study of responses at both 10 minutes and 30 minutes after strategy initiation. The times of implementation through the test day were chosen to study different loading conditions on the building, allow enough time between setpoint adjustments for recovery to normal operation, and fit within the scheduled system occupancy period of 10:00 AM to 6:00 PM on weekends. For each test, the AHU1 duct static pressure was lowered from 248.8 Pa (1 inwg) to 161.7 Pa (0.65 inwg) and the AHU2 duct static pressure setpoint was lowered from 373.2 Pa (1.5 inwg) to 248.8 Pa (1 inwg). Electrical data was recorded every one-minute and HVAC performance data was recorded every two minutes, as described in a previous section.

3.3.2 Results

Measurements from the tests are presented in Figures 3.6 to 3.8 on the following pages, while data from the test day is summarized in Tables 3.2, Table 3.3, and Figure 3.9. Figure 3.6 displays plots of outdoor air temperature and total building power for the day of the test. Figure 3.7 displays plots of AHU performance data as well as HVAC panel power consumption. Unfortunately in the case of AHU data recording, there were unknown technical difficulties with the HVAC data recorder that caused some loss of data from approximately 2:00 PM to 3:30 PM and from approximately 5:30 PM to the end of the test day. Figure 3.8 displays terminal unit data including damper position, air flowrate, and zone temperature. The data in this figure comes from five terminal units. TU102 and TU108 are on the system of AHU1 and located at approximately 1/3 and 2/3 down the main duct trunk respectively. TU125, TU135, and TU139 are on the system of AHU2 located at approximately 1/2 down the east duct branch, the start of the east duct branch, and 1/3 down the west duct branch. Table 3.2 summarizes fan speed and supply air flowrate for AHU1 and AHU2 and Table 3.3 summarizes power consumption for the main HVAC distribution panels, MPNH1 and GPNH2.

Overall, the tests were successful in implementing the static pressure adjustment. It is evident from the data that transient timescales of damper and fan speed modulation in response to adjustments in the duct static pressure setpoints occurred within the two-minute resolution of data recording. This is important to consider in the case of predicting and bidding reserve supply, as it would be possible for the air system to reach a steady-state well before the required reduction times of 10 or 30 minutes.

Additionally, whole-building power measurements plotted in Figure 3.6 show how discrete staging of the chiller makes it difficult to characterize the overall effectiveness of the curtailment strategy, as described in a previous section. It is likely that the chiller would have continued its periodic staging, whose magnitude and frequency are on the order of those of the curtailment event, through the 10:30 AM test had it not been for a reduction in AHU airflow as a result of the static pressure reductions. The apparent magnitude and duration of one of the chiller stage increments is approximately six minutes and 25 kW respectively and would have to be considered in service settlement. However, the analysis that follows will focus on the two HVAC electrical panels, and not on whole-building or chiller power, as they provide more insight into the effectiveness of the curtailment event with respect to air system operation.

As noted in Callaway and Hiskens (2011), the provision of ancillary services is related more to instantaneous load adjustments than it is to hourly deviations from a whole-day baseline model. This is especially true for service periods on the order of 10 to 30 minutes, during which time significant changes in HVAC load are unlikely to occur. Exceptions for this could be made for the transient periods of morning start-up and night shutdown. Therefore, changes in electrical and HVAC performance parameters in this analysis are determined by comparing the time-averaged value of the parameter for 30 minutes before the curtailment event to the time-averaged value for the 30 minutes during the event. Note in Tables 3.2 and 3.3, reduction magnitude and normalized reduction are defined as in Equations 3.1 and 3.2 so that curtailments with different reference magnitudes may be compared.

Lastly, the performance of TU139 in Figure 3.8 shows oscillatory damper behavior. This demonstrates how operational faults, in this case controller tuning, could interfere with ancillary service provision as indicated in the previous section. Too many terminal units operating in this way could make performance during any kind of service event erratic as the dampers adjust not only to new system conditions brought upon by the curtailment strategy, but also by each individually.

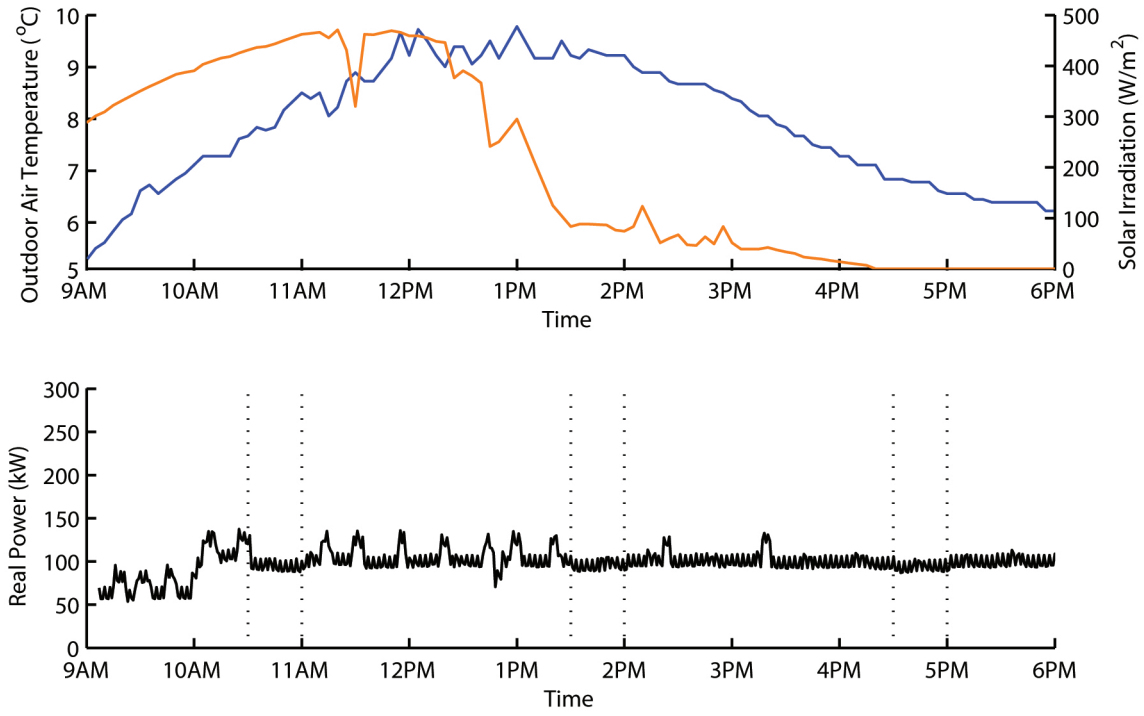

Figure 3.6 – Plot of outdoor air temperature (top, blue), solar irradiation (top, orange), and main electrical panel real power (bottom) for the duct static pressure adjustment test day, November 17th, 2012. Dotted lines indicate the beginning and end of the three test periods. Environmental data was measured at a five-minute resolution and real power data was measured at a one-minute resolution.

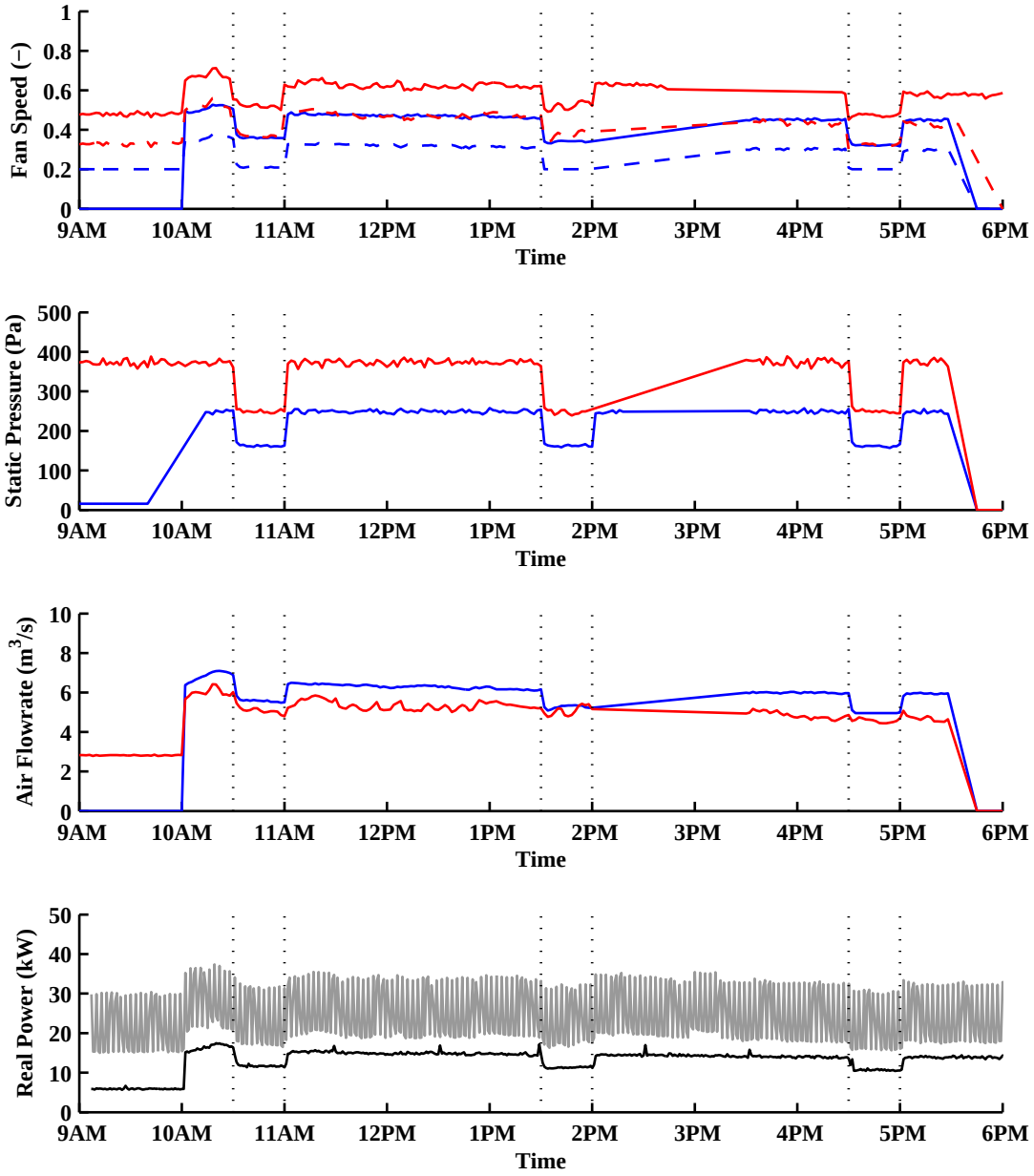

Figure 3.7 – Plots of AHU1 supply (top, solid red) and return (top, dashed red) fan speed , AHU1 duct static pressure (upper middle, red), AHU2 duct static pressure (upper middle, blue), AHU1 supply air flowrate (lower middle, blue), AHU2 supply air flowrate (lower middle, red), MPNH1 real power (bottom, black), and GPNH2 real power (bottom, gray) for the duct static pressure adjustment test day, November 17th, 2012. Dotted lines indicate the beginning and end of the three test periods. HVAC performance data was measured at a two-minute resolution and real power data was measured at a one-minute resolution.

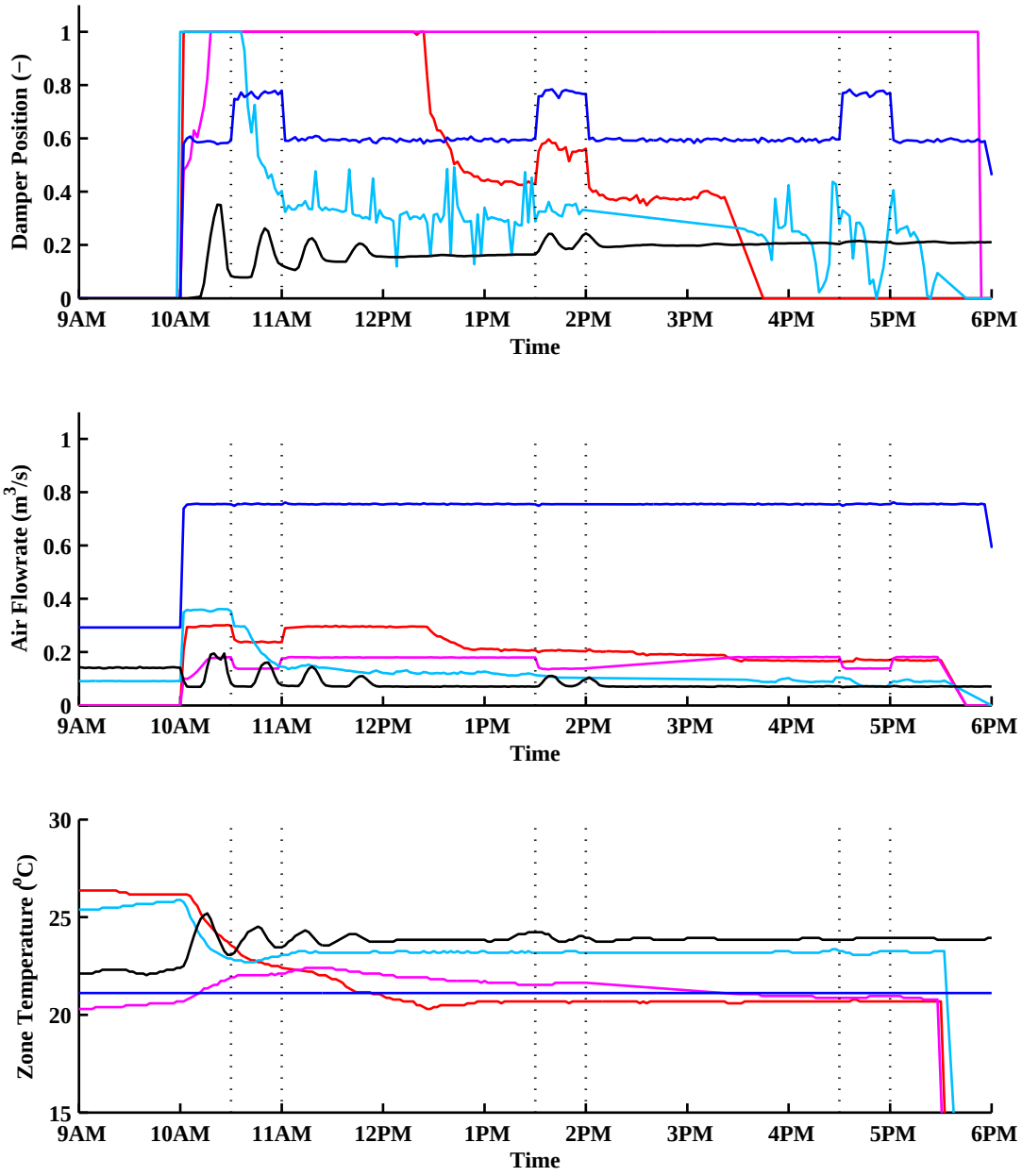

Figure 3.8 – Plots of damper position (top), air flowrate (middle) and zone temperature (bottom) for TU102 (red), TU108 (pink), TU125 (light blue), TU135 (blue), and TU139 (black) for the duct static pressure adjustment test day, November 17th, 2012. Dotted lines indicate the beginning and end of the three test periods. Data was measured at a two-minute resolution.

AHU		Supply Fan Speed				Supply Air Flowrate			
	Test Time	Normal (-)	Reduced (-)	α (-)	β (-)	Normal (m^3/s)	Reduced (m^3/s)	α (m^3/s)	β (-)
1	10:30 AM	0.48	0.37	0.11	0.78	6.41	5.67	0.75	0.88
	1:30 PM	0.46	0.36	0.11	0.77	6.16	5.32	0.84	0.86
	4:30 PM	0.45	0.32	0.12	0.73	5.98	5.03	0.95	0.84
2	10:30 AM	0.66	0.53	0.13	0.81	5.81	5.15	0.66	0.89
	1:30 PM	0.62	0.53	0.10	0.84	5.35	5.08	0.27	0.95
	4:30 PM	0.54	0.47	0.07	0.87	4.72	4.59	0.13	0.97

Table 3.2 – Summary of test building AHU performance during static pressure tests.

Electrical Panel		Real Power			
	Test Time	Normal (kW)	Reduced (kW)	α (kW)	β (-)
MPNH1	10:30 AM	15.65	12.35	3.30	0.79
	1:30 PM	13.95	11.96	1.99	0.86
	4:30 PM	13.28	11.27	2.01	0.85
GPNH2	10:30 AM	27.22	24.20	3.02	0.89
	1:30 PM	25.15	23.50	1.64	0.93
	4:30 PM	23.86	22.36	1.50	0.94

Table 3.3 – Summary of test building HVAC electrical panel performance during static pressure adjustment tests.

$$\alpha_\theta = \theta_{normal} - \theta_{reduced} \tag{3.1}$$

$$\beta_\theta = \frac{\theta_{reduced}}{\theta_{normal}} \tag{3.2}$$

Where:

θ = Parameter Value
α_θ = Reduction Magnitude of θ
β_θ = Normalized Reduction of θ

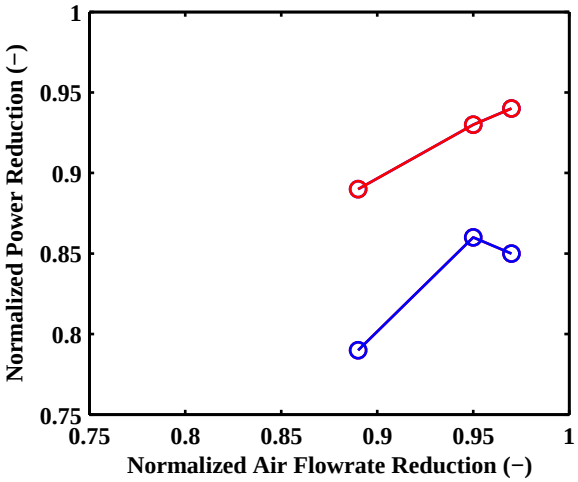

Figure 3.9 – Normalized power reduction of MPNH1 (blue) and GPNH2 (red) against normalized air flowrate reduction for AHU2 of the test building during three static pressure adjustment tests.

3.3.3 Discussion

The total power curtailment for each of the three tests, 10:30 AM, 1:30 PM, and 4:30 PM, was 6.32 kW (approximately 6% of whole-building power), 3.63 (3.6%) and 3.5 kW (3.5%) respectively. While noticeable curtailment was present for each test, the morning test was almost twice as effective as the two afternoon tests, where the curtailments were approximately equal. Normalized reduction in fan speed and air flowrate for AHU1 continued to increase slightly throughout the day, while for AHU2, the normalized reduction in fan speed decreased throughout the day and the normalized reduction in air flowrate decreased dramatically between the morning and afternoon. Figure 3.7 shows that the return fans for each AHU follow their respective supply fans very well with an offset. Therefore, it can be assumed that similar changes in return air flowrates as supply air flowrates can be expected for each AHU. Unfortunately, direct measurements of fan power could not be made. However, the AHU1 supply and return fans and the AHU2 supply fan are located on panel MPNH1 while the AHU2 return fan is located on panel GPNH2. From Table 3.2, Table 3.3, and Figure 3.9, it is clear that the dramatic decrease in supply and return air flowrate reduction in AHU2 from the morning tests to the afternoon tests had the largest impact on power consumption for both HVAC panels MPNH1 and GPNH2. Their power consumption reductions decrease as the air flowrate reductions for AHU2. This analysis reveals a strong relationship between fan power curtailment and air flowrate reduction when using a duct static pressure adjustment as a curtailment strategy. It is, therefore, important to explore the reason for higher airflow reduction in the afternoon than the morning for AHU2.

Air flowrate is reduced in response to duct static pressure adjustments when terminal units are starved. Pressure-independent terminal units develop a desired air flowrate based on the error of zone temperature from setpoint. The dampers are modulated in order to attain the desired flowrate or maintain it in the wake of small duct pressure variations. Lowering the duct static pressure setpoint reduces the pressure drop across the dampers, lowering the air flowrate through them, and requiring the dampers to modulate open to retain the desired air flowrate. If the duct static pressure is dropped low enough such that even with the dampers modulated to fully open there is still not the desired airflow through them, the terminal unit is considered starved. There is nothing the terminal unit can do to provide the correct amount of air to meet the load. Note that this can also occur if the load becomes too high compared to the static pressure setpoint. In general, if a duct static pressure setpoint reduction is made, and none of the terminal units become starved, then no change in airflow in the system will occur. However, if terminal units become starved as the result of the decrease in duct static pressure, a reduction in airflow through the system will occur.

The operation of such a process is visible in the plots shown on Figure 3.8 and Figure 3.7. TU135 is able to maintain its desired air flowrate through all three tests by modulating its dampers open in the wake of static pressure reductions during the test. TU108, however, is starved the entire day, as its damper position remains fully open throughout the entire day. Notice that during the test periods when the duct static pressure is dropped, the air flowrate through TU108 also drops. Meanwhile, TU102 is starved during the start of the day, however, is able to modulate open during the test periods of the afternoon. A loss of damper position data is a possible reason for the display of all zeros after approximately 4:30 PM. The effect on the total air flowrate through the AHU supply fans is clearly seen in Figure 3.7. Notice that both AHU air flowrates are reduced during the morning test period, indicating that terminal units on both systems were starved. However, AHU2 experiences less air flowrate reduction during the two afternoon test periods, indicating a lesser number of starved terminal units. Recognizing that fan and

chiller power consumption are strong functions of AHU air flowrate, and AHU air flowrate is dependent on the starving of terminal unit boxes, predicting when terminal units will be starved in response to a static pressure setpoint adjustment, or any other demand response strategy, can be key to determining how much power can be curtailed at a given time. In addition, since terminal unit starving is indicative of a loss of service, determining which terminal units will starve and to what magnitude can help minimize loss of service to those critical zones.

3.4 Conclusion

This chapter has used high-resolution power consumption and HVAV performance data collected from a test building on Boston University's campus to gain insights into some qualities of VAV HVAC systems that affect ancillary service provision performance. These insights should be considered by both building owners and future demand response researchers in order to improve both the ability and reliability of VAV system to provide ancillary services.

First, main and sub-panel power data during a summer week was used to compare the relative magnitude of end-use power demand in the building. From this analysis, it was determined that the HVAC system can account for up to 80% of the building power, most of which is from the air-cooled chiller. Therefore, it would be desirable in this case to use the HVAC system for any demand response service and target the chiller as the source of the service.

Second, a relationship between HVAC system power consumption and environmental conditions was observed. This led to a discussion on the reasons for this relationship. First, outdoor air temperature has a direct effect on air-cooled chiller condenser operation. Second, there is an indirect effect, through the cooling loads of the building, environmental conditions have on airflow through the AHU fans and chilled water temperature entering the chiller's evaporator. If the building is internally-load dominated or the chiller is water-cooled, occupancy and equipment loads or outdoor air wetbulb temperature could play more important roles in determining power consumption.

Third, the presence of discrete equipment operations was presented through power data on the chiller and air-compressor located on an HVAC electrical panel. Chiller compressor staging was cited as an advantage or challenge for providing ancillary services, depending on the predicted knowledge of staging and mechanical durability. On-off cycling of equipment, such as the air compressor, could be considered as noise if the frequency of oscillations is high enough or the magnitude low enough. Otherwise, the effect of on-off cycling of equipment on the settlement of ancillary services provided would have to be considered.

Fourth, the presence of HVAC operational faults must be considered in order for the system to perform as anticipated during a service event. Example faults that could alter actual performance from anticipated performance include sticky actuators, the degradation of equipment over time, or improper controller tuning.

Lastly, a common demand response strategy was implemented to observe event-specific dynamics that are important to the provision of ancillary services. The duct static pressure setpoint was lowered in each AHU for 30 minutes three times during a test day. Results of this test showed that fan speed controllers and terminal unit actuators responded to the static pressure setpoint adjustments within two minutes,

much faster than the required 10 or 30 minute responses of reserve resources. Additionally, the results displayed a strong relationship between airflow reduction and fan power consumption. It was shown that terminal unit starving plays a large role in the reduction in airflow through a system, and is a key to determining HVAC performance during ancillary service or other demand response events.

Chapter 4

VAV System Modeling For Ancillary Service Simulations

Real building tests are good for identifying real-world challenges and system performance capabilities associated with providing ancillary services. There are, however, many limitations to their use when trying to characterize the performance of curtailment strategies over a range of operating conditions. The first of which is the presence of occupants, who rely on normal building operation in their daily life and work. Manipulating normal control schemes can lead to disturbances in thermal comfort or indoor air quality that inhibit occupant productivity and willingness to continue test participation. Second, the ability for data collection can be limited by the level of metering in the building for normal operation. This includes collection points and frequencies. The installation of additional monitoring equipment may require the shutdown of building systems for periods of time, which can be a burden on facility management. Lastly, testing in a real building limits the test conditions to those experienced in real time. If a large number of tests are required over a range of operating conditions, testing must continue for a time period on the order of months, at the least, to allow environmental conditions to change.

The limitations listed above are surpassed by the use of simulations. Simulated buildings contain no occupants to dissatisfy, no laborious installation of equipment, and operating conditions that can be set at will. However, building simulations also present their own set of challenges. Fundamentally, building operation involves dynamic thermal, fluidic, and electrical physical processes. The resulting mathematical models required for simulation can quickly become large, complex, and difficult to solve. It is necessary, therefore, to do two things; 1) Define the relevant physical processes whose models are required to capture the operation of interest and 2) Define a method of solving or approximating the solution of the resulting system of algebraic and differential equations. Accordingly, Section 1 of this chapter will outline the physical processes required to study VAV-provided ancillary service provision. The remaining sections will present trials of three readily-available building-specific or dynamic system simulation packages. Section 2 will present the use of EnergyPlus v6.0 (U.S. Department of Energy, 2013a), Section 3 TRNSYS 16 (Klein, 2007), and Section 4 Modelica via Dymola 2013 FD01 (Dassault Systemes, 2013). Lastly, Section 5 will conclude the chapter by choosing a modeling and simulation package with which to move forward for ancillary service simulations in the following chapter.

4.1 Model Requirements

There are three main parts associated with VAV system operation: the thermal zones, the air system, and the central plant. The thermal zones represent the space in which occupants reside and includes the building construction and room air volumes. The air system includes air diffusers, terminal units, ducting, and fans that are responsible for moving the appropriate amount of air through the building to meet the thermal loads of the zones. Lastly, the central plant distributes hot and cold water to heating and cooling coils, which condition the air to the appropriate temperatures.

The heart of a VAV system is the air system, as the total amount of air flowing through the system plays a large role in fan and chiller power consumption. Terminal unit damper positions are set based on the required flow to meet time-varying zone-specific cooling or heating loads. While the airflow through the system is controlled by damper position, it is governed by the physical relationships between pressure and flow. The fan produces a static pressure in the supply duct sufficient to drive airflow through the terminal units and diffusers into the thermal zone. The static pressure difference between the duct and thermal zone must be sufficient to overcome the flow friction resulting from the terminal units, diffusers, and other duct lengths or fittings in order to provide the proper air flowrate. The modulation of the terminal unit dampers provides a variable resistance that may be adjusted according to the demanded air flowrate, provided the static pressure in the duct stays constant. For this reason, supply fan speed is most commonly controlled to maintain a constant static pressure in the duct while terminal unit dampers modulate to provide the proper air flowrate to the thermal zone (Montgomery and McDowall, 2008). This type of terminal unit control is called pressure-independent. The total air flowrate through the terminal units and total pressure rise across the fan determines the fan power required. Chilled water flow through the cooling coil is controlled to maintain a supply air temperature setpoint. This is accomplished through a bypass modulating valve in constant flow systems or variable speed pump or modulating two-way valve in variable flow systems. As the airflow though the coil changes, the water flowrate through the coil must modulate accordingly. The change in return water temperature in constant flow systems or the change in mass flowrate in variable flow systems ultimately determines the change in chiller power.

The primary means of load curtailment for any demand response activity is the adjustment of a setpoint for one or more of these control loops. The four most common of these strategies found in Motegi et al. (2007) include a zone dry bulb temperature setpoint adjustment (ZDBA), static pressure setpoint adjustment (SPA), supply air temperature setpoint adjustment (STA), and chilled water temperature setpoint adjustment (CWA). In order to simulate the dynamic performance of these curtailment strategies over a range of load conditions, a model describing the pressure-flow physics of the air system in response to controller signals is required. This is particularly the case for ancillary service provision because the time period of interest is on the same order as the transient time period of VAV system dynamics.

4.2 EnergyPlus

EnergyPlus v6.0 was the first simulation engine trialed due to its common use for building load and energy simulations in both industry and research. The program uses a Predictor-Corrector method to determine the energy flows through the zones, air system, and central plant (University of Illinois and Lawrence Berkeley National Laboratory, 2010). In general, this involves the prediction of system and

plant operation based on assumed zone loads and the correction of system operation and zone air temperatures based on plant and system capacity. For VAV air systems, the method begins with estimating the load on the air system by assuming the zone air temperature is equal to the setpoint temperature. The zone-specific loads are translated to corresponding required terminal unit air flowrates, which are then summed and given to the fan model as inputs. If the fan airflow capacity is not high enough, the available capacity is distributed to each terminal unit proportional to their design air flowrate and the resulting zone air temperatures are calculated.

Different fan models are possible depending on the application and are defined in EnergyPlus as *Fan:ModelName*. These include *Fan:ConstantVolume*, *Fan:VariableVolume*, textitFan:OnOff, and *Fan:ComponentModel*, which is new as of v6.0. *Fan:VariableVolume* and *Fan:ComponentModel* are most applicable to VAV systems, with *Fan:VariableVolume* calculating fan power as a function of the determined air flowrate and other definitions by the user, including design pressure rise, fan efficiency, motor efficiency, and part load ratios. The *Fan:ComponentModel* model calculates fan pressure rise as a function of air flowrate using a physically-based equation based on air flowrate, system leakage, and duct static pressure setpoint. The calculated pressure rise and air flowrate are used in various functions to calculate fan efficiency, motor efficiency, and finally total power draw. A model to evaluate the effect of a static pressure reset strategy also exists, which determines a reduction in fan pressure rise as a function of the air flowrate location between a minimum and maximum.

The above analysis, however, reveals that no explicit relationship between duct pressure and terminal unit air flowrates is present. To demonstrate this fact, a daylong simulation was run using a DOE small office reference building (U.S. Department of Energy, 2013b) in Boston, MA with a VAV template model and air-cooled electric chiller model. The supply fan had a max air flowrate capacity of 2.19 m^3/s, pressure rise of 995 Pa, and total effeciency of 0.55. The chiller had a compressor COP of 3.2 and total COP of 2.7. The simulation implemented a zone air temperature setpoint change from the normal cooling setpoint of 22 °C to the setback cooling setpoint of 29.5 °C at noon until 3:00pm. The output variable names were *Zone Mean Air Temperature*, *Chiller Electric Power*, *Fan Electric Power*, *System Node Pressure*, and *VAV Terminal Damper Positions*, each with a key value of "*", indicating the reporting of values for each instance of the variable (e.g. zone or node). The results, shown in Figure 4.1 below, indicate that there is no change in pressure from the inlet of the fan to the outlet of the fan, despite a change in air flowrate through the fan, air flowrate through the terminal unit, and terminal unit damper position. Additionally, the fan outlet pressure is reported lower than the zone pressure, which would indicate backwards flow, with one crossover point at hour 10. Lastly, there is no explicit modeling of controller dynamics, as the calculation procedure uses mass and energy balances to assume behavior over a given timestep.

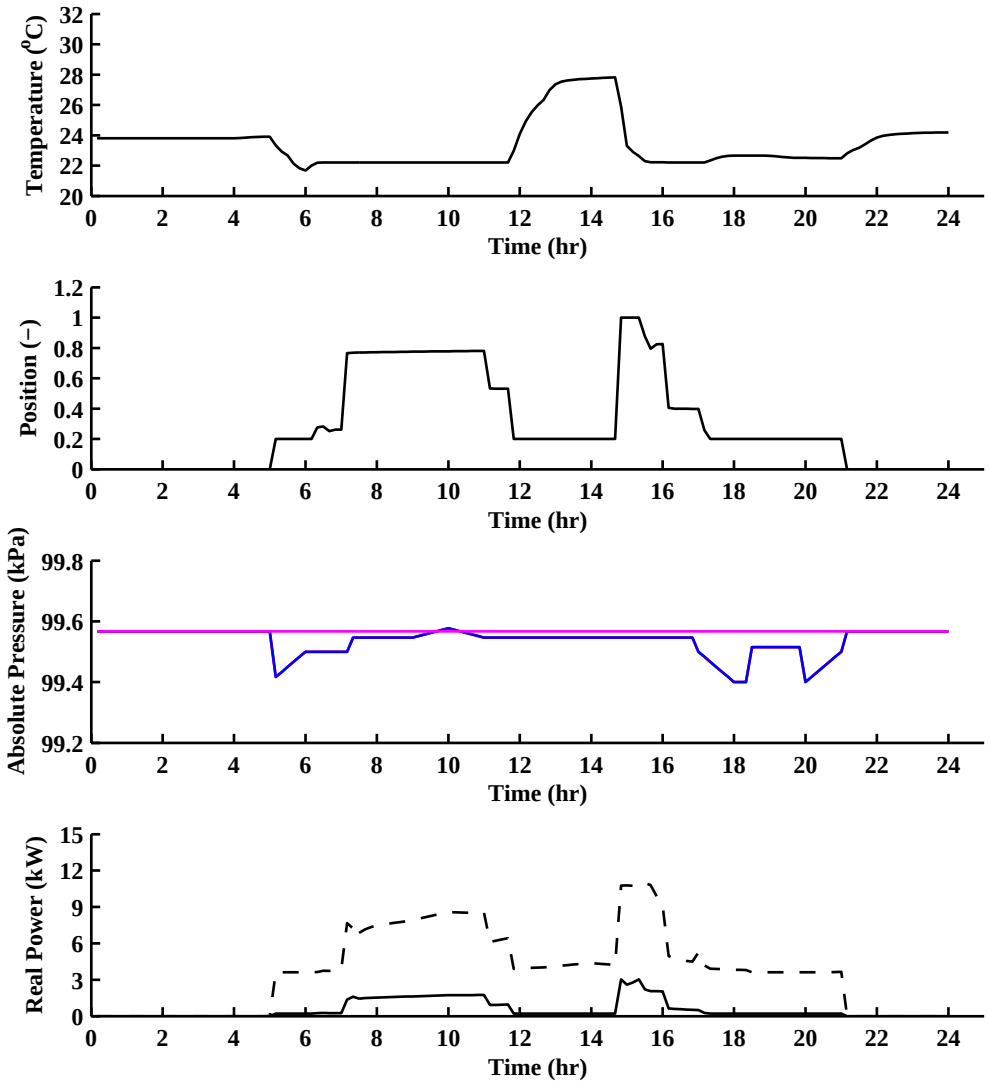

Figure 4.1 – Single day simulation in EnergyPlus with zone air temperature setpoint adjustment showing core zone air temperature (top), core zone terminal unit damper position (second), supply fan inlet node pressure (third, red), supply fan outlet node pressure (third, blue), core zone node pressure (third, magenta), supply fan power (bottom, solid), and chiller power (bottom, dashed).

4.3 TRNSYS

4.3.1 Background

TRNSYS is a Transient System Simulation tool which uses a graphically based user environmental to simulate systems made up of components. Each component, called a type, represents a portion of the system and many times represents a piece of equipment or process. Types contain inputs and outputs that are linked together through programming code and user-adjustable parameters. TRNSYS is a popular choice among engineers and researchers in the building industry due to its flexibility in the models it simulates. Largely unlike EnergyPlus, TRNSYS allows for user-created types, in addition to many standard types, to be included in simulations. This gives the possibility of simulating virtually any building or HVAC system in design, especially those on the cutting edge of study or implementation. Of particular interest to most is Type 56, which is configured to represent the heat transfer dynamics of single or multi-zone building construction.

The TRNSYS engine (Kernel) uses a solver, called the Successive Substitution Method (SSM), to solve the simulation numerically. The SSM solver initializes the inputs of each type with the user-defined or default (0) initial values. The outputs are calculated and passed to the types that take the resulting outputs as inputs. These types then calculate outputs and the process continues until all types have calculated their outputs. The whole process is iterated until the change in output values from each type is within the tolerance value set by the user or the default value (0.001). If this process does not converge to a solution, such as in the case with large oscillations in output values, a user-defined relaxation factor may be put in place. This causes only a fraction of the calculated change in successive iterative outputs to be considered for the next iteration. Additionally, an allowable number of iterations can be set by the user, above which TRNSYS reports a warning and moves on to the next timestep using the value resulting from the previous timestaep. If this occurs over enough timesteps, the simulation is stopped with an error.

Of interest to this project is the possible use of TRNSYS to model and simulate the explicit relationship that exists between pressure and flow in duct. Haves and Norford (1997) reported on a research project during which types were developed to explicitly simulate an HVAC system in the desired manner of this application. These types included fans, terminal units, heating coils, valves, controllers, and duct resistances. Types were written for use in HVACSIM+ and TRNSYS and example simulations were developed and tested in each simulation package (DeSimone, 1995; Haves and Norford, 1997). Results were acquired and presented using HVACSIM+, however, numerical difficulties were cited when attempting to use TRNSYS. Unfortunately, HVACSIM+ is no longer heavily supported. Though numerical difficulties during the use of TRNSYS to model dynamic fluid flow with thermal systems was also cited elsewhere (Wang, 1999), TRNSYS was determined as a better alternative to EnergyPlus with the underlying assumption that any numerical difficulties should be further explored and could be overcome. Additionally, the availability of the library of types created as part of ASHRAE 825-RP would greatly reduce the burden of programming the models required to study building-provided ancillary services.

4.3.2 Trials

Flow networks are simulated by a system of resistances in series and in parallel, analogues to electrical resistance networks. A pressure difference can be related to a mass flowrate and duct resistance in turbulent fluid flow using Equation 4.1 below (Haves and Norford, 1997).

$$\Delta P = RQ^2 \tag{4.1}$$

Where:

ΔP	=	Total Pressure Drop	(kPa)
Q	=	Air Mass Flowrate	(kg/s)
R	=	Air Flow Resistance	(0.001/kg-m)

Four types, 341, 342, 345, and 346, developed in ASHRAE 825-RP (Haves and Norford, 1997) use the above relation to model explicit airflow networks. Note that a linear relation between pressure and flow is employed at low mass flowrates in order to promote convergence of the model at those points. Types 341 and 342 represent flow resistances and types 345 and 346 represent flow splits and mergers. Two types are required for each model due to the input-output nature of the TRNSYS simulation. Type 341 calculates pressure drop based on a given flow, type 342 calculates mass flowrate based on a given pressure drop, type 345 is a flow split that calculates main and branch outlet mass flowrates as well as inlet pressure given an inlet mass flowrate and outlet pressures, and type 346 calculates inlet and branch outlet pressures as well as main outlet mass flowrate given an inlet mass flowrate, main outlet pressure, and branch outlet mass flowrates. Types 342 and 345 can be used at the ends of open systems to calculate mass flowrates while types 341 and 346 are used in closed or open systems. The mass flowrates through branches calculated by types 342 and/or 345 can be passed to types 341 and/or 346 to calculate resulting pressure drops and corresponding node pressures. The resulting pressures can then be passed back to types 342 and/or 345 to calculate the resulting branch mass flowrates.

After some adjustments were made to the code of each type in order to be handled by the TRNSYS kernel, initial simulations of the individual types alone were successful. However, difficulties arose when combining the types into more complex flow networks that are representative of a VAV system, such as those presented in Figure 4.2 below. Each case represents a pressure source, such as that created by a fan, and multiple pressure sinks, such as those created by thermal zones. In between, a network of resistances split the flow into each zone, which represent the terminal units and duct system. Types 342, 345, and 346 were used to simulate this model with the source and sink pressures given. Simulations were attempted that varied the inlet pressure (P_1) from 10 kPa to -10 kPa at one hour steps for 10 days and held the sink pressures constant at 0 kPa. The resistance of each resistor of the network was equal to 2000 1/kg-m.

For comparison, a MATLAB script was written which performs the same simulation by using the fsolve function on Equations 4.2 to 4.3 below, developed my performing a mass balance at each of the flow splits.

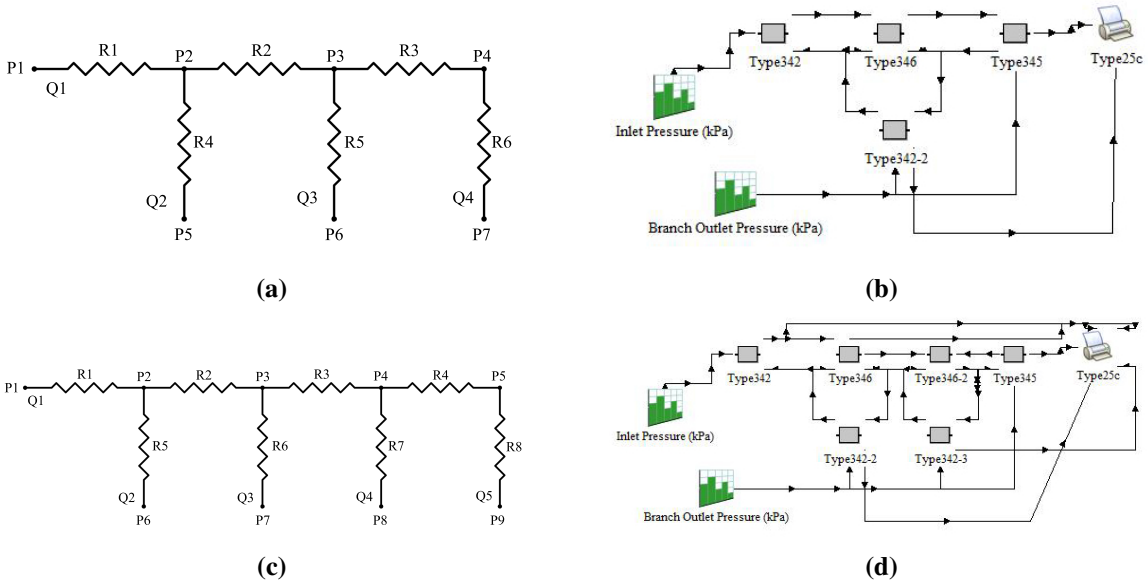

Figure 4.2 – TRNSYS dynamic flow network trial setups, including the schematic (a) and TRNSYS implementation (b) of the two flow split network and the schematic (c) and TRNSYS implementation (d) of the three flow split network.

$$0 = \sqrt{\frac{P_1 - P_2}{R_1}} - \sqrt{\frac{P_2 - P_3}{R_2}} - \sqrt{\frac{P_2 - P_5}{R_4}} \tag{4.2}$$

$$0 = \sqrt{\frac{P_2 - P_3}{R_2}} - \sqrt{\frac{P_3 - P_4}{R_3}} - \sqrt{\frac{P_3 - P_6}{R_5}} \tag{4.3}$$

$$0 = \sqrt{\frac{P_3 - P_4}{R_3}} - \sqrt{\frac{P_4 - P_7}{R_6}} \tag{4.4}$$

Where:

P	=	Pressure	(kPa)
R	=	Air Flow Resistance	(0.001/kg-m)

The two flow-split simulation was successful in TRNSYS and agreed well with the MATLAB results, as shown in Figure 4.3 below. However, the iteration limit in the TRNSYS solver had to be adjusted from the default 30 to 1,000 and the relaxation factor limited to below 0.45. The three flow-split simulation failed in TRNSYS as mass flowrates approached zero. This occurred even while increasing the iteration limit from 1,000 up to 10,000 and varying the relaxation factor between 0.1 and 1.0. Observing a large spike in the number of required solver iterations during the two flow split network simulation as the air mass flowrate approached zero, it is hypothesized that the three flow split network simulation fails due to the larger number of branch mass flowrates approaching zero flow for a longer period of time.

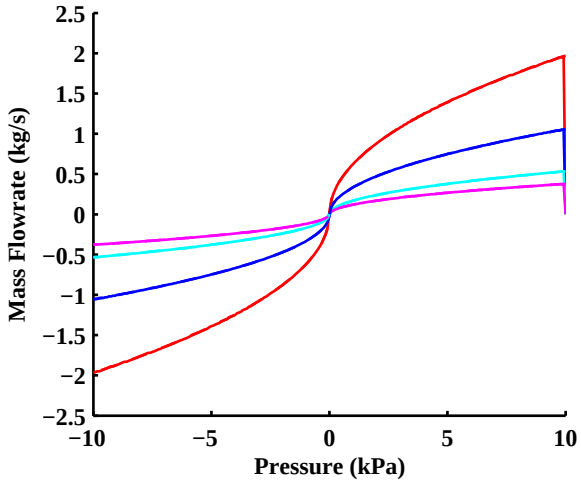

Figure 4.3 – Results of the successful TRNSYS simulation of the two flow split network showing the air mass flowrate calculated by TRNSYS (solid) and MATLAB (dashed) of Q_1 (red), Q_2 (blue), Q_3 (light blue), and Q_4 (magenta). Simulation of the three flow split network were unsuccessful in TRNSYS due to solution convergence problems at air mass flowrates close to zero.

4.4 Modelica

4.4.1 Background

Modelica (Fritzson et al., 2012) is an open-source, object-oriented programming language developed to enhance the modeling, simulation, and library sharing of complex, multi-domain physical systems. Currently supported by the Modelica Association (Modelica Association, 2013a), the development of the language specification started in 1996 by the Modelica Design Group in an effort to unite separate, but similar, ongoing efforts to advance the field of physical modeling for engineering applications (Mattsson and Elmqvist, 1997). The two results of this effort that make Modelica stand out among other engineering programming, modeling, and simulation packages are 1) acausal differential and algebraic equation (DAE) system definitions and 2) object-oriented approach for easy model library sharing.

Acausal mathematical systems are the most natural relationships that can be developed between the system state variables of interest and do not consider an input-output data flow of information. Take, for instance, the example of fluid flow through a pipe expressed by Equation 4.1. This expression describes the fundamental relationship between pressure drop and flowrate. Most modeling and simulation packages employ an assignment-based scheme of computation which requires the use of an input-output relationship among physical models. In the case of Equation 4.1, pressure drop is defined as the unknown output, with the values of resistance and mass flowrate known inputs to the model. However, if the known variable was pressure drop, the equation would have to be inverted and explicitly solved for mass flowrate in order to rearrange the input-output relationship, or causality. A simple consequence of this is the requirement to develop both types 341 and 342 of the previous section. This may not seem terribly prohibitive in this simple case, however, as systems grow in complexity, so does the choice of which flow resistance equation to use in each case within the overall model. In general, dynamic systems include both differential equations and algebraic equations, which commonly results from state and constituent

equations. The common state-space formulation of such a system inherently defines a causal relationship between input states and output states (Mattsson and Elmqvist, 1997). As the simple algebraic example above, the development of multiple models becomes required depending on the order of variable flow. Modelica alleviates this requirement through the use of acausal modeling. The user need only input the differential and algebraic equations that describe a system. In doing so, Modeclia effectively separates the processes of modeling and simulation of complex physical systems. Modelica development environments then translate the code into an assignment-based language suitable for compilation and CPU computation. While the mathematics behind the translation of code is outside the scope of this thesis, the Tarjan, Pantelides, Tearing, and Relaxation algorithms are central to its execution (Harman and Ricardo, 2005).

An object-oriented approach allows efficient development and connection of complex physical system models. This is made available in Modelica by the *connector* and *partial model* classes. The *connector* class defines the connection of a system model to another and contains a potential variable and flow variable. Potential variables, such as voltage, pressure, temperature, position, and angle, of connecting models are set equal at the point of connection. Flow variables, such as current, mass flow, heat flux, force, and torque, are summed to zero at the point of connection. Therefore, connecting two models forms additional relations between the state variables in each model. Within each model, multiple connectors can be formed to allow more than one connection. Taking resistive fluid flow in a pipe as an example, a model can be created that defines two connectors, each containing a corresponding pressure and mass flowrate. Within the model, the flow variables may be equated, while the pressure at each connection can be related to the value of the flow variable by a resistance, as in Equation 4.1. Note that other models connected to the flow resistance model may supply either the flow or pressure variable. The *partial model* class creates an instance of a model that may form fundamental physical relationships for a number of specific applications of that model. Using resistive fluid flow in a pipe again as an example, the single resistance model described above may be made a partial model that can be extended to other models that may define the resistance in other ways rather than the constant assumption made until now. When making those models, one only needs to define the relationship for resistance, while the relationship between flow, pressure, and the resistance is retained.

The acausal and object-oriented approaches to modeling lead to an ability for wide-spread sharing of models. One would only need to verify the similarity of connector variables. For this reason, the Modelica Standard Library has been created to supply a developer with 1280 models and 910 functions. Other, domain specific, libraries have also been created. One which aligns itself well to the needs of this thesis is the Modelica Library for Building Energy and Control Systems Version 1.3_build1 (Wetter, 2009; Wetter et al., 2011b, 2013). This library contains models for air and water-based HVAC systems, controls, heat transfer among rooms and the outside, and multi-zone airflow. Components from the Modelica Standard Library are indicated by *Modelica.modelname* and components from the Buildings Library are indicated by *Buildings.modelname* throughout the remainder of this thesis.

Lastly, a Modelica development environment is required to translate and compile model codes as well as to simulate the models under given conditions. As many are available (Modelica Association, 2013b), both commercially and open-source, Dymola was chosen for its high level of industry support.

4.4.2 Trials

Trials were performed to test the capability of the models developed in the Buildings Library for application in this thesis. These trials included simulating the same flow networks described in the TRNSYS trials of the last section, with each resistance equal to 2000 1/kg-m, the sink pressures held constant at 0 kPa, and the inlet pressure (P_1) being varied from -10 to 10 kPa at one hour steps for a 10 day period. Two, three, and four flow split networks were implemented in Dymola using multiple instances of *Buildings.Fluid.FixedResistances.SplitterFixedResistanceDpM* along with a pressure source and sink implemented by *Buildings.Fluid.Sources.Boundary_pT*. Figure 4.4 presents the four flow split network diagram and implementation in Dymola.

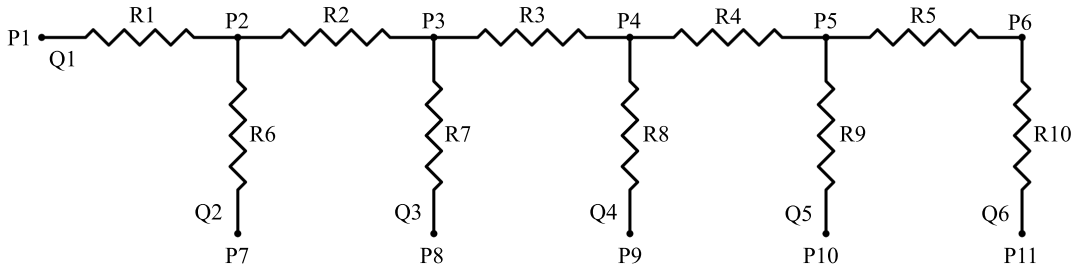

(a)

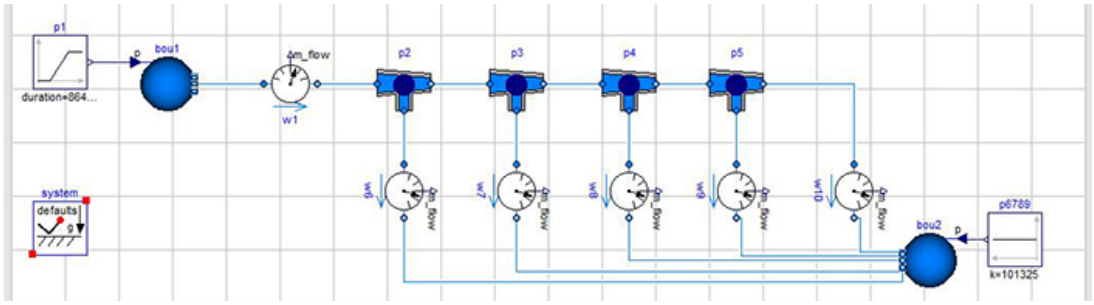

(b)

Figure 4.4 – Setup for the four flow split network trial in Dymola, including the schematic (a) and Dymola graphical implementation (b).

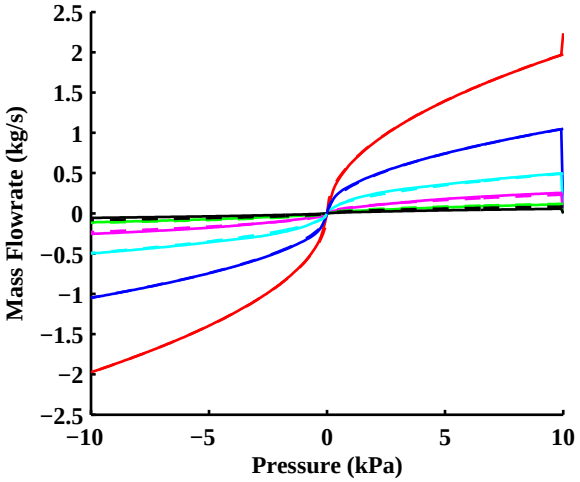

Figure 4.5 – Results of the successful Dymola simulation of the four flow split network showing the air mass flowrate calculated by Dymola (solid) and MATLAB (dashed) of Q_1 (red), Q_2 (blue), Q_3 (light blue), Q_4 (magenta), Q_5 (green), and Q_6 (black).

The integration algorithm used was Radau IIa - order 5 stiff, as recommended by (LBNL, 2012) with a tolerance of 1e-6. The simulations of each of the flow split networks performed very well when compared to calculations performed in MATLAB using the fsolve function on a system of equations defined by mass flow conservation at the points of flow split. The results are presented in Figure 4.5.

4.5 Conclusion

This chapter has outlined requirements and methods for the simulation of ancillary service provision in multi-zone commercial buildings. In order to model the response in system operation to changes in controller setpoints, explicit modeling of the physical variables by which the system is controlled is necessary. This is especially true for the air system, which plays an integral role in maintaining occupant service and affecting plant power consumption on a timescale of similar order to ancillary service delivery. As fan and terminal unit controllers are based on the pressure-flow relationship in duct systems, it is important that this relationship is modeled in conjunction with a suitable thermal zone model and central plant model.

Multiple simulation packages were presented that are common in building and dynamic system modeling and simulation. The first, EnergyPlus, does not explicitly model pressure-flow relationships in ducts or associated controllers and instead uses a predictor-corrector method of simulation. While this tool is useful for the load and energy simulation of large buildings over long time frames, the interest of this thesis is the short-term, dynamic relationship between system physical variables and controllers. The second, TRNSYS, faced solution convergence problems at small air flowrates when attempting to simulate complex flow networks representative of a VAV supply system. The third, Dymola, which is a development environment for Modelia, proved very successful in simulating complex flow networks. In addition, the user interface, availability and support for the Modelica Library for Building Energy and Control Systems, and ease of setting up complex multi-domain physical models make Dymola a very attractive option for the dynamic simulation of building HVAC systems. Therefore, the simulations presented in the following chapter as well as those planned for future work will be implemented in Dymola through the use of the Modelica programming language.

Chapter 5

Simulations

In order to better characterize relationships between demand response curtailment strategy performance and system operating conditions, simulations of a representative VAV system serving two thermal zones were conducted. Section 1 describes the design and modeling of the thermal zones and VAV system used in the simulations. Section 2 demonstrates the performance of the simulated system in design conditions as well as with step-change disturbances. Section 3 describes the batches of simulations that were conducted in order to characterize the performance of each curtailment strategy and Section 4 presents the results of those simulations. Section 5 discusses the results to give reasons for the variability in performance within and among curtailment strategies subjected to different operating conditions. Finally, Section 6 offers broader conclusions that may be drawn regarding the application of these results to ancillary service provision.

5.1 System Design and Modeling

The representative VAV system model, diagrammed in Figure 5.1, is able to capture the major dynamics associated with the provision of ancillary services by various load curtailment strategies. The components considered are the supply fan, cooling coil and associated chilled water loop, duct pressure drops, terminal units, diffuser pressure drops, and two thermal zones. Additionally, 100% recirculated air is considered. While this does not allow for the inclusion of a fraction of outdoor air mixing, it allows for the inclusion of the effects that zone air temperature variations may have on the air entering the cooling coil without the additional model complexity required to include mixing box dynamics and control. The model was implemented in Dymola using components from the Modelica Standard Library and Modelica Library for Building Energy and Control Systems Version 1.3_build1 (Wetter, 2009; Wetter et al., 2011b, 2013) where indicated by *Modelica.modelname* and *Buildings.modelname* respectively.

5.1.1 Thermal Zones

In order to provide a representative amount of thermal mass, models of two thermal zones were based on the U.S. Department of Energy's small office reference building with new construction 2004_v1.3_5.0

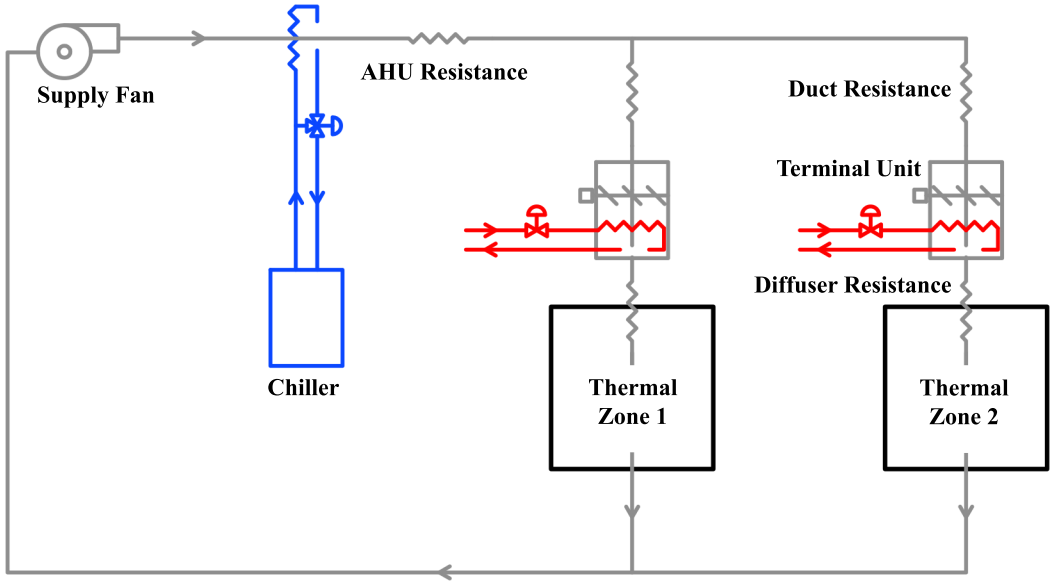

Figure 5.1 – Representative VAV system used for demand response simulations.

(U.S. Department of Energy, 2013b). This reference building is 510 m^2 (5,500 ft^2) total over one floor with a ceiling height of 3.05 m (10 ft). Each exterior wall contains 20% glazing, and is constructed by 0.0254 m (1 in) stucco on 0.203 m (8 in) concrete block with 0.0381 m (1.5 in) insulation and 0.0127 m (0.5 in) gypsum wallboard. The floor construction is 0.102 m (4 in) concrete slab on grade. The ceiling construction is 0.0127 m (0.5 in) acoustic tile ceiling, 0.0127 m (0.5 in) gypsum wallboard, 0.229 m (9 in) fiberglass insulation, and 0.0127 m (0.5 in) gypsum wallboard. Above the ceiling, there is an unconditioned attic with a height of 1.27 m (4.16 ft), after which the roof is constructed of 0.0183 m (0.06 in) metal decking and a roofing membrane. The internal loads are 10.76 W/m^2 for lighting and 10.76 W/m^2 for plug and process. The total occupancy is 27 people. The total design cooling load for the building in a climate of Albuquerque, NM is equal to 18.58 kW. Equation 5.1 was used to determine the design volumetric air flowrate for the HVAC system. This equation results from application of the First Law of Thermodynamics to a control volume around the building zones and assuming perfect mixing of indoor air, that the air leaving the zones is equal to the zone temperature setpoint, that mass is conserved from zone supply to exhaust, and that the air can be approximated as an ideal gas.

$$Q_{coolingload} = \rho_{air} \dot{V}_{air} c_{pair} (T_Z - T_{SA}) \tag{5.1}$$

Where:

$Q_{coolingload}$	=	Design Cooling Load	(W)
rho_{air}	=	Density of Air	(kg/m^3)
$\dot{V}_{air}$	=	Volumetric Supply Air Flowrate	(m^3/s)
c_{pair}	=	Specific Heat Capacity of Air	(J/Kg-K)
T_Z	=	Zone Air Dry Bulb Temperature	(°C)
T_{SA}	=	Supply Air Dry Bulb Temperature	(°C)

Using a 10 °C change in temperature from air supply to exhaust, ρ_{air} = 1.20 kg/m^3 , and c_{pair} = 1,005 J/Kg-K at 20 °C, the design air flowrate is 1.54 m^3/s.

Weather is not considered in the simulations of this model, nor is the thermal interaction between zones. Instead, a specified amount of convective load is introduced to each zone. This does not tie the model to a specific zone configuration, orientation, or location and allows for the general study of any variation of zone thermal loading. Similarly, the exterior facades of each construction element are assumed adiabatic so that the effects of construction thermal capacitance are directly studied without the influence of exterior conditions. Lastly, the temperature of each construction element is initialized to the starting zone air setpoint temperature for each simulation presented in this chapter. The two-zone thermal model was implemented in Dymola using two instances of *Buildings.Rooms.MixedAir* (Wetter et al., 2011a). The modelica code for the two-zone thermal model is presented in Appendix A.

5.1.2 Air System

The air system model is designed to represent a common VAV system. This includes the modeling of diffuser pressure drops, terminal unit performance and control, duct pressure drops, and variable speed supply fan performance and control. For this thesis, the design thermal load for this system was assumed split equally between the two thermal zones. Therefore, the design air flowrate for each zone is 0.77 m^3/s with an assumed supply air temperature of 12.78 °C. Air properties were implemented in Dymola using the media model *Buildings.Media.IdealGases.SimpleAir*, which is valid from -50 °C to 100 °C and treats air as an ideal gas. While latent heat is neglected throughout the model, this treatment of the air flow simplifies the heat transfer phenomena for basic understanding.

Diffusers were selected from a manufacturer's catalog (Titus, 2013a) on the basis of design air flowrate requirements and diffuser throw. As shown in Figure 5.2 below, the geometry of each thermal zone encourages the use of three diffusers with a characteristic room length of 4.57 m (15 ft), defined as the horizontal distance from the diffuser to the nearest boundary or half of the distance between diffusers (ASHRAE, 2005). Dividing the design air flowrate by three yields 0.257 m^3/s per diffuser. Selecting a 0.254 m (10 inch) diameter round TMR ceiling diffuser from the Titus catalog yields a diffuser throw based on a 0.25 m/s (50 fpm) terminal velocity (T_{50}) of 4.57 m (15 ft), which satisfies Air Diffusion Performance Index (ADPI) requirements (ASHRAE, 2005). The selected diffusers are rated with a Noise Criteria (NC) of 30. Although this rating is no longer the standard in verifying comfortable acoustical properties of HVAC equipment, the value is less than the generally recommended value for office spaces of 35 (ASHRAE, 2005). With this diffuser selection from the manufacturer's catalog, the static pressure drop at the design flowrate of each diffuser is 29.6 Pa (0.119 inwg). Assuming the diffusers are ducted in parallel from the exit of the terminal unit and neglecting pressure drops due to ducts from the exit of the terminal unit to each diffuser, the static pressure drop due to the diffusers can be modeled as a single resistance with the design zone air flowrate. Therefore, the diffusers were modeled in Dymola using a single instance of *Buildings.Fluid.FixedResistances.FixedResistanceDpM* for each zone. See Appendix A for the modelica code implementation of the diffuser resistance model and see Appendix B for the manufacturer's catalog selection.

Terminal units for each zone were selected from a manufacturer's catalog (Titus, 2013b) on the basis of design air flowrate, yielding a selection of a 12 in diameter DESV Pressure Independent Single Duct Terminal Unit with hot water reheat for each zone. A resulting NC rating of 35 is adequate for office

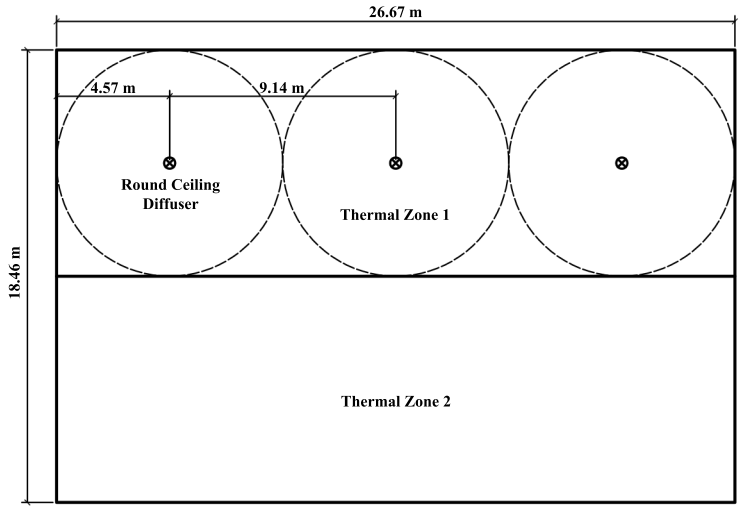

Figure 5.2 – Thermal zone layout with assumed placement of round ceiling diffusers using a T_{50} of 4.57 m (15 ft), as recommended by ASHRAE (2005).

spaces. The selected terminal unit has a maximum air flowrate of 0.944 m^3/s (2000 cfm) and a minimum air flowrate of 0.153 m^3/s (325 cfm). The static pressure drop through the unit at the design air flowrate, including one heating coil row, is equal to 66.7 Pa (0.268 inwg). The terminal units and their control were modeled in Dymola as described below.

A pressure-independent terminal unit model was developed for implementation into the Dymola simulation. The model is composed of a control damper, fixed resistance, reheat coil, and controller. The inputs to the model are an inlet fluid port, zone dry bulb temperature setpoint input port, and zone dry bulb temperature measurement input port. The outlet of the model is a fluid outlet port. The damper and fixed resistance, which represents the pressure drop through the unit with a wide open damper, are modeled in series using an instance of *Buildings.Fluid.Actuators.Dampers.VAVBoxExponential*. The control damper variable resistance model is based on that which was developed by Haves and Norford (1997). The reheat coil is implemented in series with the control damper and fixed resistance using an instance of *Buildings.Fluid.HeatExchangers.DryEffectivenessNTU*, which uses an effectiveness-NTU method to model the heat exchange of the coil. The configuration of the heat exchanger is cross flow with both streams unmixed. An ideal hot water pressure source, implemented with *Buildings.Fluid.Sources.FixedBoundary* supplies hot water to the reheat coil through a two-way modulating valve, implemented with *Buildings.Fluid.Actuators.Valves.TwoWayLinear*. The hot water supply temperature is set to 93.3 °C and the pressure drop through the reheat coil on the water side is assumed to be 5971 Pa (24 inwg), which are the design values for terminal unit reheat coils in the test building described in Chapter 3. See Appendix A for the modelica code implementation of the terminal unit physical model and see Appendix B for the manufacturer's catalog selection.

The terminal unit controller is based on that which is described in Montgomery and McDowall (2008) and applied in Englander and Norford (1992b) and Haves and Norford (1997) to represent the control of a common pressure-independent terminal unit. The controller is diagrammed in Figure 5.3 below.

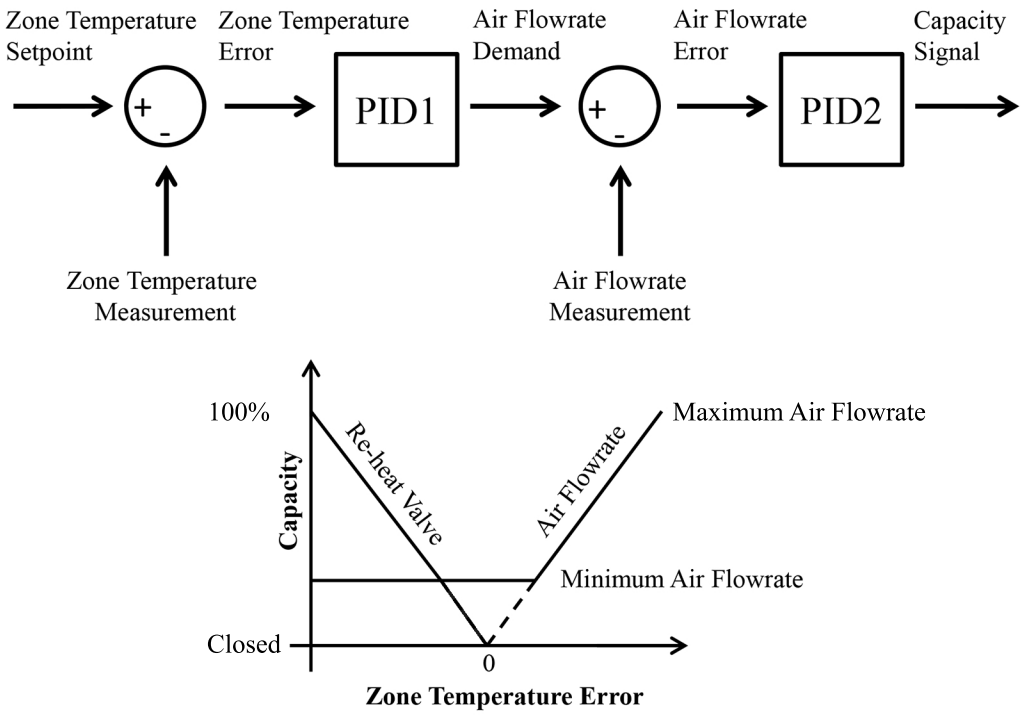

Figure 5.3 – Diagram of terminal unit control (top) and schematic of operation (bottom), based on that which is described in Montgomery and McDowall (2008) and applied in Englander and Norford (1992b) and Haves and Norford (1997).

The inputs to the controller are zone air temperature setpoint, measured zone air temperature, measured supply air temperature, and measured terminal unit air flowrate. Outputs of the controller are the damper and hot water valve positions. In general, as the cooling load decreases, the demanded air flowrate through the terminal unit is reduced until a minimum air flowrate is demanded. Once the minimum air flowrate has been reached, any further decrease in cooling load, or increase in heating load, modulates the hot water valve open. To alleviate cycling that can occur around this operating point, a hysteresis of 1 K exists between the demanding of minimum air flow and modulating of the hot water valve open. The controller consists of two cascading sub-controllers, each implemented by *Modelica.Blocks.Continuous.LimPID*, a feedback controller model that utilizes PID control with output limiting and anti-windup capabilities. The first (PID1) determines a demanded air flowrate and hot water valve position from the error between zone air temperature setpoint and measurement, while the second (PID2) determines the damper position from the error between demanded air flowrate and measured air florwate through the terminal unit. The demanded air flowrate passes through a limiter that limits the demand between a minimum and maximum value. In the case of this thesis, these are set to those found in the manufacturer's catalog for the chosen terminal unit, 0.153 m^3/s (325 cfm) and 0.944 m^3/s (2000 cfm) respectively. In practice, the minimum value should also consider the outdoor air requirements of the given zone set by ASHRAE (2010). For PID1, k_P is equal to 0.8 and T_I is equal to 600 seconds. For PID2, k_P is equal to 2 and T_I is equal to 30 seconds. PID1 gains were determined mainly based on

those used in Haves and Norford (1997), but also so that the terminal unit dampers respond to changes in duct static pressure within approximately two minutes, as seen by the response of the test building terminal unit dampers in Chapter 3. PID2 gains were tuned so that the damper response is faster than the flow demand response. It is advantageous to have the response of PID1 be slower than that of PID2 in order to allow the modulation of damper position in response to variations in duct static pressure before the modulation of demanded air flowrate. Note that the control damper model contains a first order filter on opening speed, which can be used to simulate transient dynamics associated with internal equipment controllers or limit the speed of actuation. In this case, the filter was set with a rise time of 120 seconds. Additionally, HVAC system dynamics are often slow enough to dismiss the requirement of derivative control, as seen in both Haves and Norford (1997) and Englander and Norford (1992b). See Appendix A for the modelica code implementation of the terminal unit controller model.

The total static pressure drop from the diffusers and terminal boxes equals 96.3 Pa (0.387 inwg). VAV supply duct static pressure setpoints have been found to range from 199 to 398 Pa (Haves and Norford, 1997), 373 to 622 Pa (Englander and Norford, 1992a), 199 to 597 Pa (Englander and Norford, 1992b), and 249 to 373 Pa as seen in the test building described in Chapter 3. Therefore, it was assumed the duct static pressure setpoint for this system would be 373 Pa. A detailed design and analysis of the duct system considering pressure losses through duct length and fittings is possible, for instance via the static regain method (ASHRAE, 2005), however, it is not necessary for the simple representation of common VAV system operation in this case. Therefore, the static pressure drop due to duct lengths and fittings through each terminal unit branch is 277 Pa, the difference between the static pressure setpoint of 373 Pa and that resulting from the diffusers and terminal units of 96.3 Pa. A duct splitter, implemented with *Buildings.Fluid.FixedResistances.SplitterFixedResistanceDpM*, is used to model the separation of supply air flow to each of the two terminal units and the static pressure drop associated with the duct lengths and fittings from the split to each terminal unit. An air handling unit (AHU) was selected from a manufacturer (Trane, Inc, 2012) using the design air flowrate of 1.54 m^3/s and system static pressure drop of 373 Pa (1.5 inwg). The AHU selected added an additional pressure drop of 537 Pa (2.16 inwg), from preheat and cooling coils, filters, dampers, and construction. This pressure drop was implemented using an instance of *Buildings.Fluid.FixedResistances.FixedResistanceDpM* in series with the splitter inlet. See Appendix A for the modelica code implementation of the duct and AHU static pressure drops as well as Appendix B for the manufacturer's AHU specification.

The resulting design condition of the supply fan is an air flowrate of 1.54 m^3/s (3263 cfm) at 910.7 Pa (3.66 inwg) static pressure rise. The fan model was implemented using *Buildings.Fluid.Movers.FlowMachine_Nrpm*. This model takes speed and current air flowrate as inputs and determines the pressure rise of the fan. The performance of the fan is determined based on pressure-flow data points supplied by the user from manufacturer fan curves at a single speed, which are splined together to form a functional relationship between pressure and flow. Fan similarity laws are then used to describe this pressure-flow relationship at different speeds. This method of pressure-flow modeling is not unlike that which was developed in Haves and Norford (1997). The following three data points were used to describe the pressure-flow relationship of the supply fan at a speed of 1600 RPM; (1.18 m^3/s, 746 Pa), (1.42m^3/s, 741 Pa), and (1.65 m^3/s, 697 Pa). In a similar way, the fan model uses data from manufacturer performance curves relating air flowrate to power consumption at a single speed to output fan power. The following three data points were used to describe the power-air flow relationship of the supply fan at a speed of 1600 RPM; (0 m^3/s, 0 W), (1.18m^3/s, 1641 W), and (1.65 m^3/s, 2424 W). See Appendix A for the modelica code implementation of the fan performance model and see Appendix B for the manufacturer's

supply fan performance curves.

The fan speed is controlled by a PID controller to maintain a duct static pressure just upstream of the duct splitter. The controller model is implemented using *Modelica.Blocks.Continuous.LimPID* with a k_p equal to 0.15 and T_I equal to 5 seconds. Note that the fan model also contains a first order filter on modulating speed, which can be used to simulate transient dynamics associated with internal equipment controllers or limit speed change rate, with a rise time of 30 seconds. The controller was tuned to these gains so that the fan responds to changes in static pressure setpoint within approximately two minutes, as seen by the response of the test building supply fan in Chapter 3. See Appendix A for the modelica code implementation of the supply fan controller model.

Fan power modeling for this VAV system model does not come from the use of manufacturer data points alone. As described by Englander and Norford (1992c), systems using centrifugal flow machinery, such as pumps or fans, can be placed into one of five categories depending on the operations of the system. Two of these system operation types are common to VAV air systems; 1) Variable flow, with pressure determined solely by flow and 2) Variable flow, with constant pressure offset. The first operation type considers a system where flow is the controlled variable and there exists a constant system curve. That is, the relationship between operating pressure and flow in the system is quadratic, includes the zero point, and is based on the fluid dynamics associated with pressure losses in ducts and pipes. Return fans are an example of this type of system, as they are generally controlled to maintain an air flowrate offset from the supply fan. The second operation type considers a system where the piece of centrifugal equipment must first overcome a constant pressure at all fluid flowrates before flow is achieved. An example of this is a pump pumping water up a given height from a tank and then through a pipeline. The pump must first overcome the static head associated with the height of the pipeline from the tank. This situation also applies to a VAV system in the case of a supply fan that is controlled to maintain a duct static pressure setpoint. Here, the system curve, and subsequently air flowrate, may change independently from the duct static pressure, based on the position of terminal unit dampers. It is conceivable, though theoretical in practice, that a point of operation can include zero flow with a pressure offset, if the terminal unit dampers are fully closed. To create this pressure offset, the fan must use energy at zero flow, just as the pump with a static head. This is unlike the first operation case, where zero flow corresponds to the point of zero pressure, and therefore, zero energy. Therefore, the power of the supply fan does not follow a simple cubic relation with air flowrate, as similarity laws suggest, due to the necessity of the offset at zero flow.

Englander and Norford (1992c) developed Equations 5.2 to 5.5 below to approximate the power consumption of a piece of centrifugal equipment subject to the variable flow with constant pressure offset operating condition. This model agreed well with measured data shown in that study as well as data presented in Englander and Norford (1992a). Therefore, Equations 5.2 to 5.5 are used in the simulation to model the supply fan power consumption. Note that motor efficiency curves are not considered in this model, which means the calculated power from the model is fan shaft power. See Appendix A for the modelica code implementation of this fan power model.

$$H = \left[1 - \left(\frac{p_o}{2}\right)^{1.5}\right]\left[(1-p_o)\,f^2 + p_o\right] f + \left(\frac{p_o}{2}\right)^{1.5} \tag{5.2}$$

$$H = \frac{P}{P_{max}} \tag{5.3}$$

$$p_o = \frac{p_s}{p_{max}} \tag{5.4}$$

$$f = \frac{\dot{V}}{\dot{V}_{max}} \tag{5.5}$$

Where:

H	=	Normalized Power	(-)
P_{max}	=	Maximum System Capacity Power	(W)
P	=	Operating Power	(W)
p_o	=	Normalized Duct Static Pressure Setpoint	(-)
p_{max}	=	Maximum System Capacity Duct Static Pressure Setpoint	(Pa)
p_s	=	Operating Duct Static Pressure Setpoint	(Pa)
f	=	Normalized Flowrate	(-)
$\dot{V}_{max}$	=	Maximum System Capacity Flowrate	(m^3/s)
$\dot{V}$	=	Operating Flowrate	(m^3/s)

5.1.3 Chilled Water System

A simplified chilled water system was included in the VAV system model in order to relate changes in air system performance to changes in chilled water system performance, particularly relating to chiller power. The chilled water system is designed to serve the cooling coil of the AHU described above using an ideal chiller, three-way modulating bypass valve, and constant total water flowrate. This constant flow with modulating bypass system is similar to that used in the test building described in Chapter 3.

For the cooling coil design operation and modeling, only sensible cooling is considered. Assuming the air stream transfers all of its heat to the water stream through the coil heat exchanger, and treating the air again as an ideal gas, a First Law energy balance around the cooling coil describes the required heat transfer from the air stream to the water stream through the cooling coil to satisfy the supply air temperature setpoint at the design air flowrate. The result is shown in Equation 5.6 below, where the left and right sides of the equation represent the enthalpy changes of the water and air respectively through the coil:

$$\dot{m}_{water} c_{pwater} (T_{CHWR} - T_{CHWS}) = \rho_{air} \dot{V}_{air} c_{pair} (T_{RA} - T_{SA}) \tag{5.6}$$

Where:

$\dot{m}_{water}$	=	Chilled Water Mass Flowrate	(kg/s)
c_{pwater}	=	Specific Heat Capacity of Water	(J/Kg-K)
T_{CHWR}	=	Chilled Water Return Temperature	(°C)
T_{CHWS}	=	Chilled Water Supply Temperature	(°C)
ρ_{air}	=	Density of Air	(kg/m^3)
$\dot{V}_{air}$	=	Volumetric Supply Air Flowrate	(m^3/s)
c_{pair}	=	Specific Heat Capacity of Air	(J/Kg-K)
T_{RA}	=	Return Air Dry Bulb Temperature	(°C)
T_{SA}	=	Supply Air Dry Bulb Temperature	(°C)

Using T_{CHWS} = 6 °C, T_{CHWS} = 11 °C, c_{pwater} = 4,200 J/kg-K, $\dot{V}_{air}$ = 1.54 m^3/s, ρ_{air} = 1.20 kg/m^3, c_{pair} = 1,005 J/kg-K, T_{RA} = 24.3 °C, which includes a temperature rise of 1.5 °C in zone return air from the fan, and T_{SA} = 12.78 °C, the required $\dot{m}_{water}$ = 1.02 kg/s and total sensible heat transfer through the cooling coil is 21,395 W.

The cooling coil was implemented using an instance of *Buildings.Fluid.HeatExchangers.DryEffectivenessNTU* with the heat exchanger configuration assumed to be crossflow with both streams unmixed. This model uses an effectiveness-NTU method to model the sensible heat exchange between fluids and does not consider condensation. The chilled water flow through the system originates in an ideal mass flow source and is controlled by a three-way modulating valve that diverts chilled water through a cooling coil bypass created by a pipe splitter. The chilled water return is mixed with the chilled water supply bypass in the modulating valve and exhausted to an ideal fluid sink. The ideal mass flow source, modulating bypass valve, flow splitter, and ideal fluid sink are implemented by instances of *Buildings.Fluids.Sources.MassFlowSource_T*, *Buildings.Fluids.Actuators.Valves.ThreeWayLinear*, *Buildings.Fluids.FixedResistances.SplitterFixedResistancesDpM*, and *Buildings.Fluid.Sources.FixedBoundary* respectively. The modulating bypass valve is controlled by a PID controller to maintain the supply air temperature setpoint. The controller model is implemented using *Modelica.Blocks.Continuous.LimPID* with a k_p equal to 0.06 and T_I equal to 30 seconds. Note that the modulating valve model also contains a first order filter on actuating speed, which can be used to simulate transient dynamics associated with internal equipment controllers or limit actuating speed, with a rise time of 60 seconds. The valve controller was tuned to respond relatively quickly to supply air temperature fluctuations in order to allow the terminal units to respond to disturbances with a constant supply air temperature. See Appendix A for the modelica code implementation of the cooling coil, mass flow source, modulating bypass valve, flow splitter, and chilled water valve controller.

The chiller power associated with cooling the return water to the chilled water supply setpoint is not modeled with an explicit chiller model. The added complexity of such a model is not necessary in this thesis to understand the bulk dynamics of the VAV system performing a demand response curtailment. Instead, the chiller power is approximated by taking the enthalpy difference between the return chilled water and supply chilled water and applying a constant COP equal to 3.0, as described in Equation 5.7

below. This COP is similar to the nominal COP found in the test building described in Chapter 3.

$$P_{chiller} = \frac{\dot{m}_{water} c_{pwater} (T_{CHWR} - T_{CHWS})}{COP} \tag{5.7}$$

Where:

$P_{chiller}$	=	Chiller Power	(W)
COP	=	Coefficient of Performance	(-)

Lastly, changes in chilled water supply setpoints do not occur in steps, as there are internal dynamics of a chiller that filter the actual chilled water supply temperature response. To approximate these dynamics for any adjustment to the chilled water supply setpoint, a first order filter was applied to the supply water temperature signal given to the ideal mass flow source that causes a chilled water temperature rise of 5 °C in 20 minutes, which is similar to that seen in Berardino and Nwankpa (2010).

5.2 Simulated System Performance

For all of the simulations presented in this section, the integration algorithm used in Dymola was Radau IIa - order 5 stiff, as suggested by LBNL (2012), with a tolerance of 1E-5. The output interval length was one second.

5.2.1 Design Conditions

A simulation was performed to determine the maximum capacity of the VAV system and compare operating parameters to those calculated as design values. The simulation forced the maximum air flowrate through the fan at the design static pressure setpoint of 373.2 Pa (1.5 inwg). This occurs when the terminal unit dampers for both thermal zones are fully open. This was done by subjecting both thermal zones to full cooling load (9300 W), setting the zone air temperature setpoint to 22 °C, the supply air temperature to 12.78 °C, and the chilled water temperature to 6 °C and letting the simulation run to steady state. The results of this simulation are compared to the calculated design conditions in Table 5.1 below. As can be seen, the VAV system model does a good job of simulating the design conditions determined in the previous section. The only significant discrepancy is seen in the fan power consumption, which has an approximate 18% error. This could be a result of the approximation of power consumption data points from the fan performance curve.

5.2.2 Supply Fan Power

The maximum capacity parameters of the alternative fan power model (Englander and Norford, 1992c) were set to the values obtained in the design condition simulation presented in Table 5.1. Note that this includes the fan power calculated by the similarity law method integrated into *Buildings.Fluid.Movers.FlowMachine_Nrpm*, as it is assumed that at the maximum capacity operating point the power calculated

Operating Parameter	Simulated	Designed
Fan Air Volumetric Flowrate (m^3/s)	1.540	1.540
Fan Static Pressure Rise (Pa)	910.2	910.7
Fan Speed (rpm)	1772	1764
Fan Power (W)	3054	2587
Supply Air Temperature (°C)	12.78	12.78
Cooling Coil Chilled Water Mass Flowrate (kg/s)	1.010	1.020
Cooling Coil Return Water Temperature (°C)	11.01	11.00
Chiller Power (W)	7103	7132
Zone Dry Bulb Temperature (°C)	22.55	22.78

Table 5.1 – Comparison of design conditions as designed and as simulated using the implemented VAV system model.

using the similarity law method is equal to the power calculated using the alternative method. A series of simulations were then run in order to plot the performance of the fan with respect to pressure rise across the fan and power consumption over a range of air flowrates at two different operating duct static pressure setpoints, similar to the presentation of fan performance in Englander and Norford (1992c) and Englander and Norford (1992a). These simulations slowly varied the cooling load from the design cooling load (9300 W) to zero with the minimum air flowrate setpoint on the terminal units disabled, allowing the air flowrate to go as close to zero as the model solver allowed with the fan still maintaining the static pressure setpoint. Additionally, one simulation was run to plot the performance of the model while adjusting the static pressure setpoint during a simulation. During this simulation, the operating duct static pressure setpoint was set to the actual duct static pressure to avoid a discontinuity in the power calculation, which would occur when the duct static pressure setpoint is adjusted by equations 5.2 and 5.4. The two duct static pressure setpoints used for the tests were the design setpoint of 373.2 Pa (1.5 inwg) and 248.8 Pa (1.0 inwg). Each simulation began by allowing the system operation to come to steady state at design conditions, before implementing the slow decrease in cooling load.

The results are plotted in Figure 5.4 on the following page. For comparison, the plots of operating power and normalized power also contain a curve indicating the power calculated as a result of a fan power model which uses manufacturer's data and similarity laws. Notice that at zero flow, the pressure rise across the fan indeed approaches the static pressure setpoint. In addition, the choice of using the actual duct static pressure as the operating duct static pressure setpoint allows for a well-behaved continuous power model during the transition from one static pressure setpoint to another. Lastly, the normalized power curve intersects the y-axis at 0.093. This, as well as the general form of the curve, match well with the modeled and measured data presented in Englander and Norford (1992c) and Englander and Norford (1992a) of supply fans equipped with VFDs maintaining duct static pressure setpoints in VAV systems. Note that the curl of points at the upper end of the pressure curves result from initial fan speed adjustments to maintain duct static pressure when the terminal unit dampers first begin to close.

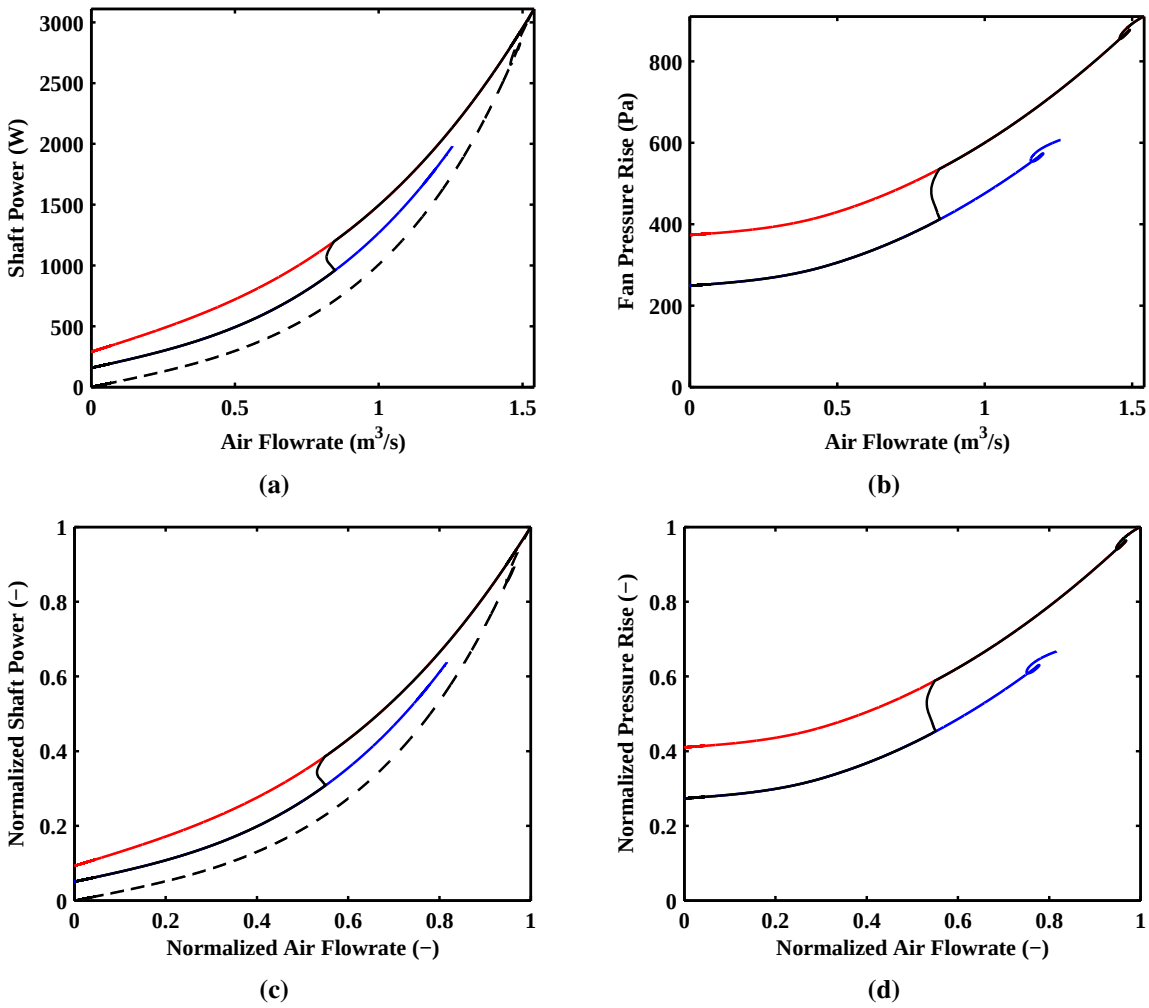

Figure 5.4 – Simulated performance of the supply fan over a range of air flowrates at static pressure setpoints of 373.2 Pa (red), 248.8 Pa (blue), and variable (black) with respect to a) power, b) fan pressure rise, c) normalized power, and d) normalized pressure rise using the fan performance model developed in Englander and Norford (1992c). Power determined from similarity laws alone is plotted (dashed black) for comparison.

5.2.3 Step Responses

A group of simulations was run to test the performance of the VAV system model in response to changes in cooling load and various system setpoints, which include zone air temperature, duct static pressure, supply air temperature, and chilled water supply temperature. For each simulation, the normal setpoints were a zone dry bulb temperature of 22 °C, static pressure of 373.2 Pa, and supply air temperature of 12.78 °C. A moderate cooling load of 5300 W was applied to both thermal zones and a chilled water supply temperature of 6 °C was used. The results of the simulations are plotted in Figures 5.5 to 5.9 on the following pages. In each plot, step changes in setpoints or operating conditions were implemented at zero seconds, and changes were reset after 2000 seconds.

The first simulation introduces a step change in cooling load from the normal 5300 W to -1300 W for thermal zone two, which represents a switch in terminal unit operation from cooling to heating. The results are plotted in Figure 5.5. When the load is adjusted, the zone two terminal unit dampers begin to close, which reduces the system air flowrate and increases the static pressure in duct until the supply fan modulates down. While the duct pressure is raised, notice that the zone one terminal unit dampers close slightly in order to maintain the demanded air flowrate through them. Also notice a small dip in supply air temperature until the chilled water valve modulates closed to maintain supply air temperature. Once the zone two terminal unit dampers reach the position for minimum flow, the reheat valve begins to modulate open until the new zone heating load is satisfied. The total system air flowrate is reduced, along with the fan power and chiller power. When the system returns to normal conditions, the reheat valve of the zone two terminal unit modulates until closed, at which point the dampers begin to modulate open. The opening of the terminal unit dampers reduces the static pressure in the duct momentarily, during which time the zone one terminal unit dampers open slightly to maintain the demanded air flowrate. The modulation of terminal unit dampers, the regain of static pressure setpoint, fan power reduction, and chiller power reduction occurs in approximately 100 seconds from step change implementation. Overall, the zone temperature setpoint of each zone is maintained very well.

The second simulation introduces a step change in duct static pressure setpoint from the normal 373.2 Pa to 248.8 Pa. The results are plotted in Figure 5.6. Upon implementation of the static pressure adjustment, the supply fan speed slows to meet the new static pressure setpoint. The total air flowrate through the system is maintained relatively constant through this process because the terminal unit dampers are tuned to respond faster than the supply fan to fluctuations in duct static pressure. In general, this keeps the supply fan from hunting the static pressure setpoint as terminal units vary their damper position in response to changes in load. No significant change in air flowrate leads to virtually no change in supply air temperature, zone air temperature, and chiller power consumption. Fan power is reduced slightly due to the reduction in static pressure. The modulation of the fan to meet the new static pressure setpoint occurs in approximately 120 seconds.

The third simulation introduces a step change in zone air temperature setpoint for both thermal zones from the normal 22 °C to 25 °C. The results are plotted in Figure 5.7. The change in zone air temperature setpoint has an immediate effect on the demanded air flowrate through the terminal units, and the dampers modulate quickly closed, within 60 seconds of the change. This is in contrast to the step change in load of the first simulation, where the dampers do not modulate closed until the zone experiences a change in temperature. In summary, this third simulation directly impacts PID2 of the terminal unit controller described in the previous section, whereas the first simulation directly impacts PID1, which is tuned

to respond slower. Once the terminal unit dampers reach their minimum position, the reheat valve is modulated open until the new zone air setpoint is reached, which occurs 320 seconds after step change implementation. At this point, the reheat valve is modulated to closed and the dampers are modulated open to a lesser degree than the normal condition. The reheat valve does not stay open because there is still ultimately a cooling load in the zone. However, this cooling load can be met with less supply air due to contributions of convective cooling by construction elements that are slow to respond to changes in air temperature due to their thermal capacitance. Therefore, the resulting damper position is smaller. Notice that this modulation process of the damper position causes an initial decrease in fan air flowrate and chiller power until the new zone air setpoint is reached, at which point these values increase slightly and remain steady for the duration of the setpoint change. Upon returning to normal conditions, the terminal unit dampers are modulated wide open to cool the space until the normal zone air setpoint is reached, during which time the fan air flowrate and chiller power consumption is increased above the normal condition.

The fourth simulation introduces a step change in supply air temperature setpoint from the normal value of 12.78 °C to 17.78 °C. The results are plotted in Figure 5.8. The supply air temperature increases sharply in response to the setpoint change as the chilled water valve closes. The new supply air temperature is reached in approximately 90 seconds. The increase in supply air temperature causes the zone air temperatures to rise slowly, which then causes the terminal unit dampers to slowly modulate open. They end up reaching the fully open position after about 240 seconds, indicating the new supply air temperature is not cool enough to meet the cooling loads of each zone with maximum supply air. Notice that the chiller initially experiences a sharp drop in power consumption followed by a slow rise to a steady value, reached when the terminal unit dampers reach their maximum position. The steady state power consumption of the chiller during the setpoint change is actually slightly more than observed during normal operation. An increase in fan power is also observed, though without an initial reduction. Both phenomenon are ultimately due to the increase in system air flowrate and will be explored further in the next section with regard to implementing supply air temperature setpoint increase as a curtailment strategy. Once the supply air temperature setpoint is returned to its normal value, the chiller power is increased for approximately 500 seconds to cool the supply air until the normal operating temperature is reached, at which point the system returns to normal performance.

The last simulation introduces a step change in chilled water supply temperature from the normal value of 6 °C to 9°C. The results are plotted in Figure 5.9. A similar trend to raising the supply air temperature is seen, however, over a longer period of time due to the time it takes the chilled water supply temperature to rise to the new setpoint, approximately 20 minutes. Once again, after an initial sharp decrease, chiller power and fan power are ultimately increased during the setpoint change due to the increase in system air flowrate. Additionally, because of an increase in supply air temperature, is is apparent that the chilled water valve is starved open.

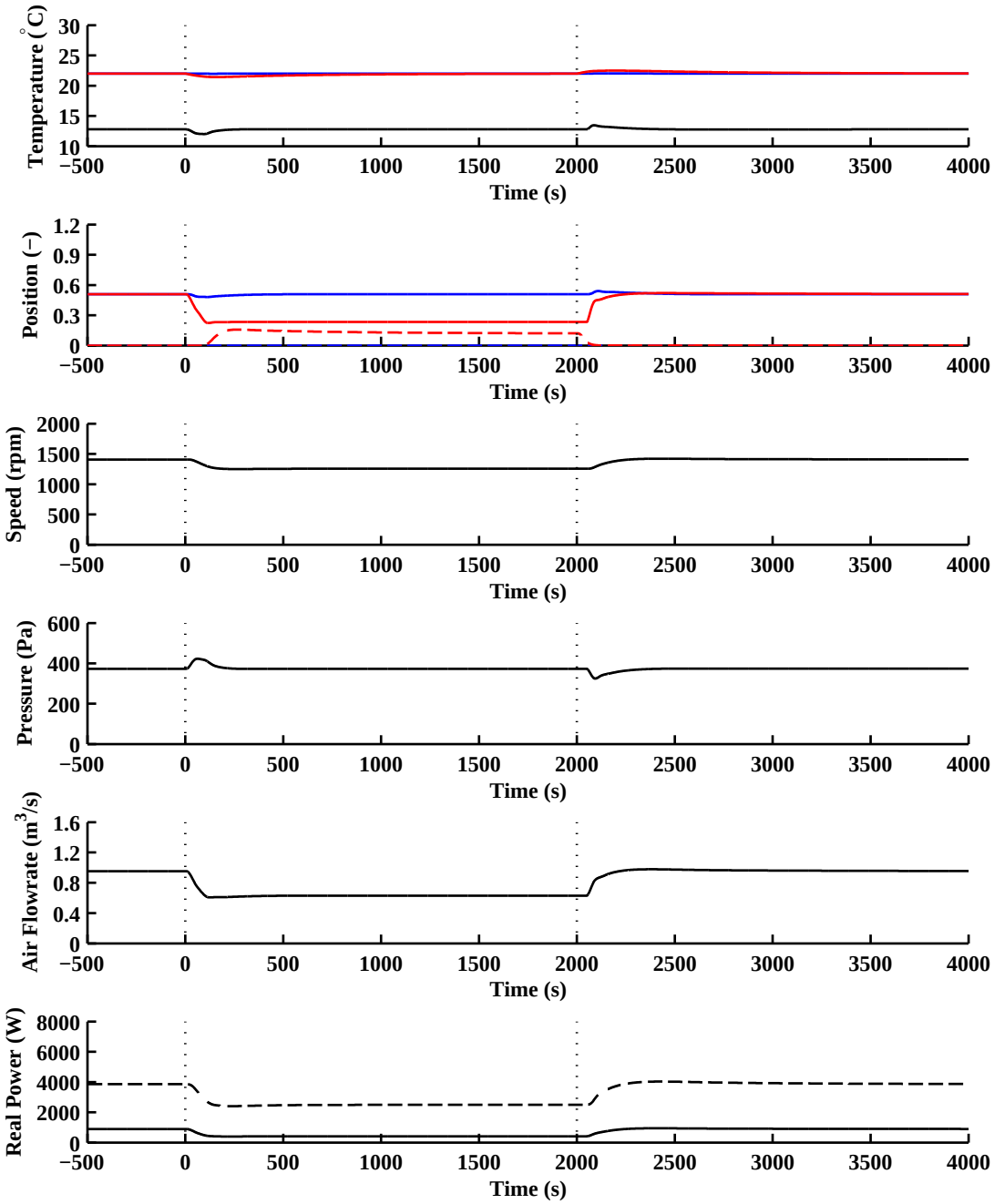

Figure 5.5 – Simulated response of a representative VAV system to a step change in cooling load from 5300 W to -1300 W in thermal zone 2 and a constant cooling load of 5300 W in thermal zone 1. Plots are shown for (first) zone air dry bulb temperature for thermal zones 1 (blue) and 2 (red) as well as supply air temperature (black), (second) terminal unit damper position (solid) and reheat valve position (dashed) for each thermal zone, (third) supply fan speed, (fourth) duct static pressure, (fifth) supply fan air flowrate, and (sixth) fan power (solid) and chiller power (dashed).

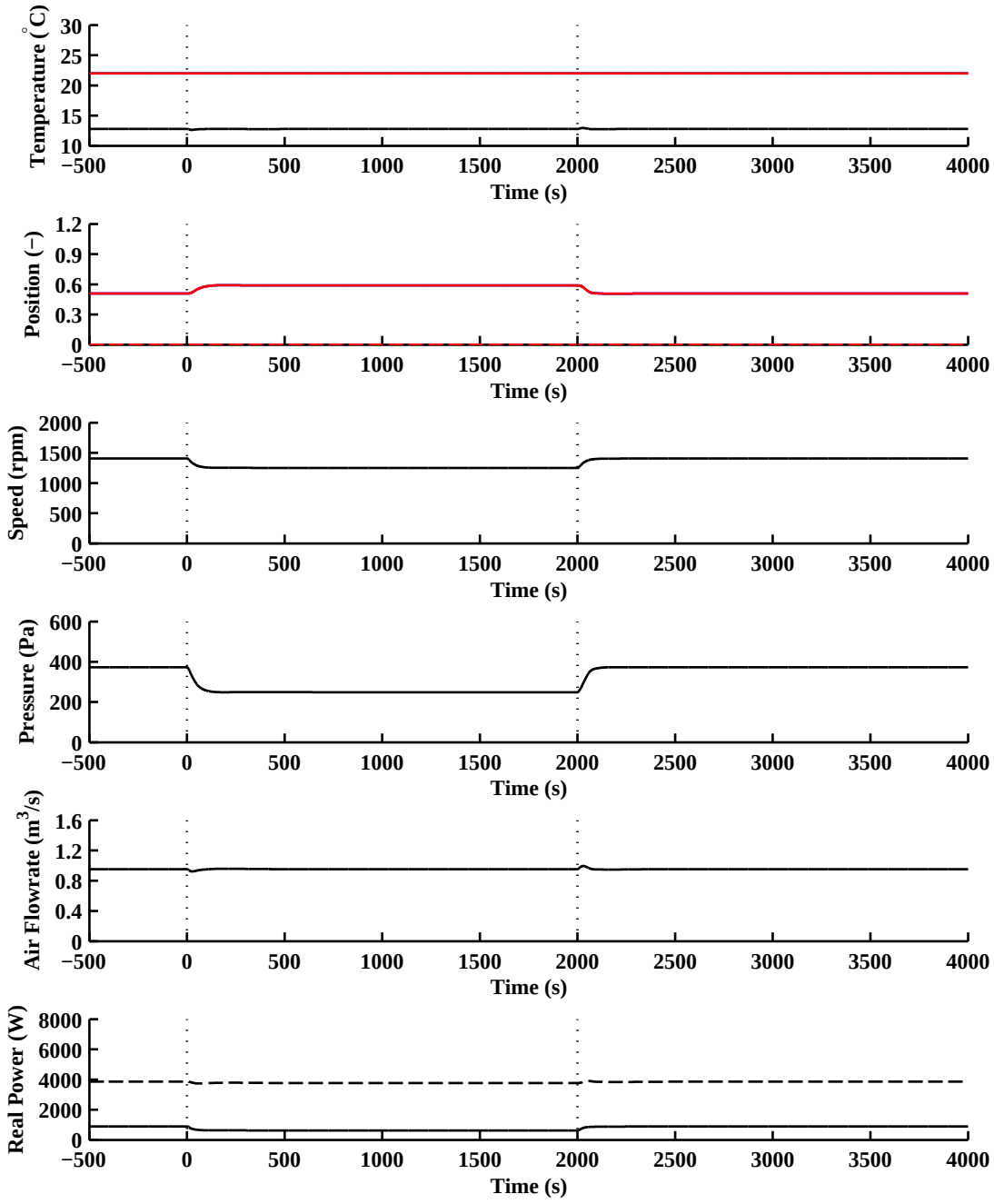

Figure 5.6 – Simulated response of a representative VAV system to a step change in duct static pressure setpoint from 373.2 Pa to 248.8 Pa. Plots are shown for (first) zone air dry bulb temperature for thermal zones 1 (blue) and 2 (red) as well as supply air temperature (black), (second) terminal unit damper position (solid) and reheat valve position (dashed) for each thermal zone, (third) supply fan speed, (fourth) duct static pressure, (fifth) supply fan air flowrate, and (sixth) fan power (solid) and chiller power (dashed).

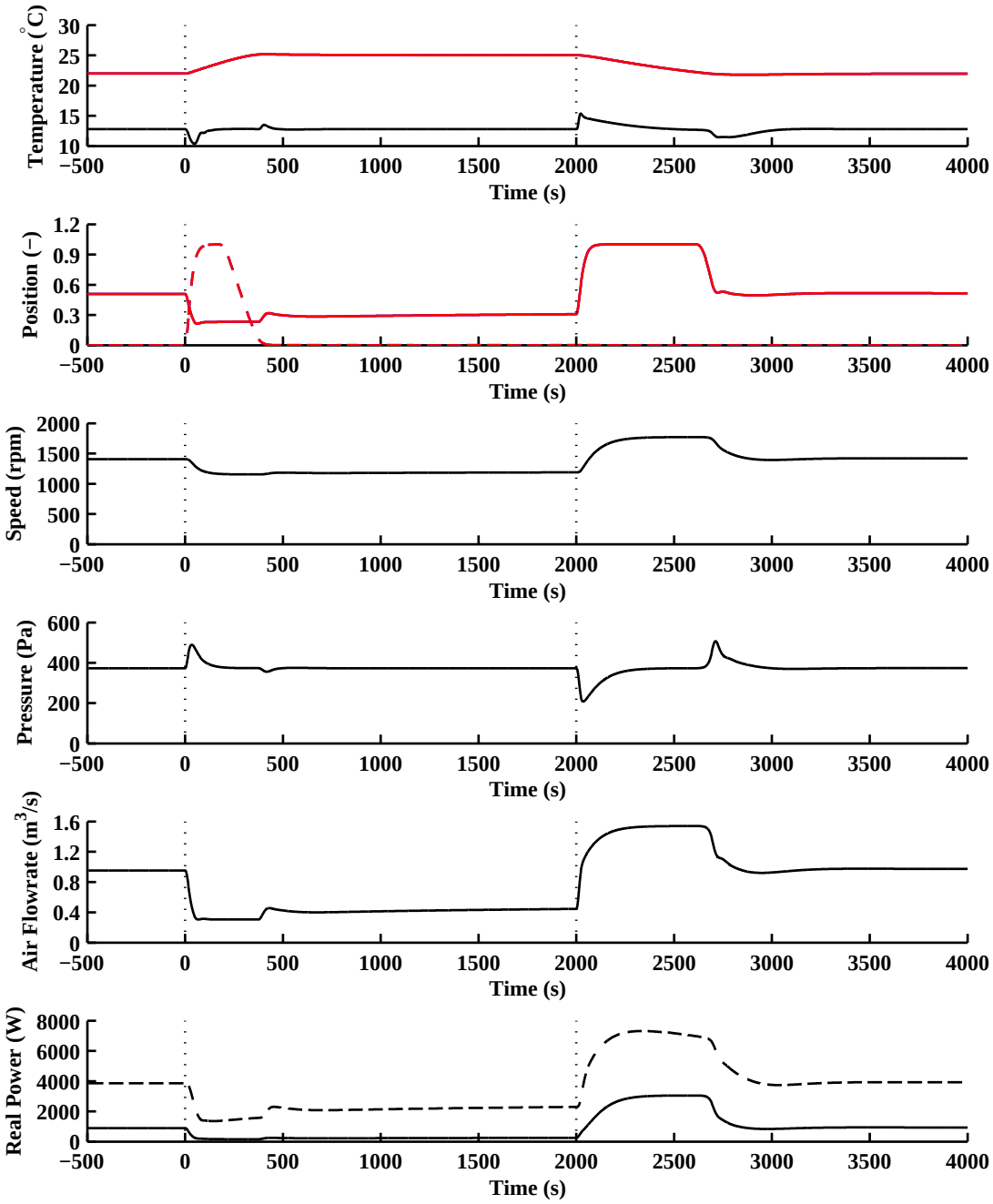

Figure 5.7 – Simulated response of a representative VAV system to a step change in zone air temperature setpoint from 22 °C to 25 °C. Plots are shown for (first) zone air dry bulb temperature for thermal zones 1 (blue) and 2 (red) as well as supply air temperature (black), (second) terminal unit damper position (solid) and reheat valve position (dashed) for each thermal zone, (third) supply fan speed, (fourth) duct static pressure, (fifth) supply fan air flowrate, and (sixth) fan power (solid) and chiller power (dashed).

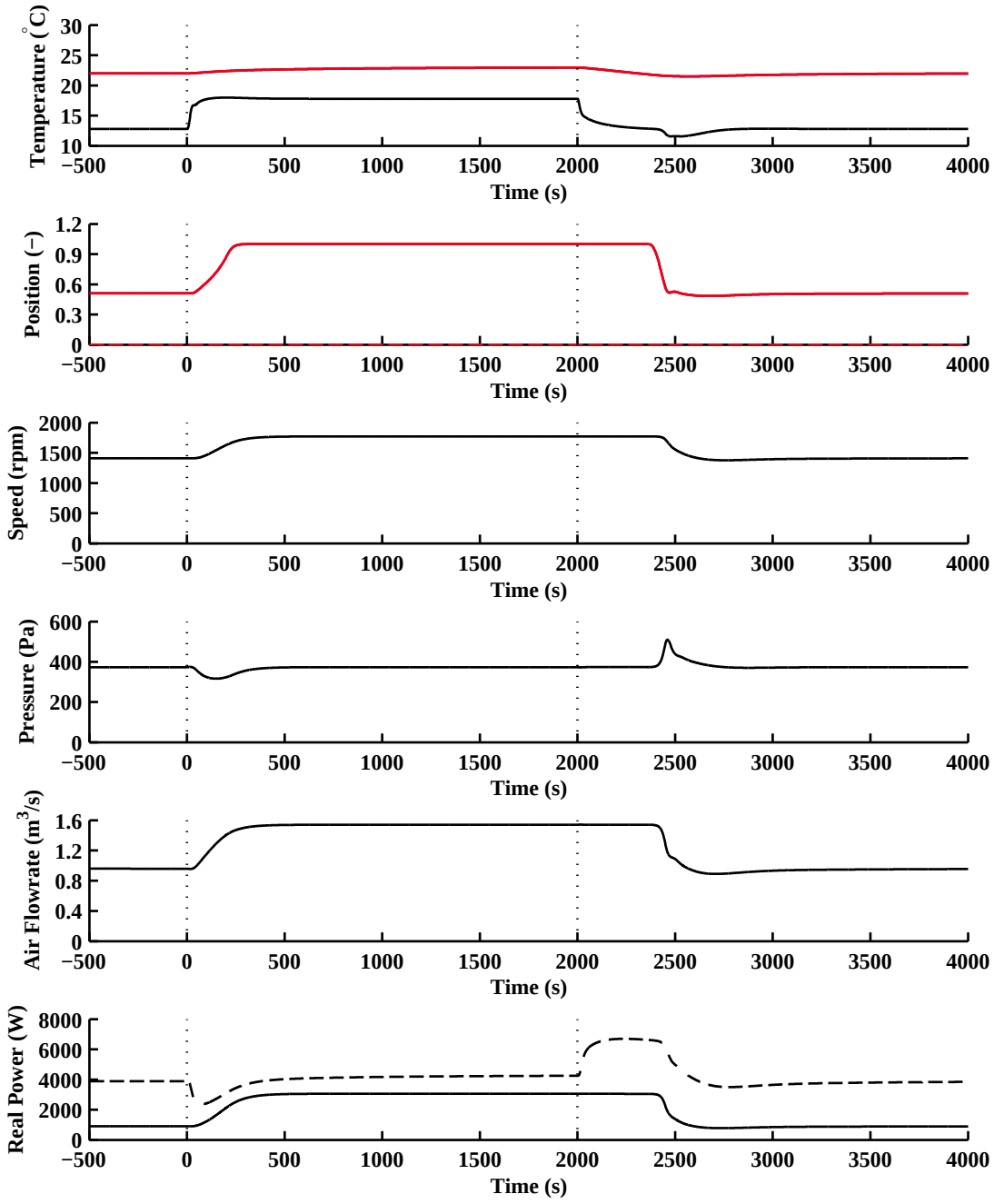

Figure 5.8 – Simulated response of a representative VAV system to a step change in supply air temperature setpoint from 12.78 °C to 17.78 °C. Plots are shown for (first) zone air dry bulb temperature for thermal zones 1 (blue) and 2 (red) as well as supply air temperature (black), (second) terminal unit damper position (solid) and reheat valve position (dashed) for each thermal zone, (third) supply fan speed, (fourth) duct static pressure, (fifth) supply fan air flowrate, and (sixth) fan power (solid) and chiller power (dashed).

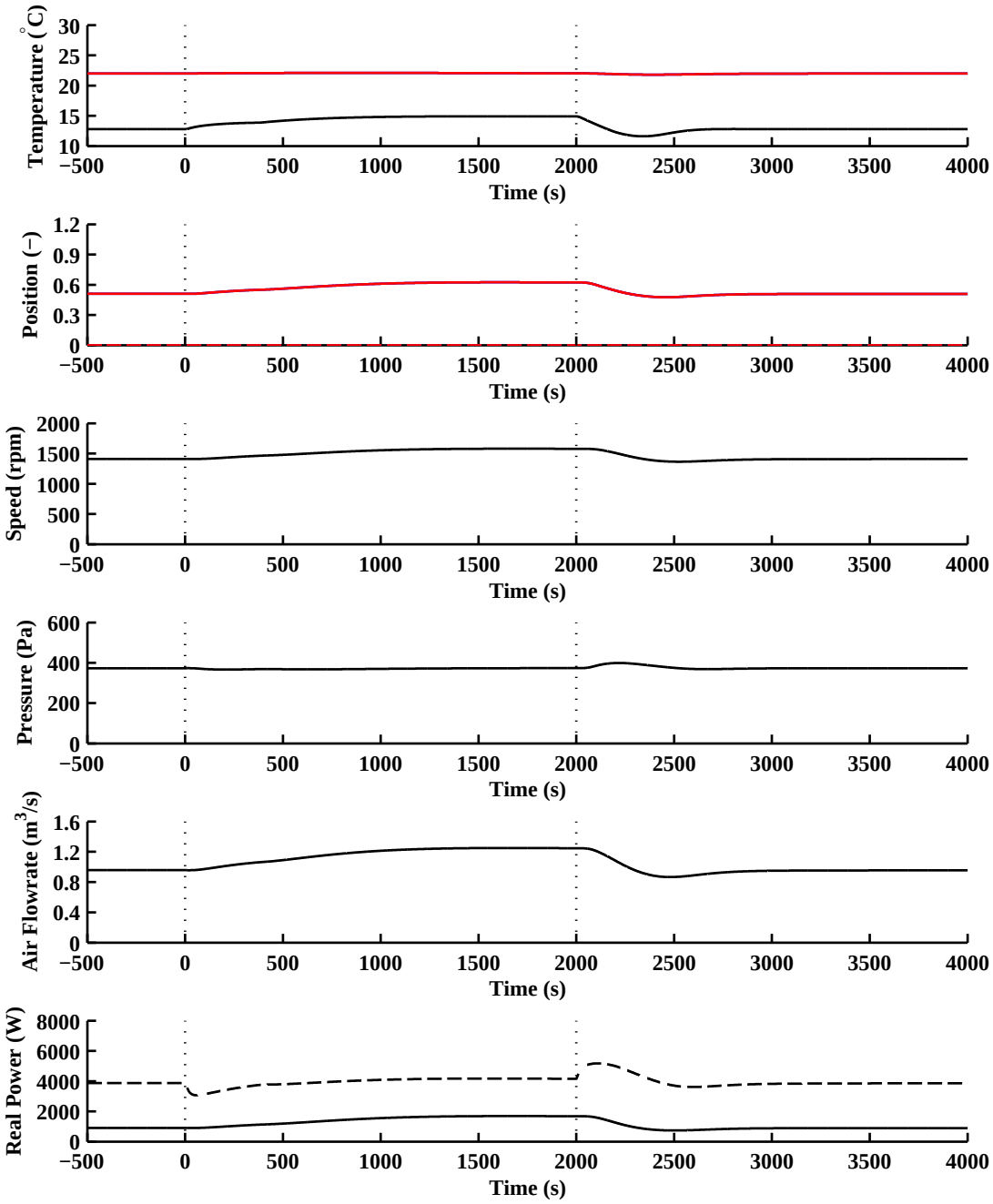

Figure 5.9 – Simulated response of a representative VAV system to a step change in chilled water temperature setpoint from 6 °C to 9°C. Plots are shown for (first) zone air dry bulb temperature for thermal zones 1 (blue) and 2 (red) as well as supply air temperature (black), (second) terminal unit damper position (solid) and reheat valve position (dashed) for each thermal zone, (third) supply fan speed, (fourth) duct static pressure, (fifth) supply fan air flowrate, and (sixth) fan power (solid) and chiller power (dashed).

5.3 Curtailment Characterization Setup

Four batches of simulations were run in order to evaluate the performance of four different VAV curtailment strategies under a wide range of operating conditions. This evaluation includes both how and why variations occur in the power consumption curtailment observed at 10 and 30 minutes after strategy implementation under different curtailment intensities and load conditions. The strategies tested include a zone dry bulb temperature setpoint adjustment (ZDBA), static pressure setpoint adjustment (SPA), supply air temperature setpoint adjustment (STA), and chilled water temperature setpoint adjustment (CWA). For each of the four curtailment strategies, the curtailment strategy was varied over a range of intensities, according to Table 5.2 below. For each strategy intensity, the cooling load applied to each zone was varied from the design cooling load of 9300 W to 1300 W by increments of 1000 W. Note that the normal operating zone setpoint temperature is 22 °C in order to include the case where the system is operating just beyond its design capacity. Also, for the STA and CWA tests, the fan speed was locked at the point of curtailment implementation to avoid speed-up for increased air flow, as suggested in Motegi et al. (2007) and Raustad and Basarkar (2011). Lastly, all simulations were run with the reheat coil in the terminal units disabled, which is representative of a building operating in summer mode with no heating available.

The simulations were run for 10,000 seconds with the first 5,000 seconds under normal operating setpoints and the second 5,000 seconds under curtailment setpoints, which were implemented as step changes at 5,000 seconds. Each zone air temperature and construction element was initialized to the normal operating temperature setpoint of 22 °C. As noted above for these simulations, the operating conditions of each zone were identical and the air system design is symmetric, so that inter-zone interactions are not considered.

Curtailment Strategy	Normal Setpoint	Intensity Range	Intensity Increment
Zone Dry Bulb Temeprature Setpoint Adjustment	22 °C	plus 0 to 5 °C	0.5 °C
Static Pressure Setpoint Adjustment	910.2 Pa	minus 0 to 80 %	5%
Supply Air Temperature Adjustment	12.78 °C	plus 0 to 5 °C	0.5 °C
Chilled Water Setpoint Adjustment	6 °C	plus 0 to 5 °C	0.5 °C

Table 5.2 – Curtailment strategy intensities implemented for simulated VAV system demand response curtailment evaluations.

Each of the four simulation groups were run in batches controlled by a MATLAB script (file.m). This script initialized inputs and saved them as MATLAB data files to the hard disk, wrote a Dymola script file (file.mos) that outlined simulation and output parameters, commanded Dymola to run the script file, collected the data output from the simulation, and saved the data to comma-separated files on the hard disk for future processing. For Dymola, the integration algorithm used was Radau IIa - order 5 stiff, as suggested by LBNL (2012), with a tolerance of 1E-5. The output interval length was one second. The simulation time for each individual simulation in Dymola was 20 seconds, where 15 of those seconds were used for model compilation and translation. For each simulation batch in MATLAB, the time was 45 minutes except for the static pressure adjustment batch which took approximately one hour because of a larger number of simulations.

5.4 Curtailment Characterization Results

Results of the simulations are plotted in Figures 5.10 to 5.21 of this section and are organized by curtailment strategy. Of two sets of plots, the first presents dynamic performance data of pertinent HVAC parameters over the time interval of interest. A select number of operating conditions was chosen to plot, as plotting all of the data for all simulations is unnecessary and would lack clarity. The conditions plotted were the 4 °C temperature setpoint adjustment for ZDBA, STA, and CWA, or the 50% static pressure setpoint reduction for SPA and the 9300 W, 6300 W, and 3300 W load cases, as they clearly show the transients of interest through the progression of load conditions. The parameters plotted include zone air dry bulb temperature, supply air temperature, terminal unit damper position, terminal unit reheat valve position, duct static pressure, fan air flowrate, chilled water valve position, fan power, and chiller power. Note that because of identical operating conditions for each of the two zones, only the data from thermal zone one is presented and referenced in the discussions below.

The second set of data presents characterization curves formulated by the plotting of a value of interest with curtailment strategy intensity and load condition, which present clear correlations between these variables. The values of interest include both the magnitude (α) of and normalized (β) total power reduction, chiller power reduction, fan power reduction, and fan air flowrate reduction, as defined by Equations 5.8 and 5.9 below, at 10 minutes after the curtailment implementation. This time after implementation is representative of spinning reserve provision. An additional value of interest is the time required for the zone temperature to rise. A rise of 2 °C is presented on the following pages. This value is modified for the ZDBA tests to represent the time required for the zone dry bulb temperature to reach within 5% of the new setpoint. For all tests, a value of zero indicates that the temperature did not rise the indicated amount during the simulation time period.

$$\alpha_\theta = \theta_{normal} - \theta_{reduced} \tag{5.8}$$

$$\beta_\theta = \frac{\theta_{reduced}}{\theta_{normal}} \tag{5.9}$$

Where:

θ	=	Parameter Value
α_θ	=	Reduction Magnitude of θ
β_θ	=	Normalized Reduction of θ

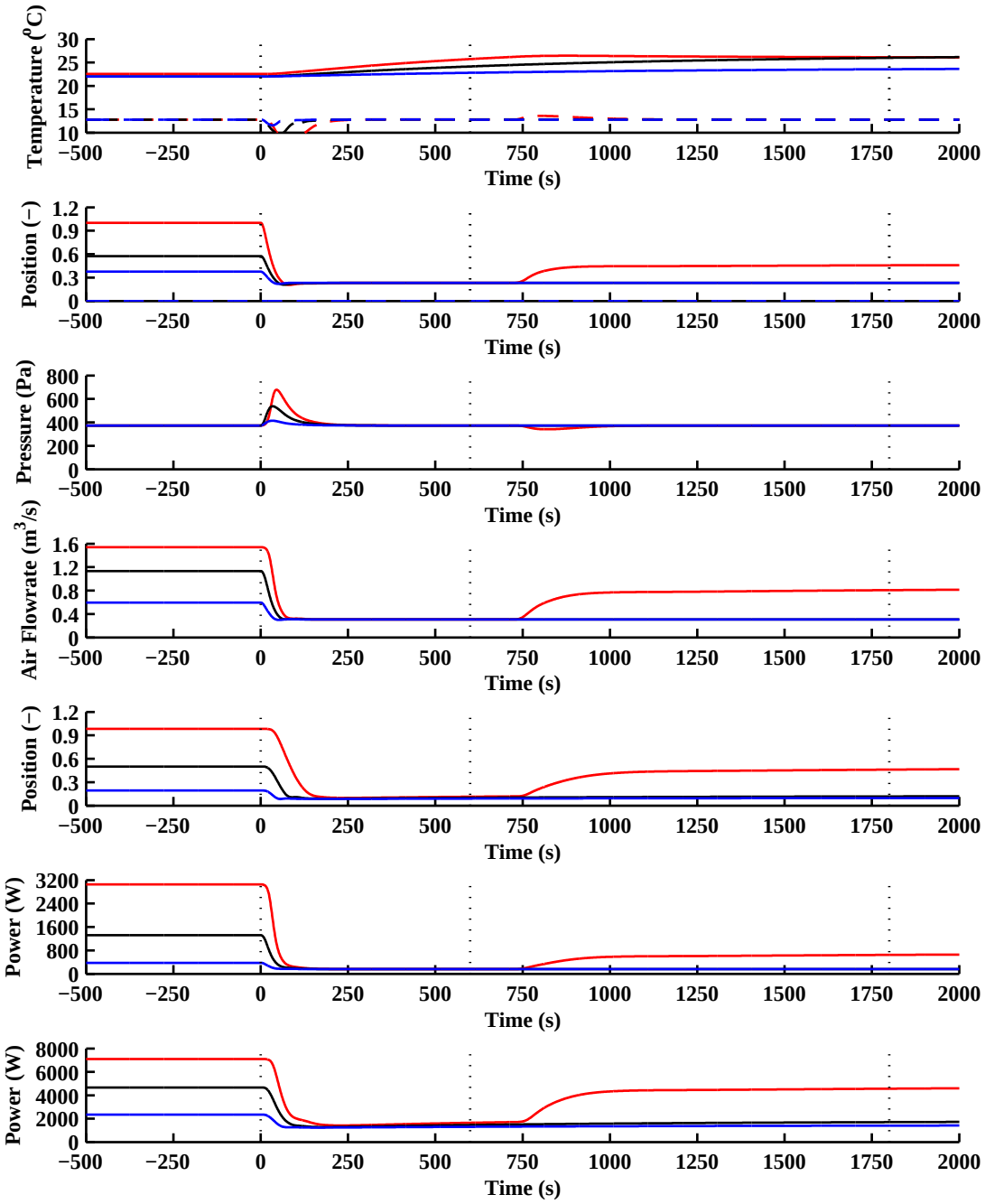

Figure 5.10 – Simulated response of a representative VAV system to a step change in zone air temperature setpoint from 22 °C to 26 °C at thermal zone cooling load intensities of 9300 W (red), 6300 W (black), and 3300 W (blue). Plots are shown for (first) zone air dry bulb temperature, (second) terminal unit damper position (solid) and reheat valve position (dashed), (third) duct static pressure, (fourth) supply fan air flowrate, (fifth) chilled water valve position, (sixth) supply fan power, and (seventh) chiller power. Dotted lines indicate the starting, 10-minute, and 30-minute points of curtailment implementation.

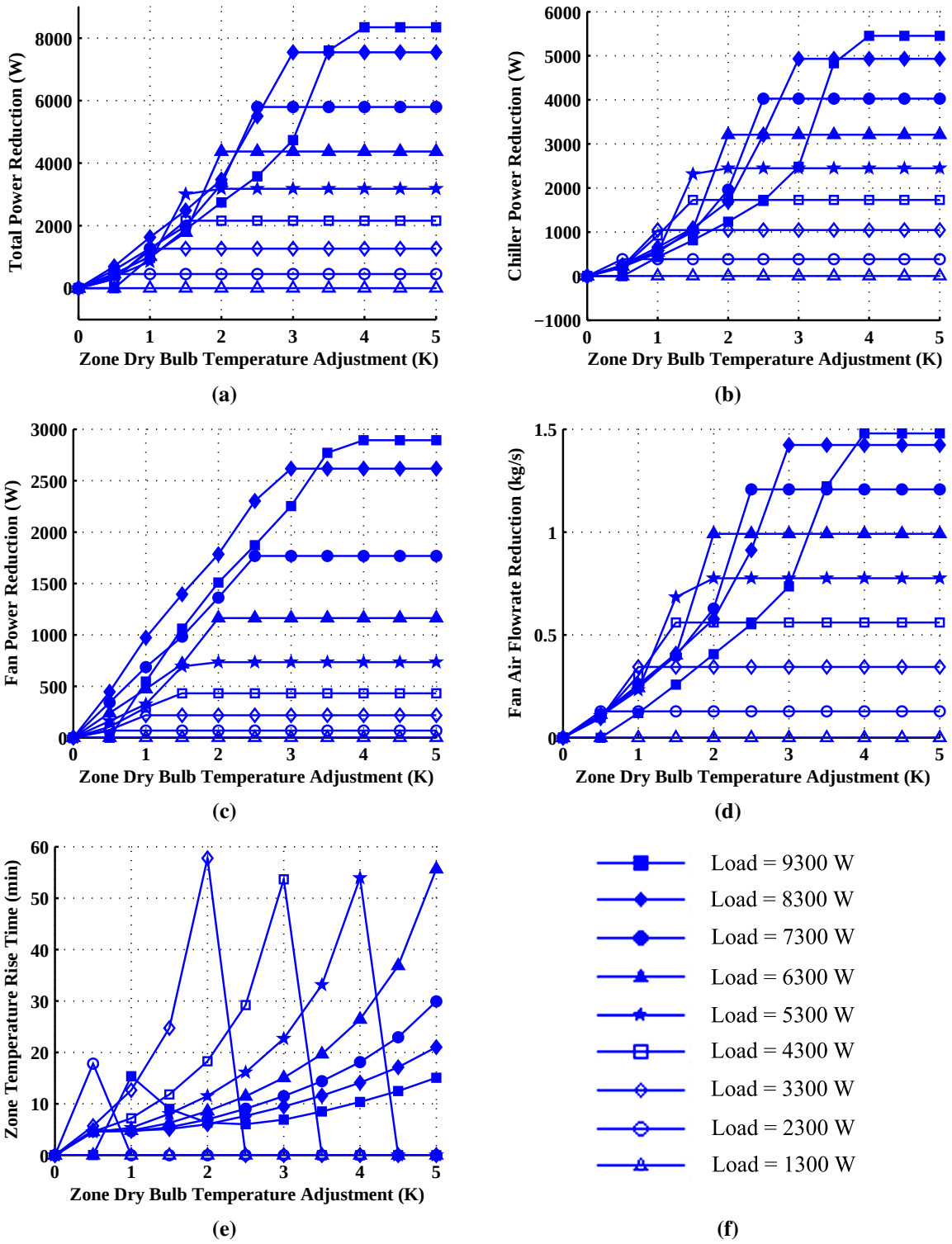

Figure 5.11 – Reduction magnitude characterization curves for ZDBA for a) total power, b) chiller power, c) fan power, and d) the supply fan air flowrate measured at 10 minutes after implementation. The time for thermal zone temperature rise to new setpoint is plotted in e).

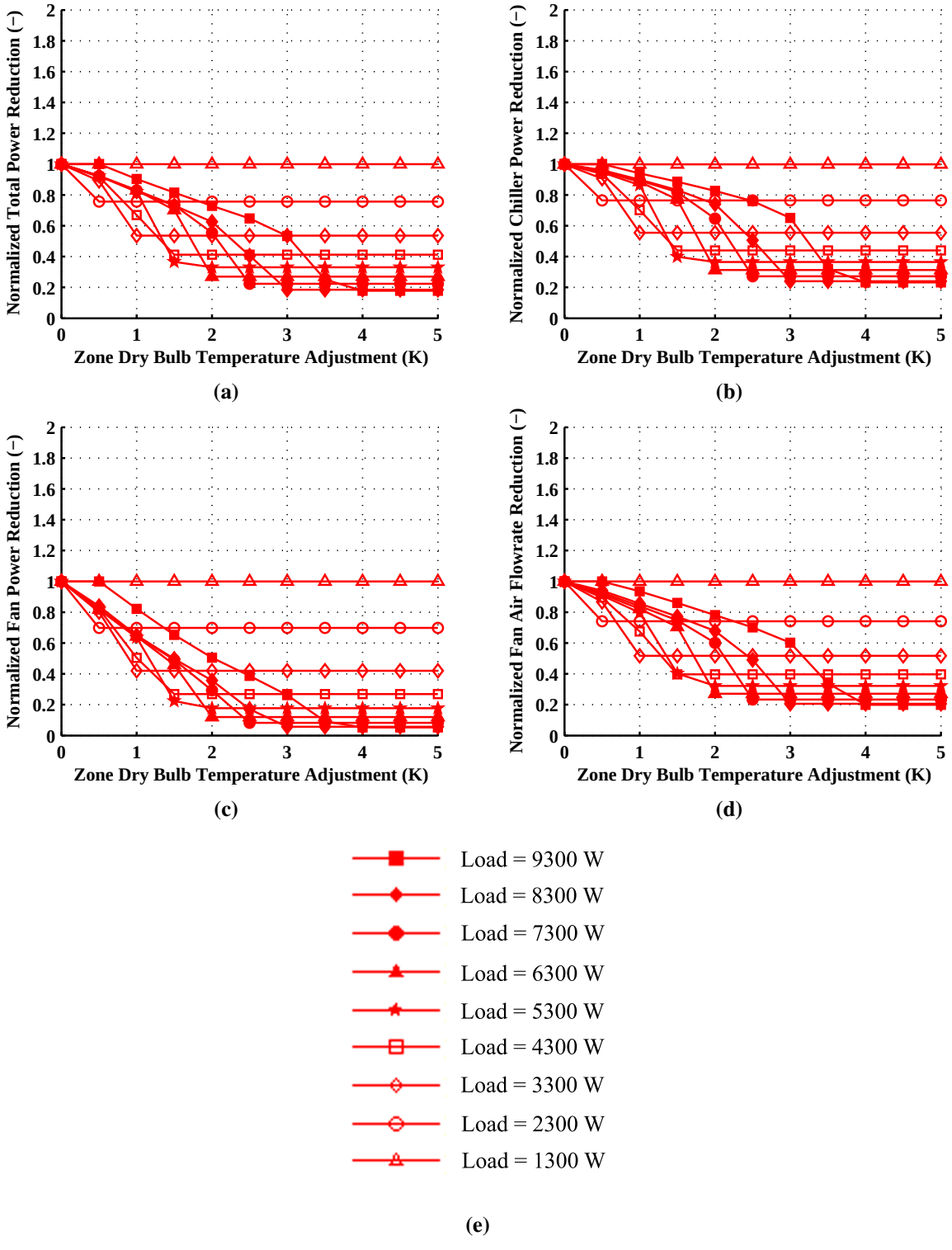

Figure 5.12 – Normalized reduction characterization curves for ZDBA for a) total power, b) chiller power, c) fan power, and d) the supply fan air flowrate measured at 10 minutes after implementation.

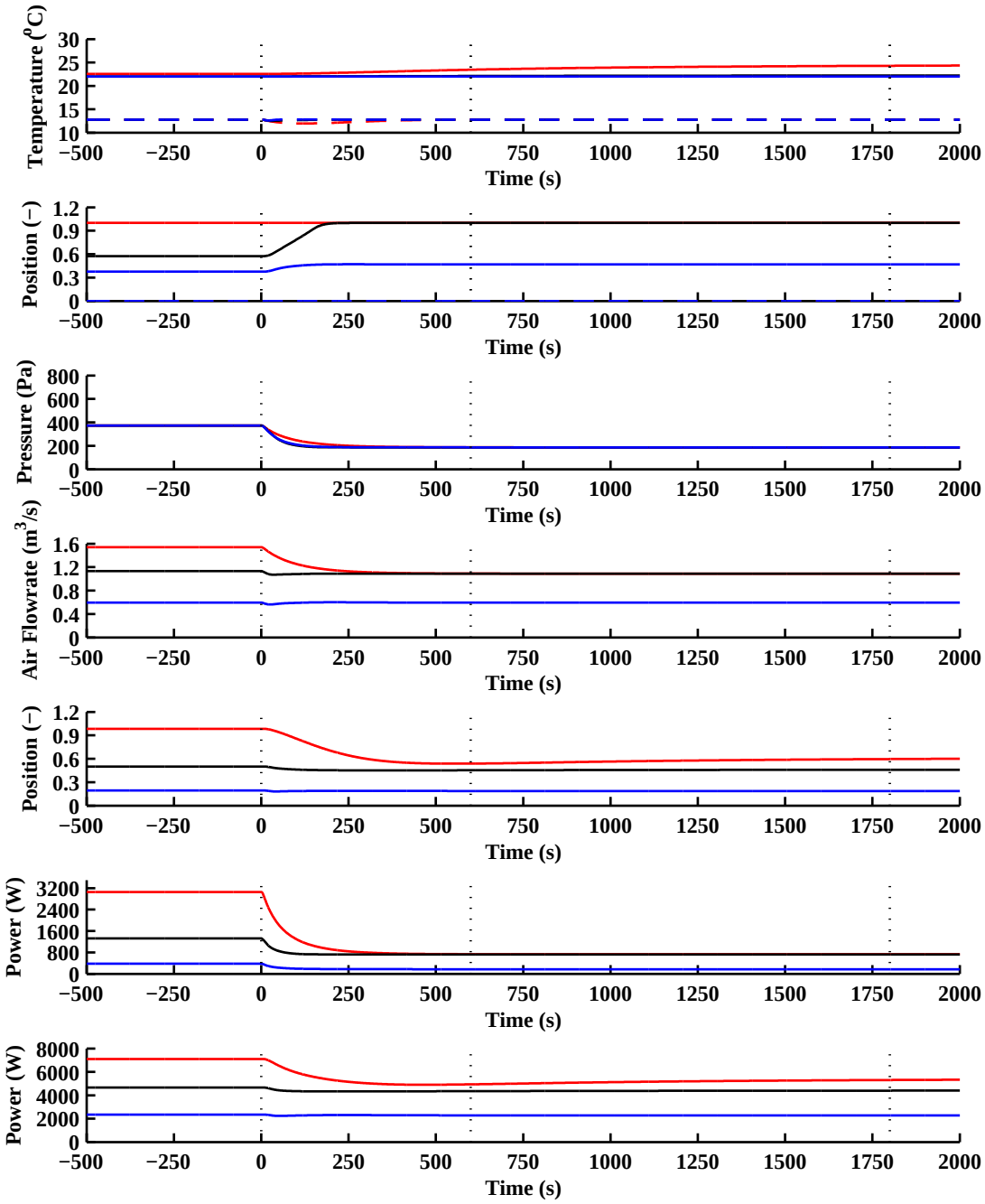

Figure 5.13 – Simulated response of a representative VAV system to a step change in duct static pressure setpoint from 373.2 Pa to 186.6 Pa at thermal zone cooling load intensities of 9300 W (red), 6300 W (black), and 3300 W (blue). Plots are shown for (first) zone air dry bulb temperature, (second) terminal unit damper position (solid) and reheat valve position (dashed), (third) duct static pressure, (fourth) supply fan air flowrate, (fifth) chilled water valve position, (sixth) supply fan power, and (seventh) chiller power. Dotted lines indicate the starting, 10-minute, and 30-minute points of curtailment implementation.

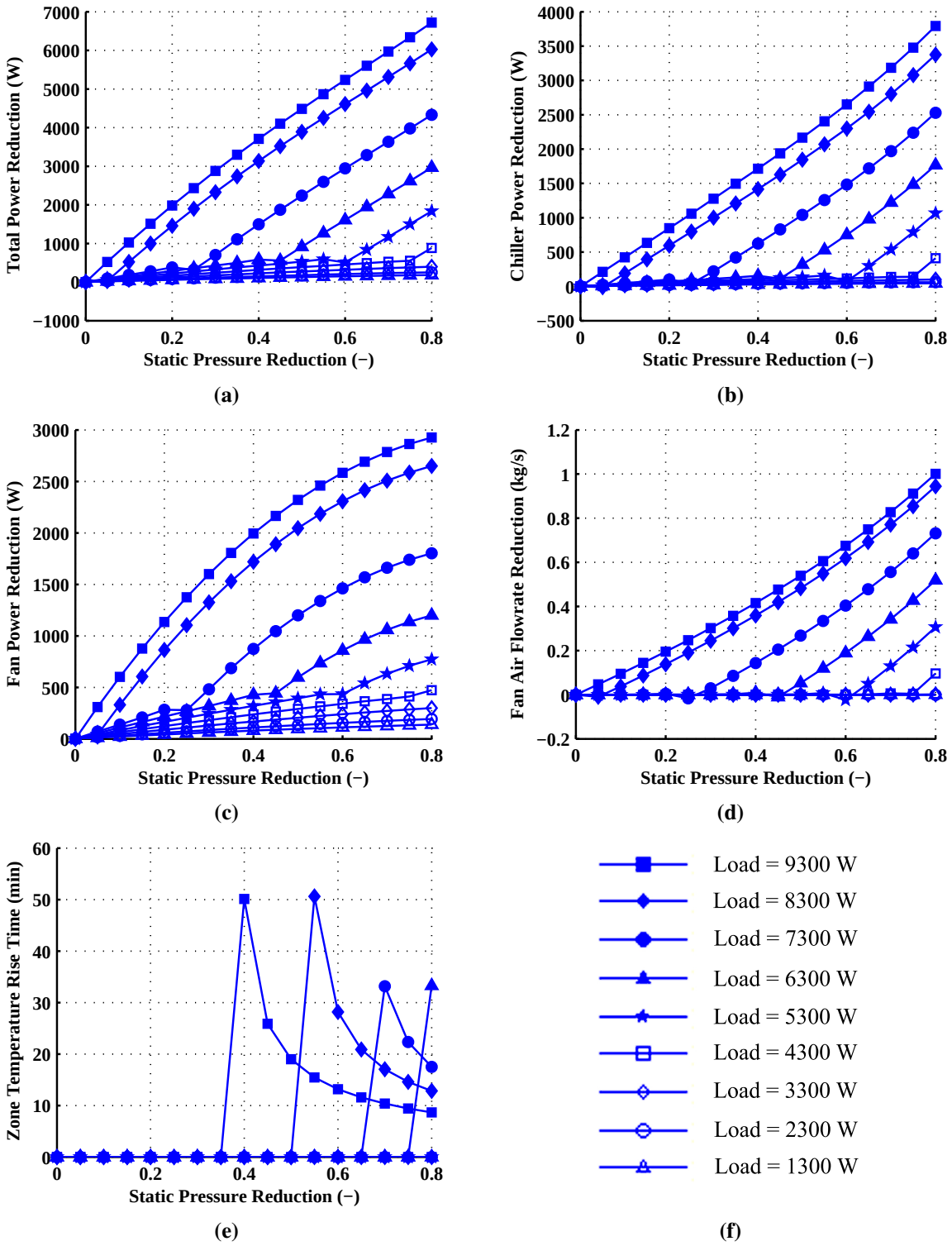

Figure 5.14 – Reduction magnitude characterization curves for SPA for a) total power, b) chiller power, c) fan power, and d) the supply fan air flowrate measured at 10 minutes after implementation. The time for thermal zone temperature rise of 2 °C is plotted in e).

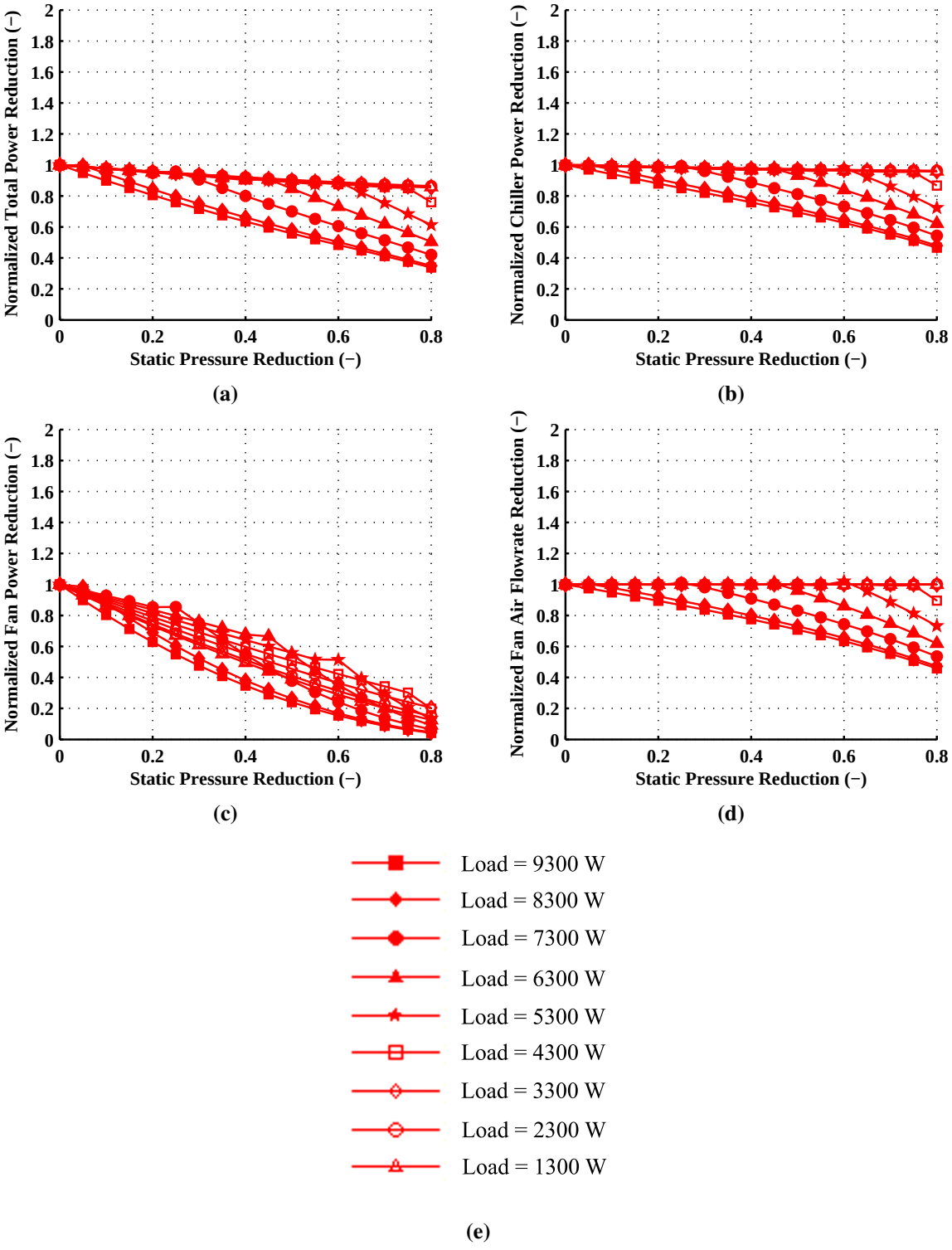

Figure 5.15 – Normalized reduction characterization curves for SPA for a) total power, b) chiller power, c) fan power, and d) supply fan air flowrate measured at 10 minutes after implementation.

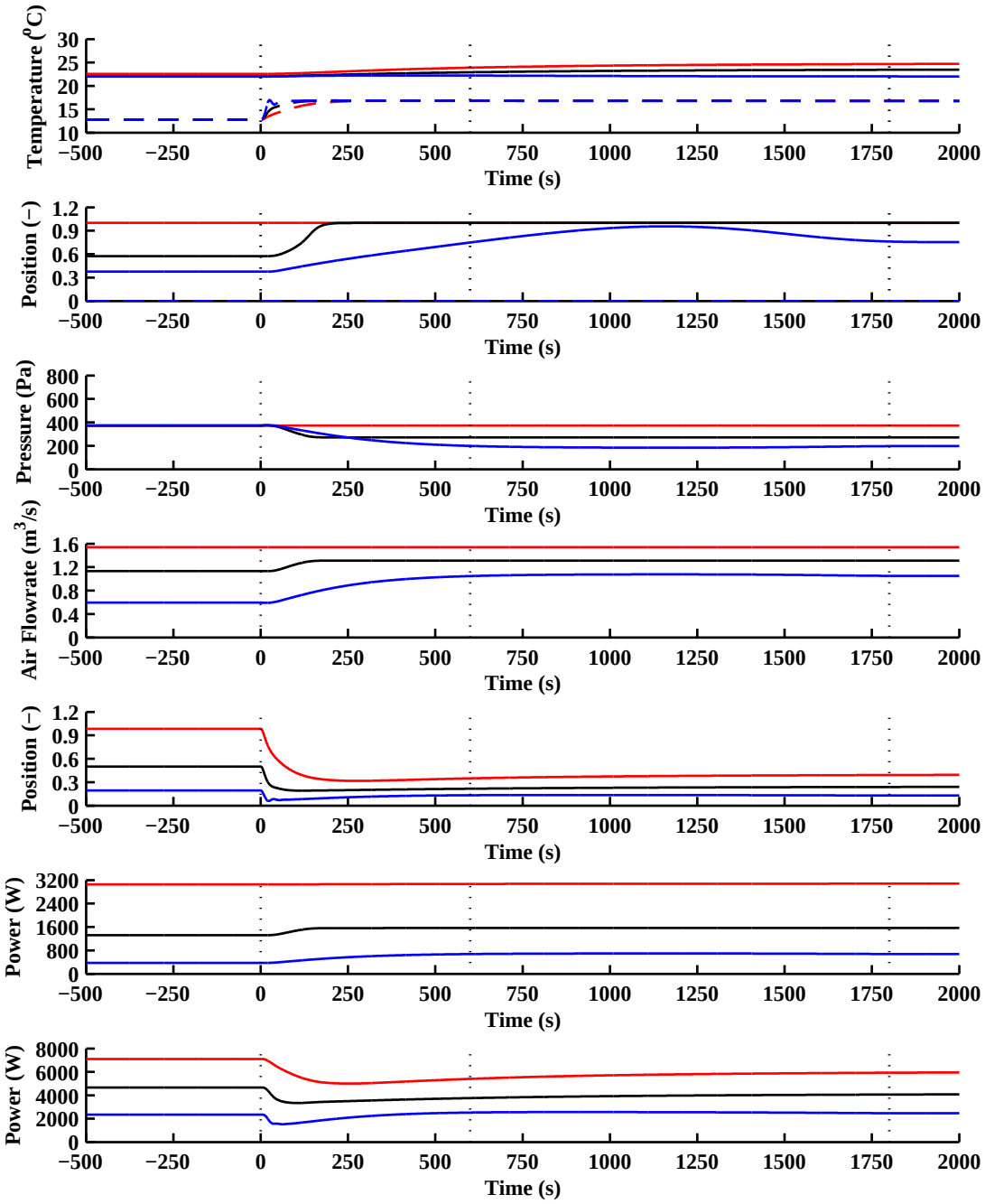

Figure 5.16 – Simulated response of a representative VAV system to a step change in supply air temperature setpoint from 12.78 °C to 16.78 °C at thermal zone cooling load intensities of 9300 W (red), 6300 W (black), and 3300 W (blue). Plots are shown for (first) zone air dry bulb temperature, (second) terminal unit damper position (solid) and reheat valve position (dashed), (third) duct static pressure, (fourth) supply fan air flowrate, (fifth) chilled water valve position, (sixth) supply fan power, and (seventh) chiller power. Dotted lines indicate the starting, 10-minute, and 30-minute points of curtailment implementation.

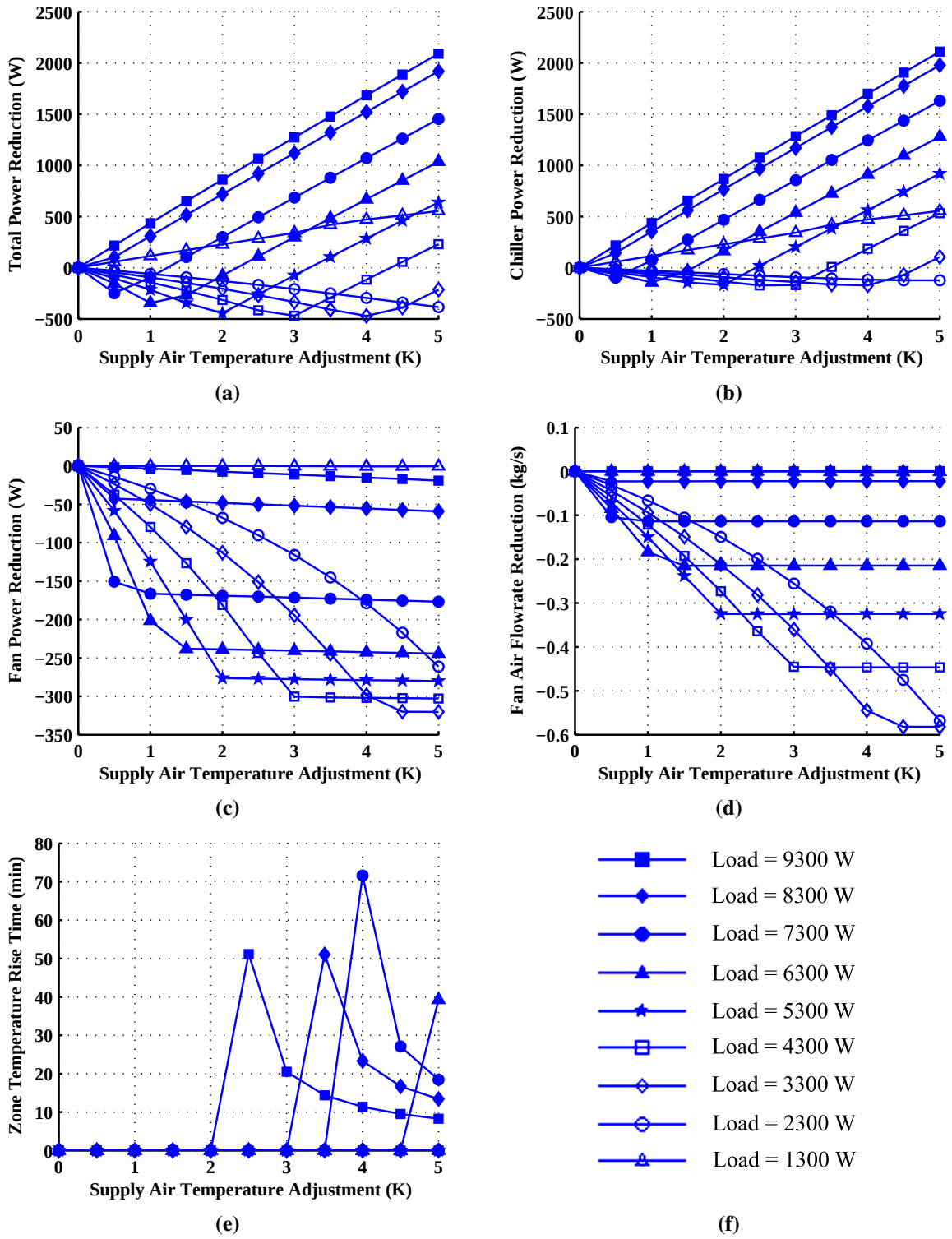

Figure 5.17 – Reduction magnitude characterization curves for STA for a) total power, b) chiller power, c) fan power, and d) the supply fan air flowrate measured at 10 minutes after implementation. The time for thermal zone temperature rise of 2 °C is plotted in e).

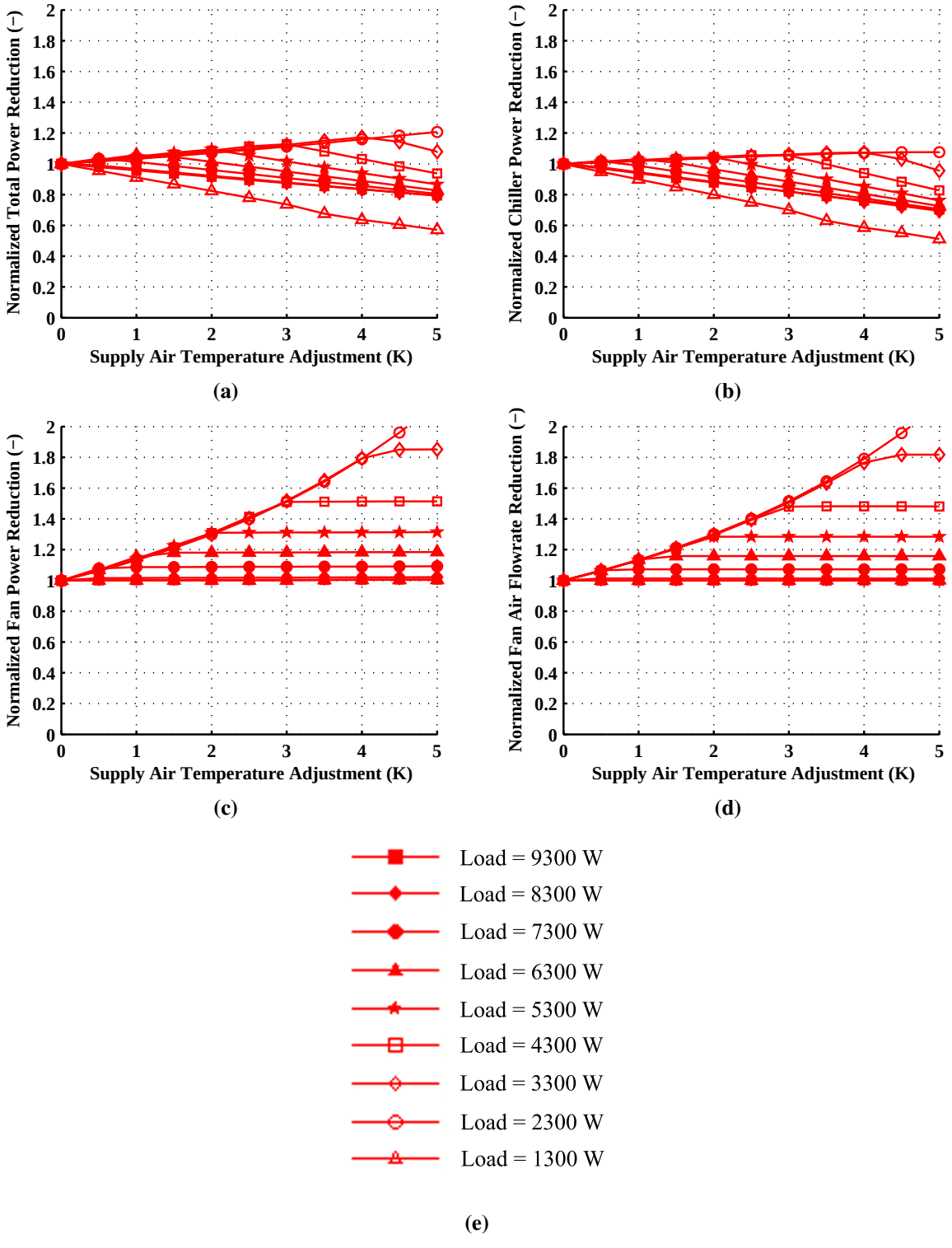

Figure 5.18 – Normalized reduction characterization curves for STA for a) total power, b) chiller power, c) fan power, and d) the supply fan air flowrate measured at 10 minutes after implementation.

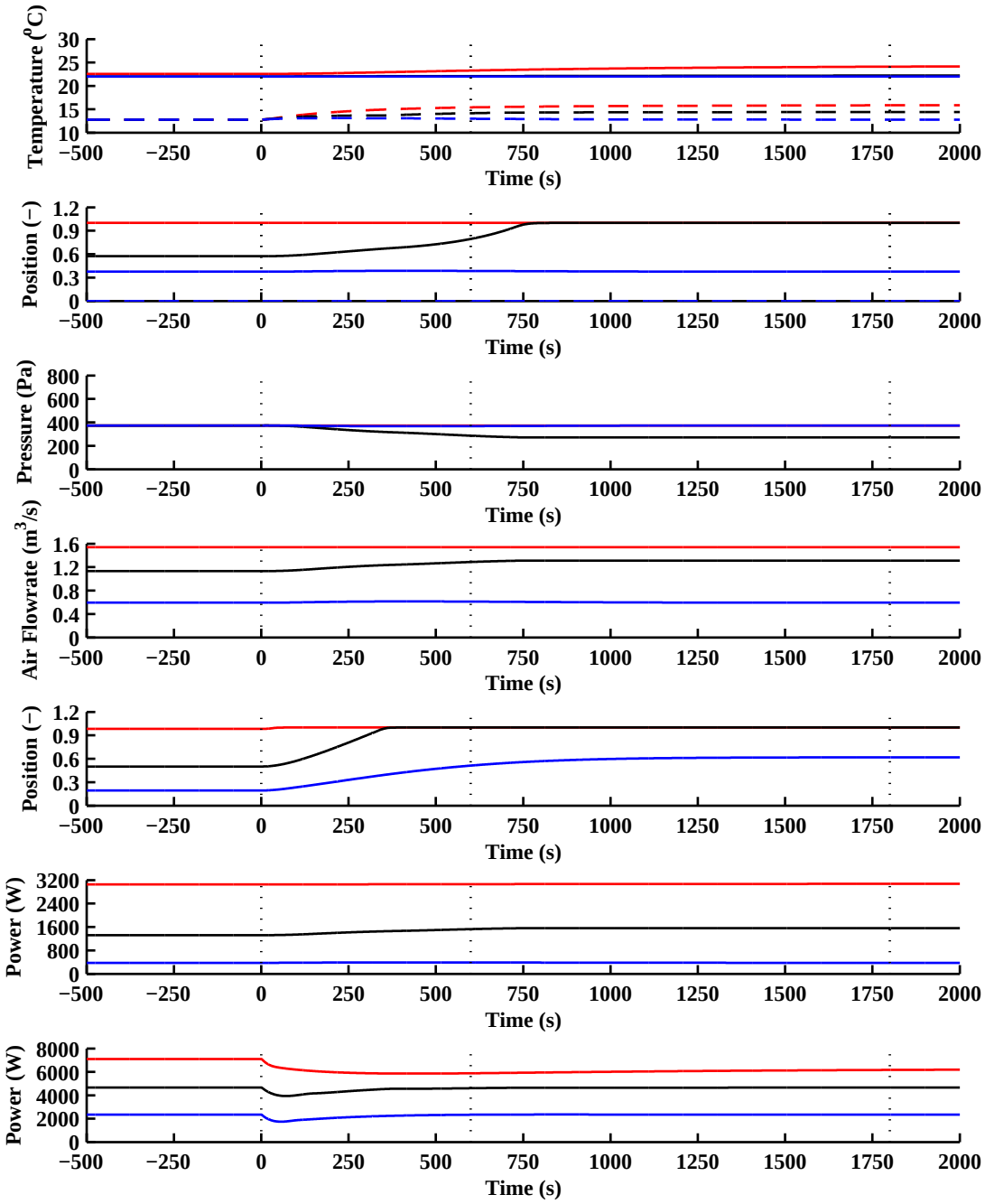

Figure 5.19 – Simulated response of a representative VAV system to a step change in chilled water temperature setpoint from 6 °C to 10 °C at thermal zone cooling load intensities of 9300 W (red), 6300 W (black), and 3300 W (blue). Plots are shown for (first) zone air dry bulb temperature, (second) terminal unit damper position (solid) and reheat valve position (dashed), (third) duct static pressure, (fourth) supply fan air flowrate, (fifth) chilled water valve position, (sixth) supply fan power, and (seventh) chiller power. Dotted lines indicate the starting, 10-minute, and 30-minute points of curtailment implementation.

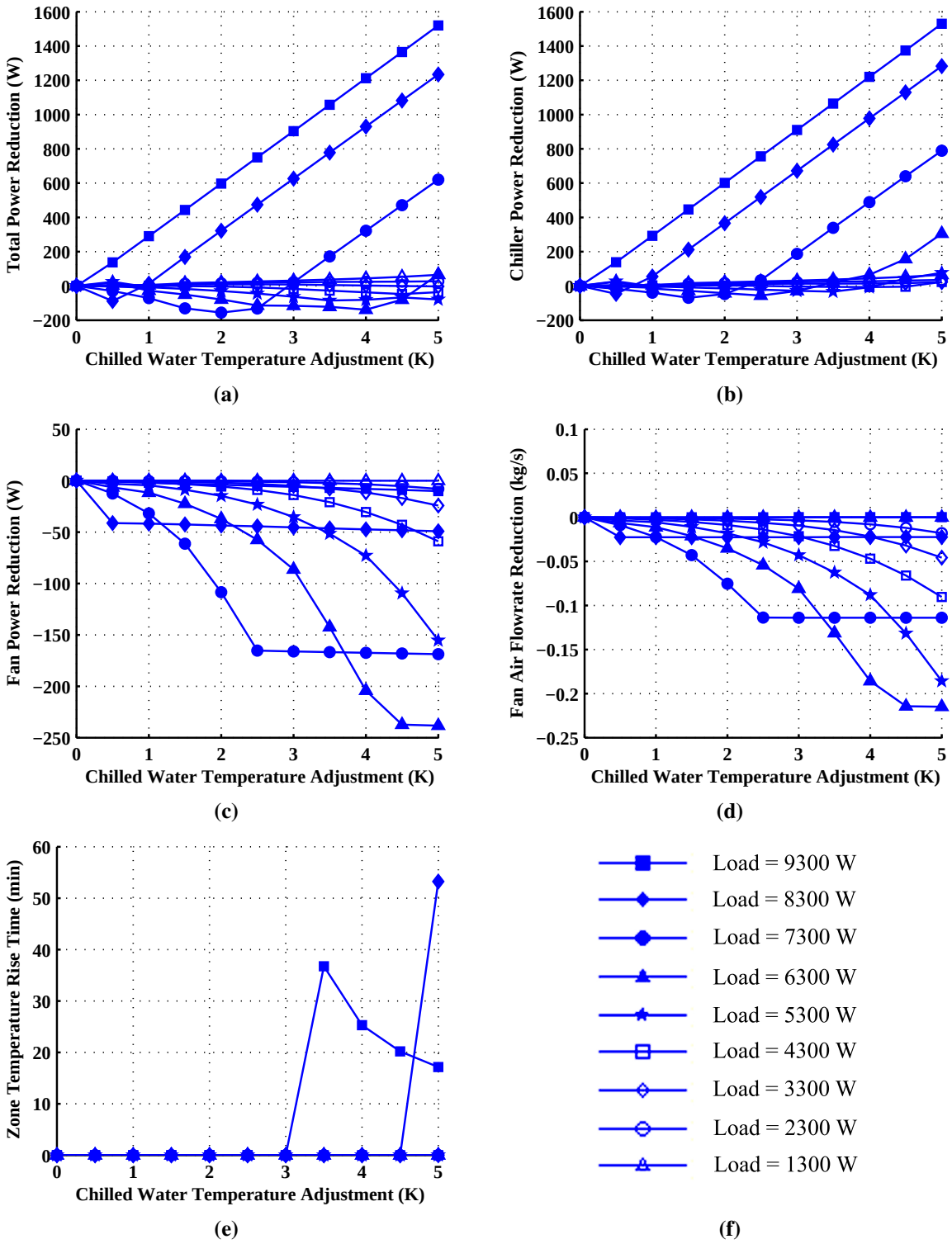

Figure 5.20 – Reduction magnitude characterization curves for CWA for a) total power, b) chiller power, c) fan power, and d) the supply fan air flowrate measured at 10 minutes after implementation. The time for thermal zone temperature rise of 2 °C is plotted in e).

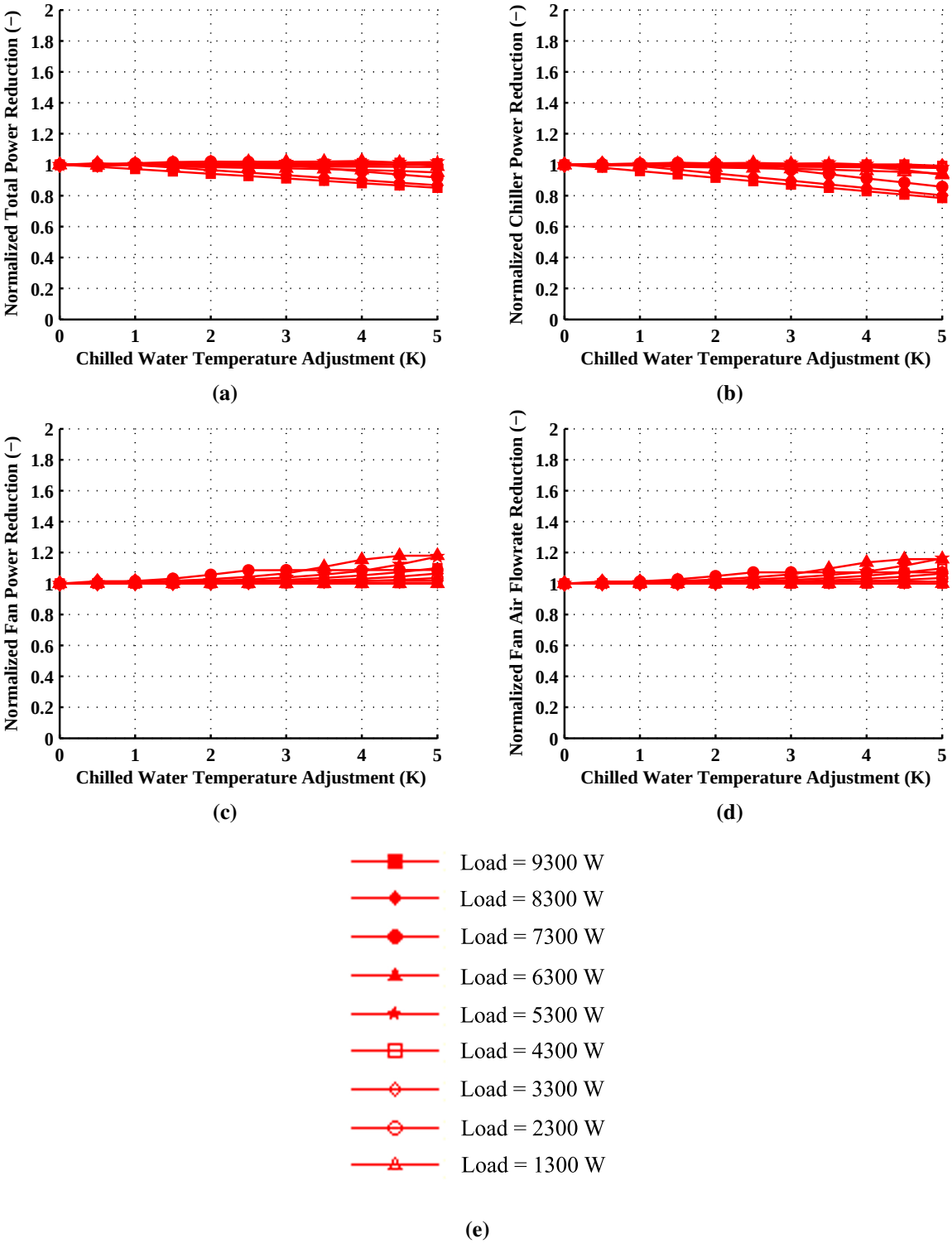

Figure 5.21 – Normalized reduction characterization curves for CWA for a) total power, b) chiller power, c) fan power, and d) the supply fan air flowrate measured at 10 minutes after implementation.

5.5 Discussion

5.5.1 Zone Dry Bulb Temperature Adjustment

As seen in Figure 5.10, upon implementation of the zone dry bulb temperature adjustment, the error between the zone temperature and zone temperature setpoint immediately becomes negative, indicating a heating load. This causes the terminal unit damper position to modulate to the minimum. This sudden closing of the dampers sharply reduces air flow, reduces the supply air temperature, and increases the duct static pressure. The chilled water valve closes to maintain supply air temperature setpoint and the fan slows down to maintain the static pressure setpoint, leading to both fan and chiller reductions in power. The fan power reduction occurs over 60 seconds while the chiller power reduction occurs over 90 seconds. Upon reaching the new zone temperature setpoint, the damper modulates open to maintain the zone setpoint at the new cooling load. The new required air flowrate is decreased, as the system is now taking advantage of the thermal capacitance of the construction, which is providing convective cooling to the zone. Simultaneous with the opening of terminal unit dampers, the air flowrate increases, supply air temperature increases, and duct static pressure decreases. This causes the fan to speed up and chilled valve to modulate open, increasing chiller power and fan power to a new steady state value for the duration of the curtailment. Notice that if the load in the room is not high enough to raise the air temperature to the new setpoint, the reopening of terminal unit dampers does not occur. Also, at high loads, the supply air flowrate is reduced faster than the chilled water valve can maintain supply air temperature. The result of this is an initial chiller unloading due to the sharp reduction in supply air flowrate, and a continued, smaller, unloading rate as the chilled water valve reaches its new position.

Figure 5.11 shows that total power reduction at 10 minutes after implementation increases with setpoint adjustment until a particular value, depending on the load condition. The exception to this is in the highest load case, where the curves are shifted one unit to the right on the x-axes. This is due the terminal units beginning starved due to the high load and remaining starved with a small setpoint adjustment. Figure 5.12a shows that power is reduced with an increase in setpoint adjustment until a particular value, where a further increase in temperature adjustment has no further effect on reduction amount. It is seen from 5.12d that this inflection point occurs at the setpoint adjustment that causes the air flowrate through the terminal unit to no longer decrease. This point corresponds to when the minimum damper position is required to maintain the new setpoint and occurs with high setpoint adjustments or low initial cooling loads.

It is important to note the effect of disabling the hot water reheat systems for these tests. If the reheat were enabled, the sudden increase in setpoint temperature would cause the reheat valve to open in order to heat the room as quickly as possible to the new setpoint. This phenomenon is seen in the first step test simulation and is not advantageous to ancillary service provision because it shortens the time in which the dampers are at minimum position to less than 10 minutes after implementation. This faster change in zone temperature is also more likely to be sensed by occupants and could lead to thermal discomfort.

5.5.2 Static Pressure Adjustment

As seen in Figure 5.13, upon implementation of the static pressure setpoint adjustment, the fan slows to meet the new static pressure setpoint. This reduces the pressure in the duct, which decreases air flow

through the terminal unit. The terminal unit dampers are then modulated open until the demanded air flowrate is once again met. The initial decrease in air flowrate decreases the supply air temperature slightly until the combination of increased airflow and slight chilled water valve modulation correct the temperature to the setpoint. The fan power is reduced due to a decrease in pressure, however, chiller power reduction is small. The exception is the highest cooling load case, where the terminal damper positions are at their maximum during normal operation. In this case, their inability to modulate further open causes the air flowrate to reduce in the wake of the static pressure adjustment. This decrease in air flowrate reduces the temperature of the supply air until the chilled water valve modulates closed. Fan power is reduced due to a decrease in pressure and air flowrate and chiller power is reduced due to a decrease in air flowrate. With the terminal units starved and unable to meet the cooling load, note that the chiller power rises slightly over time as the zone air, and corresponding return air, warms.

Figures 5.14 and 5.15 show that total power reduction is increased with increasing intensity of static pressure adjustment. However, there is an obvious inflection point in all of the curves of both figures that corresponds to the point where terminal unit starving takes place. From this point, further reduction in static pressure continues to reduce air flow, which increases the reduction in fan power and initializes a reduction in chiller power. Also note that the zone temperature does not rise drastically, as shown in Figure 5.14e. Only in the highest load cases with high setpoint adjustments does the zone temperature rise 2 °C in an appreciable amount of time relative to the time periods of ancillary service provision. In practice, static pressure reset controllers operate the system as close to the inflection point of the correlation curves as possible. However, for truly effective demand response applications, the point of operation should extend beyond this inflection point to the degree occupant service is not severely impacted.

5.5.3 Supply Air Temperature Adjustment

As seen in Figure 5.16, upon implementation of the supply air temperature setpoint adjustment, the cooling valve modulates closed until the supply air temperature rises to the new setpoint. The increased supply air temperature begins to warm the zone air, which causes the terminal unit to increase its demanded air flowrate and modulate its dampers open. The modulation of the dampers open decreases the duct static pressure and increases the air flowrate. Unlike the previous two curtailment strategies, however, the fan speed has been locked to avoid speed-up. Therefore, the duct static pressure remains below the setpoint. The fan power ultimately increases, as it is now riding a constant speed fan performance curve with increasing air flowrate. The chiller power decreases sharply initially and then begins to increase as air flowrate increases or zone air temperature increases, which occurs in the case that terminal unit dampers are or become starved.

Figures 5.17 and 5.18 show that fan power increases with increased supply air temperature adjustment until the setpoint adjustment where terminal unit boxes become starved and air flow can no longer increase. If the terminal units do not become starved, the zone air temperature is maintained at the normal setpoint and airflow is increased. Although the fact that the zone air temperature does not change implies that the chiller must be providing the same rate of cooling as normal conditions, there is additional energy added to the system in the form of fan work. If the same amount of heat is added to the air system from the zone cooling load, and additional work is added to the air system from the fan, the First Law of Thermodynamics says that the total amount of energy the chiller must remove from the system increases.

Once the terminal unit becomes starved, any further increase in setpoint adjustment will only increase the supply air temperature and not the air flowrate, causing an increase in chiller power reduction. At higher cooling load intensities, this transition to terminal unit starving occurs at small supply air temperature adjustments. It should be noted, however, that the magnitude that power increases due to the effects of added fan work is small compared to the magnitude of power curtailed after terminal unit starving takes place.

The exception to the above process is in the case with the lowest cooling load. In this case, the minimum position of the damper provides more cooling than is necessary to maintain the zone air temperature setpoint. When the supply air temperature is increased, the damper position and corresponding flowrate do not change from minimum. Without an increase in supply air flowrate, the supply air temperature increase unloads the chiller. It is hypothesized that the slope of this curve is less than the unloading slope of the other load cases due to the smaller air flowrate (minimum compared to maximum), however the discussion of forming functional relationships for these curves and relating them to physical parameters of operation is saved for future work.

5.5.4 Chilled Water Temperature Adjustment

As seen in Figure 5.19, upon implementation of the chilled water temperature setpoint adjustment, the cooling valve modulates open so that the supply air temperature is maintained. In the case that the cooling valve modulates fully open, the supply air temperature is increased. The increase in supply air temperature begins to heat the zone air and causes the terminal unit dampers to modulate open, increasing the air flowrate and dropping the duct static pressure. This process, as in the case of the supply air temperature adjustment, ultimately increases fan power. Chiller power is reduced sharply initially, however begins to increase as the air flowrate increases and the chilled water valve modulates to maintain supply air flowrate setpoint.

Figures 5.20 and 5.21 show similar trends to that of the supply air temperature adjustment. That is, fan power only increases with chilled water temperature setpoint adjustment due to the resulting increase in air flowrate. Once the terminal unit is starved, a continued increase in setpoint adjustment unloads the chiller.

5.6 Conclusion

This chapter has developed a representative VAV model to analyze the performance of four demand response curtailment strategies; zone air dry bulb temperature setpoint adjustment (ZDBA), duct static pressure setpoint adjustment (SPA), supply air temperature adjustment (STA), and chilled water temperature adjustment (CWA). The model was used to simulate each strategy under various load conditions and strategy implementation intensities in order to formulate correlation curves between these two parameters and performance variables of interest, which included absolute and normalized total power reduction, chiller power reduction, fan power reduction, and fan air flowrate reduction at a time 10 minutes from implementation. This time was chosen as representative of providing spinning reserve ancillary services. Additionally, zone temperature rise times were plotted to gauge the impact on occupant service. From the results and discussion presented in this chapter, the following conclusions can be drawn.

First, terminal unit position plays the largest role in determining the performance of each curtailment strategy. This is because they ultimately control the airflow through the central system and into each zone. While this fact is almost obvious, the results show a clear distinction in curtailment performance before and after operating conditions are met that cause a terminal unit to reach minimum or maximum position. These points are indicated by inflection points of the correlation curves presented for each strategy. For ZDBA, terminal unit damper position minimization marks the point of maximum curtailment, beyond which further curtailment does not affect the performance. For SPA, terminal unit starvation marks the point of increased curtailment effectiveness, which results from the additional decrease in air flowrate as well as static pressure. After this point, there is no physically relevant limit to effectiveness, however until this point, the curtailment strategy has minimal effectiveness. Though operation in this range should be considered as a year-round energy conservation strategy. For STA and CWA, terminal unit starvation marks the point of any positive curtailment effectiveness except for the initial moments after implementation. This observation is also noted in Motegi et al. (2007) and is true even with fan speed locking. Until this point, an increase in supply air flowrate from terminal unit damper modulation at constant fan speed results in increased fan power added to the system, as can be seen on any fan performance curve. This analysis makes it clear that effective load curtailment is not possible without some impact on service, as ZDBA load curtailment increases when zone temperature can be risen higher and SPA, STA, and CWA load curtailment increases when terminal units become starved. The key is to predict curtailment performance so that the optimum strategy may be chosen to minimize occupancy service loss and maximize ancillary service provision.

Second, the results show clear families of curves associated with each curtailment strategy. While the simplicity of the developed VAV model contributes to the relative simplicity of the correlation curves, this method of visualizing data proves to be effective in determining the general performance effectiveness of each strategy under different load conditions and implementation intensities. Simulations that add additional complexities (e.g. unbalanced thermal load or asymmetrical duct design) may reveal additional important governing parameters to that of terminal unit position described above. Examples include the relative number or duct location of terminal units, especially with respect to the location of the duct static pressure sensor and amount of flow resistance to different terminal units. Additionally, the presence of exterior weather conditions that play a role in driving cooling loads as a function of zone air temperature (such as wall conduction) will affect the shape of the curves in the cases in which zone air temperature changes.

Third, this analysis reveals important insights to fundamental differences in these curtailment strategies with application to ancillary services. SPA could be considered the "cleanest" of the curtailment strategies from a dynamics point of view. That is, once the strategy is implemented, there is only one transient period that occurs. The duct pressure is reduced, the terminal unit dampers modulate open, and if they become starved, the chiller unloads. This is unlike any of the other curtailment strategies, which involve multiple transients. In ZDBA, there is an initial decrease in air flow when terminal unit dampers close and then a re-opening of these dampers to a new position once the new zone air setpoint has been reached. For STA and CWA, there is an initial unloading of the chiller in order to order meet the new supply air or chilled water setpoints, however, as terminal unit dampers open and air flow increases, the chiller and fan increase in power consumption. Also, the impact of each curtailment strategy on occupant service is important to consider. Only at high loads and high curtailment intensities is it possible that SPA, STA, or CWA contributes to zone over-heating within a time period relevant to ancillary service provision. This is because terminal units are supplying as much air as possible to the zones during curtailment, which

may still be at an acceptable temperature or flowrate for relative thermal comfort. For ZDBA, thermal comfort is definitely affected for each load intensity, although the degree is completely controllable.

It could be concluded, then, that SPA represents an attractable strategy for spinning or non-spinning reserve provision due to the relative simplicity of the implementation dynamics and small thermal comfort impact below some critical high-load condition. This makes curves such as those presented above attractable for predicting performance. CWA and STA may be attractable options for regulation provision, as curtailment is immediate with slow secondary transients. However, mechanical durability is a large concern in this case. Lastly, ZDBA may be an attractable option for long-term demand response due to its ability to control thermal comfort at a high level.

Chapter 6

Conclusions and Future Work

Increasing penetration of intermittent renewable power generation from solar and wind sources requires the operation of future electric grids to be flexible. Buildings account for the largest portion of electricity consumption in the U.S., providing them with an incredible opportunity to help shape the operation of future electric grids. Additionally, the coupling of a building's electric power consumption with its thermal energy storage through HVAC systems make building HVAC systems prime targets for electric demand flexibility. Termed *demand response*, there has been much study of this application for building HVAC systems over the last decade. However, much of this study lacked the evaluation of multi-zone commercial building HVAC systems at a level fine enough to capture the physical processes and system dynamics responsible for demand response performance. This is especially important when considering the use of HVAC systems in providing grid ancillary services, which are of most importance when considering the high use of renewable intermittent generation and have timescales of implementation on the order of transient HVAC dynamics. Through this type of study, it will be possible to better predict performance in the face of varying operating conditions, as occurs on a daily basis. Therefore, this thesis set out to analyze and characterize the performance of a common multi-zone HVAC system, the VAV system, providing grid ancillary services.

Initially, high resolution electrical and HVAC data from a real test building was analyzed to gain insights into real-world operational qualities that affect the provision of ancillary services. The first observation was that the HVAC system accounted for approximately 80% of whole building power demand, with the air-cooled chiller accounting for approximately 50% of whole building power demand, giving the HVAC system significant authority over building power consumption. Second, the direct and indirect relationship between environmental conditions and HVAC power were observed, pointing out the need to consider these conditions with HVAC power curtailment. Third, the discrete operation of staged or cycled equipment was presented and considered to be advantageous to ancillary service provision only if properly controlled. Fourth, the effect of operational faults on service provision was discussed, including sticky actuators and improper controller tuning. Lastly, three static pressure adjustments were applied to the test building throughout one day. The results showed that the damper and fan controllers responded quickly, within two minutes and well within the response time required to provide 10-minute spinning reserves. Additionally, observations were made about the strong effect terminal unit starvation has on fan airflow and power reduction, something that was further explored through simulations.

In order to study the operation of VAV systems providing ancillary services under varying operating conditions and curtailment strategies, a representative VAV model was developed and simulated. The strengths of Modelica, a progressive physical modeling language, were shown in simulating pressure-flow relationships in complex flow networks that are required to study the dynamic operation of VAV systems. Dymola was used to implement a Modelica model of a VAV system containing a fan, cooling coil, two terminal units with hot water reheat, various duct resistances, two thermal zones, and various equipment controllers. Explicit control of terminal unit damper position, reheat valve position, fan speed, and chilled water valve position based on operating temperatures, pressures, and air flowrates was demonstrated through a series of simulations with various setpoint step changes. The VAV model was then used to simulate five different load curtailment strategies at various intensities and load conditions, including zone dry bulb temperature setpoint adjustment (ZDBA), static pressure setpoint adjustment (SPA), supply air temperature setpoint adjustment (STA), and chilled water temperature setpoint adjustment (CWA). Characterization curves were developed that map the power curtailment, air flowrate reduction, and zone temperature rise of each strategy. These curves are helpful in visualizing the performance and could form a basis of performance prediction. The influence of terminal unit damper position was observed through the presence of inflection points in the curves that drastically changed curtailment performance. For ZDBA, terminal unit damper position minimization marks the point of maximum power curtailment, while for SPA, STA, and CWA, terminal unit damper starvation marks the point beyond which power curtailment performance significantly increases. In the case of STA and CWA, if the setpoint temperatures are not raised high enough to starve the terminal units for a given load condition, the increase in required air flowrate by the opening of terminal unit dampers will ultimately lead to an increase in total power consumption.

In conclusion, the work of this thesis has contributed to the investigation of how multi-zone commerical HVAC systems may provide reliable ancillary services from a system dynamics point of view. In general, it has revealed that highly effective grid service provision only comes with an amount of occupant service loss. More specifically, it has identified and begun to characterize important processes by which this occurs so that the performance of different strategies under various load conditions can be better predicted in real applications. Groups of buildings on institution campuses or under regional curtailment service provider control may better deal with variability in performance due to the flexibility given by controlling multiple systems. However, understanding and predicting performance in individual buildings is still important for facility managers and owners without this luxury and can enhance the reliability and optimization of the services provided by those with it.

Future work associated with this thesis includes both the test building and simulations. The static pressure setpoint adjustment in the test building was performed in November, a time of low cooling loads for the building and little chiller operation. Similar tests during the summer would allow the study of chiller performance in addition to that of the air system. Additionally, a range of tests could be designed similar to those performed in the simulations to map the performance of the HVAC system with different strategy and load intensities through characterization curves. These curves could be compared with those developed in this thesis. Future simulations should include cases with differential loading across the thermal zones as well as asymmetrical terminal unit duct branch design. Both of these cases will cause terminal unit dampers to reach their maximum or minimum position at different points, likely adding additional inflection points in the characterization curves. Further exploration of the characterization curves should be performed to identify their mathematical functional relationship to physical variables and determine whether these functions can be identified without the explicit mapping of data, which is

not likely to be so available in real buildings. These functions may not only be used in ancillary service bidding algorithms that predict service performance, but also optimization routines that determine the implementation strategy that maximizes ancillary service provision and minimizes occupancy service loss for a given load condition.

Bibliography

Armstrong, P. R., S. B. Leeb, and L. K. Norford (2006a). Control with building mass - part I: thermal response model. *ASHRAE Transactions 112*(1), 449. 29

Armstrong, P. R., S. B. Leeb, and L. K. Norford (2006b). Control with building mass - part II: simulation. *ASHRAE Transactions 112*(1), 462. 29

ASHRAE (2005). *ASHRAE Handbook - Fundamentals*. Atlanta, GA: American Society of Heating, Refrigerating and Air-Conditioning Engineers. 74, 75, 77

ASHRAE (2010). *ANSI/ASHRAE Standard 62.1-2010 - Ventilation for Acceptable Indoor Air Quality*. Atlanta, GA: American Society of Heating, Refrigerating and Air-Conditioning Engineers. 76

ASHRAE (2011). *ANSI/ASHRAE/USGBC/IES Standard 189.1-2011. Standard for the Design of High-Performance Green Buildings*. Atlanta, GA: American Society of Heating, Refrigerating and Air-Conditioning Engineers. 29

Berardino, J. and C. Nwankpa (2010). Dynamic load modeling of an HVAC chiller for demand response applications. In *Smart Grid Communications (SmartGridComm), 2010 First IEEE International Conference*, Gaithersburg, MD, pp. 108–113. 81

California ISO (2011). *Demand Response and Proxy Demand Resource - Frequently Asked Questions*. Folsom, CA: California Independent System Operator Corporation. 34

California ISO (2013). *Conformed fifth replacement California ISO Tariff*. Folsom, CA: California Independent System Operator Corporation. 34

Callaway, D. S. (2009). Tapping the energy storage potential in electric loads to deliver load following and regulation, with application to wind energy. *Energy Conversion and Management 50*(5), 1389–1400. 32

Callaway, D. S. and I. A. Hiskens (2011). Achieving controllability of electric loads. *Proceedings of the IEEE 99*(1), 184–199. 32, 51

Commission of the European Communities (2008). *COM(2008) 30 final; 20 20 by 2020 Europe's climate change cpportunity*. Brussels, Belgium. 16

Cvetkovic, I. (2010). *Modeling, Analysis and Design of Renewable Energy Nanogrid Systems*. MS thesis, Virginia Polytechnic Institute and State University, Blacksburg, VA. 32

Dassault Systemes (2013, April). Dymola. http://www.3ds.com/products/catia/portfolio/dymola. Accessed April, 2013. 60

Deane, J., B. Ó Gallachóir, and E. McKeogh (2010). Techno-economic review of existing and new pumped hydro energy storage plant. *Renewable and Sustainable Energy Reviews 14*(4), 1293–1302. 18

DeSimone, M. (1995). *A standard simulation testbed for the evaluation of control algorithms & strategies related to variable air volume HVAC systems*. MS thesis, Massachusetts Institute of Technology, Cambridge, MA. 64

DSIRE (2013). Renewable portfolio standard polocies. http://www.dsireusa.org/documents/summarymaps/RPS_map.pdf. Accessed March, 2013. 16

EIA (2012). *Annual Energy Outlook 2013 Early Release*. U.S. Energy Information Administration. 15, 16, 17, 18, 19, 46

Englander, S. L. and L. K. Norford (1992a). Saving fan energy in VAV systems - part 1: Analysis of a variable-speed-drive retrofit. *ASHRAE Transactions 98*(1). 77, 78, 82

Englander, S. L. and L. K. Norford (1992b). Saving fan energy in VAV systems - part 2: Supply fan control for static pressure minimization using DDC zone feedback. *ASHRAE Transactions 98*(1). 29, 75, 76, 77

Englander, S. L. and L. K. Norford (1992c). Variable speed drives: Improving energy consumption modeling and savings analysis techniques. *ACEEE Summer Study Proceedings Paper*. 78, 81, 82, 83

ERCOT (2007, June). *Load Participation in the ERCOT Nodal Market, Financial Opportunities for Reducing Electricity Load*. Electric Reliability Council of Texas. 34

Eto, J., J. Nelson-Hoffman, E. Parker, C. Bernier, P. Young, D. Sheehan, J. Kueck, and B. Kirby (2009). Demand response spinning reserve demonstration - phase 2 findings from the summer of 2008. Technical Report LBNL-2490E, Lawrence Berkeley National Laboratory, Berkeley, CA. 31

Eto, J., J. Nelson-Hoffman, C. Torres, S. Hirth, B. Yinger, J. Kueck, B. Kirby, C. Bernier, R. Wright, A. Barat, and D. S. Watson (2007). Demand response spinning reserve demonstration. Technical Report LBNL-62761, Lawrence Berkeley National Laboratory, Berkeley, CA. 31

eurelectric (2009). CEO meeting, 18 march 2009 - a declaration by european electricity sector chief executives. http://www.eurelectric.org/CEO/CEODeclaration.asp. Accessed March, 2013. 16

eurelectric (2010). *Integrating Intermittent Renewables Sources into the EU Electricity System by 2020*. eurelectric. 16

European Commission (2011). *SEC 463; Definition, Expected Services, Functionalities and Benefits of Smart Grids*. Brussels, Belgium. 13

EWEA (2012). *Wind in power; 2011 European statistics*. The European Wind Energy Association. 16

FERC (2011a). Order 745; demand response compensation in organized wholesale energy markets. 29, 33, 34

FERC (2011b). Order 755; frequency regulation compensation in the organized wholesale power markets. 33

FERC (2012). Regional transmission organizations. http://www.ferc.gov/industries/electric/indus-act/rto/elec-ovr-rto-map.pdf. Accessed March, 2013. 14

Fraunhofer USA, Inc (2011). Fraunhofer CMI. http://www.fhcmi.org/. Accessed March, 2013. 40

Fritzson, P., H. Olsson, and M. Otter (2012). *Modelica - A Unified Object-Oriented Language for Systems Modeling, Language Specification* (3.3 ed.). Modelica Association. 67

Gayeski, N. T. (2010). *Predictive pre-cooling control for low lift radiant cooling using building thermal mass*. PhD thesis, Massachusetts Institute of Technology, Cambridge, MA. 29, 31, 47

Ghatikar, G. and R. Bienert (2011). Smart grid standards and systems interoperability: a precedent with OpenADR. In *Grid-Interop 2011*, Phoenix, AZ. 19, 32

Greensfelder, E. M., H. P. Gregor, and C. Felsmann (2011). An investigation of optimal control of passive building thermal storage with real time pricing. *Journal of Building Performance Simulation 4*(2), 91–104. 31

Hammerstrom, D., R. Ambrosio, T. Carlon, J. DeSteese, G. Horst, R. Kajfasz, L. Kiesling, P. Michie, R. Pratt, M. Yao, J. Brous, D. Chassin, R. Guttromson, O. Jarvegren, S. Katipamula, N. Le, T. Oliver, and S. Thompson (2007). Pacific northwest GridWise testbed demonstration projects: Part I, olympic peninsula project. Technical Report PNNL-17167, Pacific Northwest National Laboratory, Richland, WA. 30

Hammerstrom, D., J. Brous, D. Chassin, G. Horst, R. Kajfasz, P. Michie, T. Oliver, T. Carlon, C. Eustis, O. Jarvegren, W. Marek, R. Munson, and R. Pratt (2007). Pacific northwest GridWise testbed demonstration projects: Part II, grid friendly appliance project. Technical Report PNNL-17079, Pacific Northwest National Laboratory, Richland, WA. 31

Harman, P. and U. K. Ricardo (2005). Visualisation of model transformation algorithms for a modelica translator. In *4th International Modelica Conference*, Hamburg, Germany, pp. 155–158. 68

Haves, P. and L. K. Norford (1997). A standard simulation testbed for the evaluation of control algorithms and strategies. Technical Report 825-RP, American Society of Heating, Refrigerating and Air-Conditioning Engineers, Inc., Atlanta, GA. 64, 65, 75, 76, 77

ISO New England (2011). *ISO New England Operating Procedure No. 8, Operating Reserve and Regulation*. Holyoke, MA: ISO New England, Inc. 25, 26

ISO New England (2012a). *Manual M-20, Forward Capacity Market (FCM)*. Holyoke, MA: ISO New England, Inc. 34

ISO New England (2012b). *Wholesale Markets Project Plan 2012*. Holyoke, MA: ISO New England, Inc. 29

ISO New England (2013a). *Manual M-28, Market Rule 1 Accounting*. Holyoke, MA: ISO New England, Inc. 23, 24, 25

ISO New England (2013b). *Transmission, Markets and Services Tariff, Section III Market Rule 1, Standard Market Design*. Holyoke, MA: ISO New England, Inc. 23, 34

Itron (2013). MetrixIDR retail. 2111 N Molter Road Liberty Lake, WA 99019 U.S.A. 32

KEMA (2010). *Demand Response Reserve Pilot Evaluation*. Holyoke, MA: ISO New England, Inc. 35, 36

Kempton, W. and J. Tomić (2005a). Vehicle-to-grid power fundamentals: Calculating capacity and net revenue. *Journal of Power Sources 144*(1), 268–279. 18

Kempton, W. and J. Tomić (2005b). Vehicle-to-grid power implementation: From stabilizing the grid to supporting large-scale renewable energy. *Journal of Power Sources 144*(1), 280–294. 18

Kiliccote, S., M. A. Piette, G. Ghatikar, E. Koch, D. Hennage, J. Hernandez, A. Chiu, O. Sezgen, and J. Goodin (2009). Open automated demand response communications in demand response for wholesale ancillary services. In *Grid Interop Forum*, Denver, CO. 32

King, J., T. Mousseau, and R. Zavadil (2011). *Eastern Wind Integration and Transmission Study*. Golden, CO: National Renewable Energy Laboratory. 14, 17

Kirby, B., J. Kueck, T. Laughner, and K. Morris (2008). Spinning reserve from hotel load response: Initial progress. Technical Report ORNL/TM-2008/217, Oak Ridge National Laboratory, Oak Ridge, TN. 31

Kirby, B., M. O'Malley, O. Ma, P. Cappers, D. Corbus, S. Kiliccote, O. Onar, M. Starke, and D. Steinberg (2011). *Load Participation in Ancillary Services*. U.S. Department of Energy. 38

Klein, S. (2007). *TRNSYS 16: A Transient System Simulation Program*. University of Wisconsin, Madison, USA: Solar Energy Laboratory. 60

Koch, S., J. L. Mathieu, and D. S. Callaway (2011). Modeling and control of aggregated heterogeneous thermostatically controlled loads for ancillary services. In *PSCC Proceedings*, Stockholm, Sweden, pp. 1–7. 32

LBNL (2012). Users guide of the modelica buildings library. http://simulationresearch.lbl.gov/modelica/userGuide/. Accessed April, 2013. 71, 81, 91

Lee, K.-H. and J. E. Braun (2008). Model-based demand-limiting control of building thermal mass. *Building and Environment 43*(10), 1633–1646. 31

Li, S. (2009). *A Model-Based Fault Deterction and Diagnostic Methodology for Secondary HVAC Systems*. PhD thesis, Drexel University, Philadelphia, PA. 50

Mathieu, J. L. and D. S. Callaway (2012). State estimation and control of heterogeneous thermostatically controlled loads for load following. In *45th Hawaii International Conference on System Sciences (HICSS)*, Maui, HI, pp. 2002–2011. IEEE. 32

Mathieu, J. L., D. S. Callaway, and S. Kiliccote (2011). Variability in automated responses of commercial buildings and industrial facilities to dynamic electricity prices. *Energy and Buildings 43*(12), 3322–3330. 30

Mathieu, J. L., P. N. Price, S. Kiliccote, and M. A. Piette (2011). Quantifying changes in building electricity use, with application to demand response. *IEEE Transactions on Smart Grid 2*(3), 507–518. 30, 47

Mattsson, S. E. and H. Elmqvist (1997). Modelica - an international effort to design the next generation modeling language. Gent, Belgium. 67, 68

McAnany, J. (2013). 2012 load response activity report. Accessed March, 2013. 34, 35, 37

MISO (2010). *Demand Response Primer and Training Guide*. Carmel, IN: Midwest Transmission System Operator, Inc. 34

MIT (2011). *The Future of the Electric Grid*. Cambridge, MA: Massachusetts Institute of Technology. 17, 18

Modelica Association (2013a). Modelica and the modelica association. https://www.modelica.org/. Accessed April, 2013. 67

Modelica Association (2013b). Modelica tools. https://www.modelica.org/tools. Accessed April, 2013. 68

Montgomery, R. and R. McDowall (2008). *Fundamentals of HVAC Control Systems*. Atlanta, GA: American Society of Heating, Refrigerating and Air-Conditioning Engineers. 61, 75, 76

Motegi, N., M. Piette, D. Watson, S. Kiliccote, and P. Xu (2007). Introduction to commercial building control strategies and techniques for demand response. Technical Report LBNL-59975, Demand Response Research Center, Lawrence Berkeley National Laboratory, Berkeley, CA. 29, 50, 61, 91, 108

NERC (2013a). *Glossary of Terms Used in NERC Reliability Standards*. Washington, DC: North American Electric Reliability Corporation. 15

NERC (2013b). *Reliability Standards for the Bulk Electric Systems of North America*. Washington, DC: North American Electric Reliability Corporation. 14

NYISO (2013). *NYISO 2012 Annual Report on Demand Response Programs*. Rensselaer, NY: New York Independent System Operator. 34, 35

Oldak, M. (2012, November). Electric utilities and the HVAC industry. *ASHRAE Journal 54*(11), BS10–BS15. 18

Piette, M. A., G. Ghatikar, S. Kiliccote, E. Koch, D. Hennage, P. Palensky, and C. McParland (2009). Open automated demand response communications specification (version 1.0). Technical Report CEC-500-2009-063, California Energy Commission, PIER Program. 19, 32

Piette, M. A., S. Kiliccote, and G. Ghatikar (2008). Linking continuous energy management and open automated demand response. Technical Report LBNL-1361E, Lawrence Berkeley National Laboratory, Berkeley, CA. 19

PJM (2010). *PJM Manual 18B: Energy Efficiency Measurement and Verification*. Norristown, PA: PJM Interconnection. 29

PJM (2013). *PJM Demand Response Fact Sheet for End-Use Customers*. Norristown, PA: PJM Interconnection. 34

Rastler, D. (2008). New demand for energy storage. *Electric Perspectives 33*(5), 30–47. 18

Raustad, R. and M. Basarkar (2011). ASHRAE research project report: Short-term curtailment of HVAC loads in buildings. Technical Report RP-1390, American Society of Heating, Refrigerating and Air-Conditioning Engineers, Inc., University of Central Florida, Cocoa, FL. 30, 91

Rubinstein, F., D. Bolotov, M. Levi, K. Powell, and P. Schwartz (2010). The advantage of highly controlled lighting for offices and commercial buildings. Technical Report LBNL-2514E, Lawrence Berkeley National Laboratory, Berkeley, CA. 18

Rubinstein, F. and S. Kiliccote (2007). Demand responsive lighting: A scoping study. Technical Report LBNL-62226, Demand Response Research Center, Lawrence Berkeley National Laboratory, Berkeley, CA. 18

Samouhos, S. V. (2010). *Building condition monitoring*. PhD Thesis, Massachusetts Institute of Technology, Cambridge, MA. 29, 50

Schneider Electric (2013a). Automatic extended log archiver for andover continuum. http://www.schneider-electric.com/download/hk/en/details/2000508-Automatic-Extended-Log-Archiver-for-Andover-Continuum/?reference=SDS-C-EXTENDEDLOGS. Accessed March, 2013. 45

Schneider Electric (2013b). Building management system. http://www2.schneider-electric.com/sites/corporate/en/products-services/buildings/products-offer/range-presentation.page?c_filepath=/templatedata/Offer_Presentation/3_Range_Datasheet/data/en/shared/buildings/andover_continuum.xml. Accessed March, 2013. 41

SPP (2013). *Market Protocols, SPP Integrated Marketplace, Revision 13.0a*. Little Rock, AR: Southwest Power Pool. 34

Titus (2013a). Performance data, diffusers, TMR, TMR-AA. http://www.titus-hvac.com/utility/getfile2.aspx?fileid=823. Accessed April, 2013. 74

Titus (2013b). Performance data, Single/Dual duct terminals. http://www.titus-hvac.com/utility/getfile2.aspx?fileid=1163. Accessed April, 2013. 74

Trane, Inc (2012). Trane. http://www.trane.com/Index.aspx. Accessed April, 2013. 77

University of Illinois and Lawrence Berkeley National Laboratory (2010). *EnergyPlus Engineering Reference* (6.0 ed.). 61

U.S. Department of Energy (2013a). EnergyPlus. http://apps1.eere.energy.gov/buildings/energyplus/. 30, 60

U.S. Department of Energy (2013b). New construction - commercial reference buildings. http://www1.eere.energy.gov/buildings/commercial/ref_new_construction.html. Accessed April, 2013. 62, 73

U.S. House, 110th Congress (2007). *H.R. 6; Energy Independence and Security Act of 2007*. Washington D.C. 13

Veris Industries (2013a). Current transducer. http://www.veris.com/product_results.aspx?category_guid=10245aee-e3d4-4119-b7c9-208ad77f7278. Accessed March, 2013. 45

Veris Industries (2013b). H8238. http://www.veris.com/Item/H8238.aspx. Accessed March, 2013. 45

Veris Industries (2013c). H8822. http://www.veris.com/Item/H8822.aspx. Accessed March, 2013. 45

Wang, S. (1999). Dynamic simulation of building VAV air-conditioning system and evaluation of EMCS on-line control strategies. *Building and Environment 34*(6), 681–705. 64

Warren, M. and L. K. Norford (1993). Integrating VAV zone requirements with supply fan operation. *ASHRAE Journal 34*(4), 43–46. 29

Weather Underground, Inc (2013). History for KMACAMBR4. http://www.wunderground.com/weatherstation/WXDailyHistory.asp?ID=KMACAMBR4. Accessed March, 2013. 47

Wetter, M. (2009). Modelica library for building heating, ventilation and air-conditioning systems. In *Proc. of the 7th Modelica Conference*, Como, Italy, pp. 393–402. 68, 72

Wetter, M., W. Zuo, and T. S. Nouidui (2011a). Modeling of heat transfer in rooms in the modelica "Buildings" library. In *Proc. of the 12th IBPSA Conference*, Sydney, Australia, pp. 1096–1103. 74

Wetter, M., W. Zuo, and T. S. Nouidui (2011b). Recent developments of the modelica buildings library for building energy and control systems. In *Proc. of the 8th International Modelica Conference*, Dresden, Germany, pp. 266–275. 68, 72

Wetter, M., W. Zuo, T. S. Nouidui, and X. Pang (2013). Modelica buildings library. *Journal of Building Performance Simulation*, 1–18. 68, 72

Zakula, T. (2013). *Model predictive control for energy efficient cooling and dehumidification*. PhD thesis, Massachusetts Institute of Technology, Cambridge, MA. 29, 31

Appendix A

Simulation Models

A.1 VAV System - Top Level

A.2 Supply Fan

```
Buildings.Fluid.Movers.FlowMachine_Nrpm Fan(
    N_nominal=1600,
    dp(start=0),
    riseTime=30,
    N_start=1765,
    redeclare package Medium = Buildings.Media.IdealGases.SimpleAir,
    filteredSpeed=true,
    m_flow(start=1.8),
    use_powerCharacteristic=true,
    pressure(V_flow={1.1798,1.4158,1.6517}, dp={746.45,741.48,696.69}),
    addPowerToMedium=true,
    power(V_flow={0,1.1798,1.6517}, P={0,1640.57,2423.56}),
    T_start=303.15);
```

A.3 Supply Fan Power Model

```
model FanPower_wPressureHead
    parameter Modelica.SIunits.Pressure designPressure;
    parameter Modelica.SIunits.MassFlowRate designMassFlowRate;
    parameter Modelica.SIunits.Power designShaftPower;
    parameter Real designFanSpeed;
    Real a;
    Real b;
```

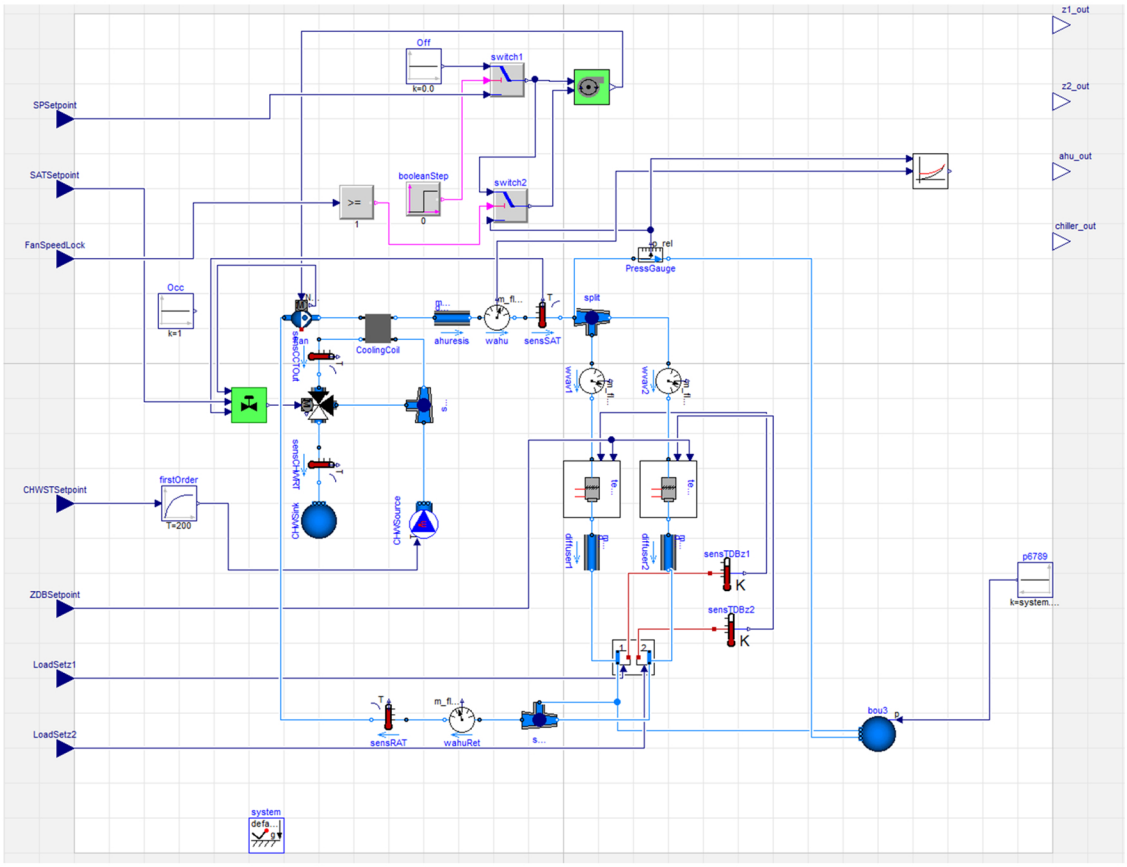

Figure A.1 – Graphical implementation of representative VAV system model in Dymola used for Chapter 5 simulations.

```
    Real d;
    Real po;
    Real f;
    Real H;
    Modelica.Blocks.Interfaces.RealInput FanAirflow;
    Modelica.Blocks.Interfaces.RealOutput FanPower;
    Modelica.Blocks.Interfaces.RealInput SPSetpoint;
equation
    po = if abs(SPSetpoint/designPressure) < 1e-4 then 0
        else SPSetpoint/designPressure;
    f = FanAirflow/designMassFlowRate;
    a = (po/2)^(3/2);
    b = po*(1-a);
    d = 1 - a - b;
    H = a + b*f + d*f^3;
    FanPower = H*designShaftPower;
end FanPower_wPressureHead;
```

A.4 Supply Fan Controller

```
model SFController
    parameter Real Nmax "Maximum Fan Speed";
    parameter Real Nmin "Minimum Fan Speed";
    Modelica.Blocks.Continuous.LimPID PI(
        yMax=Nmax,
        yMin=Nmin,
        k=0.15,
        Ti=5);
    Modelica.Blocks.Interfaces.RealOutput FanSpeedSet;
    Modelica.Blocks.Interfaces.RealInput SAPSetpoint;
    Modelica.Blocks.Interfaces.RealInput SAPMeasure;
equation
    connect(PI.y, FanSpeedSet);
    connect(PI.u_s, SAPSetpoint);
    connect(PI.u_m, SAPMeasure);
end SFController;
```

A.5 Cooling Coil

```
Buildings.Fluid.HeatExchangers.DryEffectivenessNTU CoolingCoil(
    redeclare package Medium1 = Modelica.Media.Water.StandardWater,
    redeclare package Medium2 = Buildings.Media.IdealGases.SimpleAir,
```

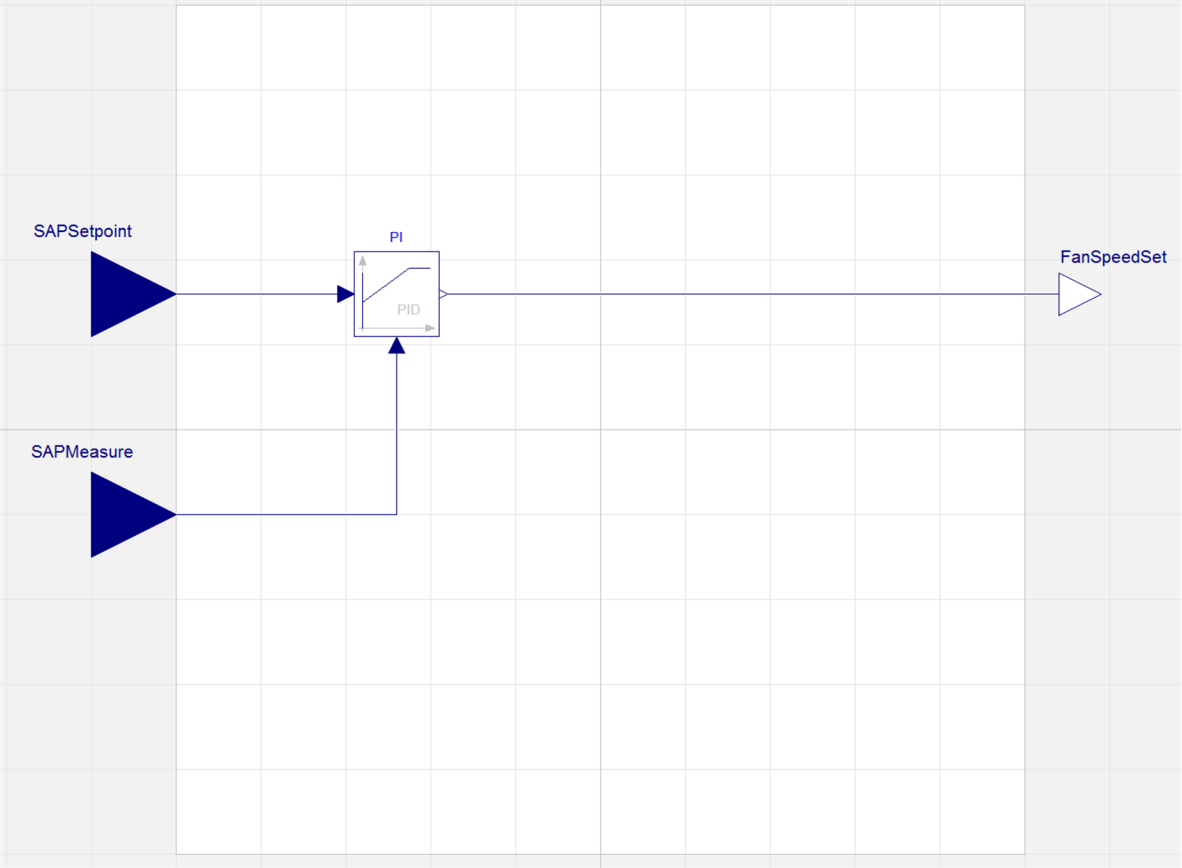

Figure A.2 – Graphical implementation of supply fan controller model in Dymola used for Chapter 5 simulations.

```
    dp1_nominal=0,
    dp2_nominal=0,
    m2_flow_nominal=1.848,
    configuration=
     Buildings.Fluid.Types.HeatExchangerConfiguration.CrossFlowUnmixed,
    r_nominal=2/3,
    m1_flow_nominal=1.02,
    Q_flow_nominal=21395,
    T_a1_nominal=279.15,
    T_a2_nominal=297.45);
```

A.6 AHU Resistance

```
Buildings.Fluid.FixedResistances.FixedResistanceDpM ahuresis(
    redeclare package Medium = Buildings.Media.IdealGases.SimpleAir,
    m_flow_nominal=1.54*1.2,
    dp_nominal=537);
```

A.7 Supply Duct Splitter

```
Buildings.Fluid.FixedResistances.SplitterFixedResistanceDpM split(
    dh={1,2,3},
    res1(m_flow(start=0)),
    res2(m_flow(start=0)),
    res3(m_flow(start=0)),
    p_start(displayUnit="Pa") = system.p_ambient,
    redeclare package Medium = Buildings.Media.IdealGases.SimpleAir,
    T_start(displayUnit="degC") = 285.93,
    dp_nominal(displayUnit="kPa") = {0,-277,-277},
    m_flow_nominal={1,-0.77,-0.77}*1.2) "Splitter";
```

A.8 Terminal Unit

Terminal unit model code:

```
model TermUnit
    parameter Modelica.SIunits.Velocity v_nominal
        "Nominal Air Velocity";
    parameter Modelica.SIunits.Velocity v_max
        "Maximum Air Velocity at Max Flow";
```

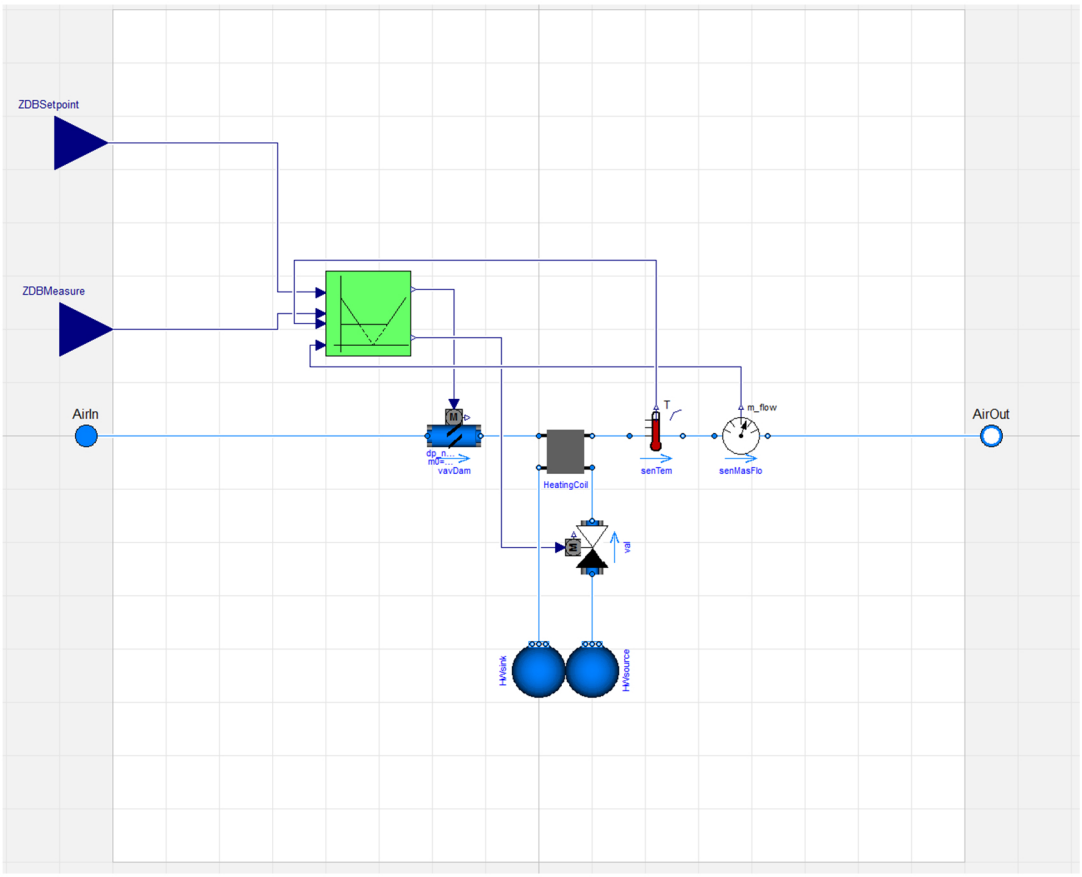

Figure A.3 – Graphical implementation of terminal unit model in Dymola used for Chapter 5 simulations.

```
parameter Modelica.SIunits.MassFlowRate m_flow_nominal
    "Nominal Air Mass Flowrate";
parameter Modelica.SIunits.MassFlowRate m_wflow_nominal
    "Nominal HW Water Mass Flowrate";
parameter Modelica.SIunits.Pressure dp_nominal
    "Nominal Pressure Drop (w/ Damp Open)";
parameter Modelica.SIunits.Pressure dp_max
    "Maximum Pressure Drop (w/ Damp Open at Max Flow)";
parameter Modelica.SIunits.MassFlowRate m_flow_max
    "Maximum Terminal Unit Air Mass Flowrate";
parameter Modelica.SIunits.MassFlowRate m_flow_min
    "Minimum Terminal Unit Air Mass Flowrate";
parameter Modelica.SIunits.Power Q_flow_nominal
    "Nominal Heating Coil Heat Flow";
parameter Modelica.SIunits.Temperature T_a1_nominal
    "Nominal Entering Water Temperature";
parameter Modelica.SIunits.Temperature T_a2_nominal
    "Nominal Entering Air Temperature";
Modelica.Blocks.Interfaces.RealInput ZDBSetpoint;
Modelica.Blocks.Interfaces.RealInput ZDBMeasure;
Buildings.Fluid.Actuators.Dampers.VAVBoxExponential vavDam(
    redeclare package Medium = Buildings.Media.IdealGases.SimpleAir,
    use_v_nominal=true,
    m_flow_nominal=m_flow_nominal,
    dp_nominal=dp_nominal,
    v_nominal=v_nominal);
Buildings.Fluid.HeatExchangers.DryEffectivenessNTU HeatingCoil(
    redeclare package Medium1 = Modelica.Media.Water.StandardWater,
    redeclare package Medium2 = Buildings.Media.IdealGases.SimpleAir,
    m1_flow_nominal=m_wflow_nominal,
    dp1_nominal=0,
    dp2_nominal=0,
    Q_flow_nominal=Q_flow_nominal,
    T_a1_nominal=T_a1_nominal,
    T_a2_nominal=T_a2_nominal,
    m2_flow_nominal=0.18405,
    configuration=
     Buildings.Fluid.Types.HeatExchangerConfiguration.CrossFlowUnmixed);
Modelica.Fluid.Interfaces.FluidPort_b AirOut(
    redeclare package Medium = Buildings.Media.IdealGases.SimpleAir);
Modelica.Fluid.Interfaces.FluidPort_a AirIn(
    redeclare package Medium = Buildings.Media.IdealGases.SimpleAir);
Buildings.Fluid.Actuators.Valves.TwoWayLinear val(
    redeclare package Medium = Modelica.Media.Water.StandardWater,
    m_flow_nominal=m_wflow_nominal,
```

```
        dpFixed_nominal=5971,
        dpValve_nominal=6000,
        l=0.000001,
        y_start=0);
    Buildings.Fluid.Sensors.MassFlowRate senMasFlo(
        redeclare package Medium = Buildings.Media.IdealGases.SimpleAir);
    Buildings.Fluid.Sensors.TemperatureTwoPort senTem(
        redeclare package Medium = Buildings.Media.IdealGases.SimpleAir,
        m_flow_nominal=m_flow_nominal);
    TUController terminalUnit(
        m_flow_max=m_flow_max,
        m_flow_min=m_flow_min,
        hysteresis(displayUnit="K") = 0.5);
    Buildings.Fluid.Sources.FixedBoundary HWsink(
        nPorts=1,
        p(displayUnit="Pa") = 101325,
        redeclare package Medium = Modelica.Media.Water.StandardWater)
        "Sink for terminal box ";
    Buildings.Fluid.Sources.FixedBoundary HWsource(
        nPorts=1,
        redeclare package Medium = Modelica.Media.Water.StandardWater,
        p(displayUnit="Pa") = 101325 + 12000,
        T=366.45) "Source for terminal box";
equation
    connect(vavDam.port_b, HeatingCoil.port_a2);
    connect(val.port_b, HeatingCoil.port_a1);
    connect(senMasFlo.port_b, AirOut);
    connect(terminalUnit.DamperSet, vavDam.y);
    connect(terminalUnit.HWValveSet, val.y);
    connect(val.port_a, HWsource.ports[1]);
    connect(HWsink.ports[1], HeatingCoil.port_b1);
    connect(ZDBSetpoint, terminalUnit.ZDBSetpoint);
    connect(ZDBMeasure, terminalUnit.ZDBMeasure);
    connect(senMasFlo.m_flow, terminalUnit.TUm_flow);
    connect(senTem.port_b, senMasFlo.port_a);
    connect(HeatingCoil.port_b2, senTem.port_a);
    connect(vavDam.port_a, AirIn);
    connect(senTem.T, terminalUnit.ATMeasure);
end TermUnit;
```

Implementation of terminal unit model within VAV model:

```
Controls.TermUnit_idealair termUnit1(
    m_flow_max=1.133,
    Q_flow_nominal=6982,
```

```
    dp_nominal(displayUnit="Pa") = 66.6,
    m_wflow_nominal=6982/(4200*10),
    m_flow_nominal=0.77*1.2,
    dp_max(displayUnit="Pa") = 98.3,
    v_nominal=6.66,
    v_max=8.07,
    m_flow_min=0.184,
    T_a1_nominal=366.45,
    T_a2_nominal=285.93);

Controls.TermUnit_idealair termUnit2(
    m_wflow_nominal=6982/(4200*10),
    m_flow_max=1.133,
    Q_flow_nominal=6982,
    dp_nominal(displayUnit="Pa") = 66.6,
    m_flow_nominal=0.77*1.2,
    dp_max(displayUnit="Pa") = 98.3,
    v_nominal=6.66,
    v_max=8.07,
    m_flow_min=0.184,
    T_a1_nominal=366.45,
    T_a2_nominal=285.93);
```

A.9 Terminal Unit Controller

```
model TUController
    parameter Modelica.SIunits.MassFlowRate m_flow_max
     "Maximum airflow through TU";
    parameter Modelica.SIunits.MassFlowRate m_flow_min
     "Minimum airflow through TU";
    parameter Modelica.SIunits.Temperature hysteresis
     "Half of full range";
    parameter Real cbreak = 0
     "Break between damper actuation and valve actuation";
    Real norm_flow_min "Normalized minimum VAV airflow";
    Real FlowDem "Normalized VAV flow demand";
    Real HWDem "Hot water valve demand";
    Modelica.Blocks.Interfaces.RealInput ZDBSetpoint;
    Modelica.Blocks.Interfaces.RealInput ZDBMeasure;
    Modelica.Blocks.Interfaces.RealInput TUm_flow;
    Modelica.Blocks.Interfaces.RealInput ATMeasure;
    Modelica.Blocks.Interfaces.RealOutput DamperSet;
    Modelica.Blocks.Interfaces.RealOutput HWValveSet;
```

```
    Modelica.Blocks.Continuous.LimPID PIDSig(
        controllerType=Modelica.Blocks.Types.SimpleController.PI,
        yMax=1,
        y_start=0.8,
        yMin=-1,
        k=0.8,
        Ti=600);
    Modelica.Blocks.Continuous.LimPID PIDDamper(
        controllerType=Modelica.Blocks.Types.SimpleController.PI,
        yMax=1,
        y_start=0.8,
        yMin=m_flow_min/m_flow_max,
        Ti=30,
        k=2);
    Modelica.Blocks.Nonlinear.Limiter FlowDemLim(
        uMax=1.0,
        uMin=m_flow_min/m_flow_max);
    Deadband deadband(deadband=0);
    Hysteresis hysteresis1;
equation
    // Define normalized minimum flow
    norm_flow_min = m_flow_min/m_flow_max;
    // Determine normalized demanded flow setpoint.
    // If the supply air temperature is warmer than the zone air temperature,
    // the box is heating and minimum flow should be demanded.
    // If the supply air temperature is colder than the zone air temperature,
    // the box is cooling and flow is set based on cooling need.
    hysteresis1.uLow = ZDBSetpoint - 0.5;
    hysteresis1.uHigh = ZDBSetpoint + 0.5;
    FlowDem = if hysteresis1.y then norm_flow_min else
        (PIDSig.y - cbreak)*(1.0 - norm_flow_min)/(-1.0 - cbreak) + norm_flow_min;
    // Limit normalized flow demand to minimum normalized flow
    FlowDemLim.u = FlowDem;
    // Determine the hotwater demand based on zone temperature error
    HWDem = (PIDSig.y - cbreak)*(1.0-0)/(1.0 - cbreak)+0;
    // Limit hot water valve set to greater than 0 and to only open
    // when the box is demanding minimum normalized flow.
    HWValveSet = if HWDem > 0 and FlowDem <= norm_flow_min then HWDem else 0;
    PIDDamper.u_m = TUm_flow/m_flow_max;
    connect(ZDBMeasure, PIDSig.u_m);
    connect(PIDDamper.y, DamperSet);
    connect(FlowDemLim.y, PIDDamper.u_s);
    connect(deadband.SetEff, PIDSig.u_s);
    connect(ZDBMeasure, deadband.VarMea);
    connect(ZDBSetpoint, deadband.VarSet);
```

```
    connect(ATMeasure, hysteresis1.uComp);
end TUController;
```

A.10 Diffuser Resistance

```
    Buildings.Fluid.FixedResistances.FixedResistanceDpM diffuser1(
        redeclare package Medium = Buildings.Media.IdealGases.SimpleAir,
        dp_nominal=29.6,
        m_flow_nominal=0.77*1.2);

    Buildings.Fluid.FixedResistances.FixedResistanceDpM diffuser2(
        redeclare package Medium = Buildings.Media.IdealGases.SimpleAir,
        dp_nominal=29.6,
        m_flow_nominal=0.77*1.2);
```

A.11 Thermal Zones

```
record datConstr
    // DEFINE BUILDING MATERIALS ////////////////////////////////////
    // x [m]
    // k [W/m-k]
    // d [kg/m^3]
    // c [J/kg-k]
    // *If c == 0 or d == 0 --> Steady State Conduction

    Buildings.HeatTransfer.Data.Solids.Generic matDOEstucco(
        x = 0.0253,
        k = 0.6918,
        d = 1858.0,
        c = 837.0) "1 in Stucco";
    Buildings.HeatTransfer.Data.Solids.Generic matDOEconc(
        x = 0.2032,
        k = 1.3110,
        d = 2240.0,
        c = 836.8) "8 in Concrete";
    Buildings.HeatTransfer.Data.Solids.Generic matDOEwallins(
        x = 0.036539,
        k = 0.049,
        d = 265.0,
        c = 836.8) "1 1/2 in Ext Wall Insulation";
    Buildings.HeatTransfer.Data.Solids.Generic matDOEgyp(
        x = 0.0127,
```

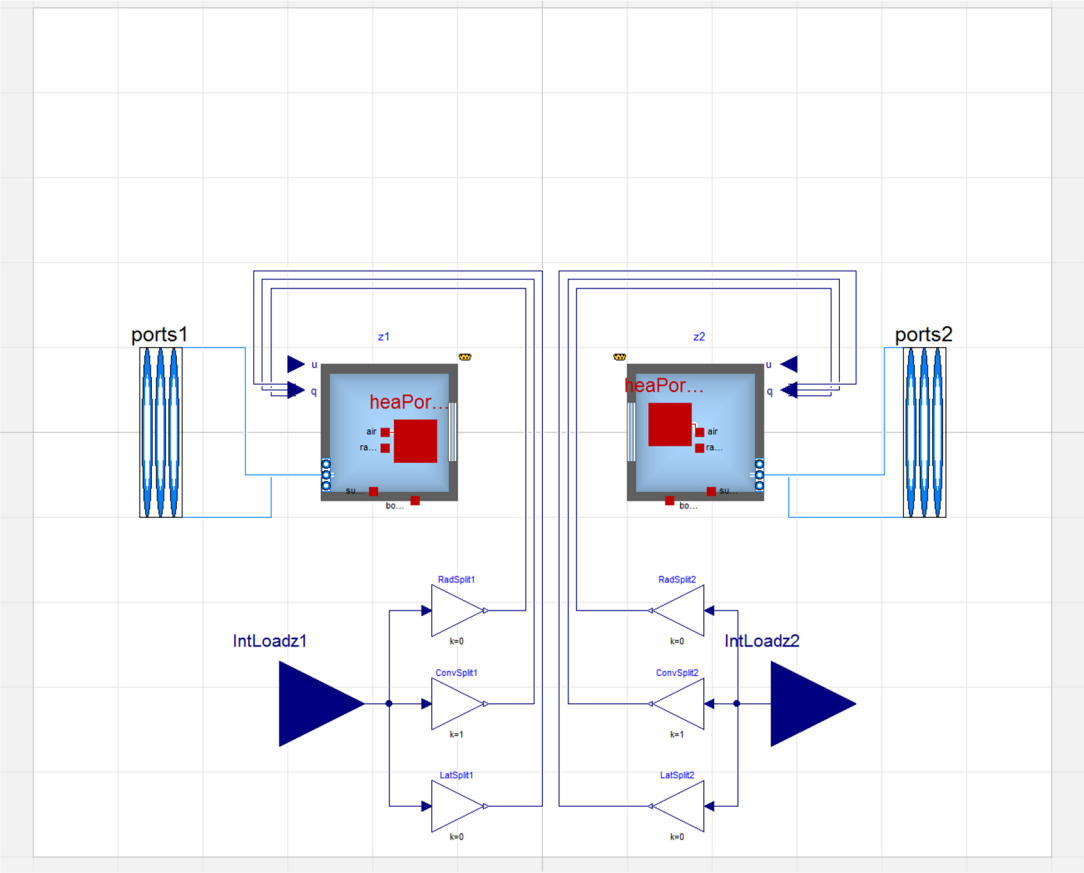

Figure A.4 – Graphical implementation of thermal zone models in Dymola used for Chapter 5 simulations.

```
    k = 0.1600,
    d = 784.9,
    c = 830.0) "1/2 in Gypsum";
Buildings.HeatTransfer.Data.Solids.Generic matDOEsog(
    x = 0.1016,
    k = 1.311,
    d = 2240.0,
    c = 836.8) "4 in SOG";
Buildings.HeatTransfer.Data.Resistances.Generic matDOEcarp(
    R = 0.2165) "Carpet";
Buildings.HeatTransfer.Data.Solids.Generic matDOEacoutile(
    x = 0.0127,
    k = 0.0570,
    d = 288.0,
    c = 1339.0) "Acoustic Tile Drop Ceiling";
Buildings.HeatTransfer.Data.Solids.Generic matDOEroofmem(
    x = 0.0095,
    k = 0.1600,
    d = 1121.3,
    c = 1460.0) "1/16 in Roofing Membrane";
Buildings.HeatTransfer.Data.Solids.Generic matDOEatticins(
    x = 0.23413,
    k = 0.049,
    d = 265.0,
    c = 836.8) "9 in Attic Insulation";
Buildings.HeatTransfer.Data.Solids.Generic matDOEmetdeck(
    x = 0.0015,
    k = 45.0060,
    d = 7680.00,
    c = 418.40) "3/8 in Metal Decking";

// DEFINE BUILDING CONSTRUCTIONS (outside to roomside) ////////////
Buildings.HeatTransfer.Data.OpaqueConstructions.Generic conDOEextwall(final
    nLay = 4,
    material = {matDOEstucco,matDOEconc, matDOEwallins, matDOEgyp})
    "Exterior Wall";
Buildings.HeatTransfer.Data.OpaqueConstructions.Generic conDOEintwall(final
    nLay = 2,
    material = {matDOEgyp, matDOEgyp}) "Interior Wall";
Buildings.HeatTransfer.Data.OpaqueConstructions.Generic conDOEfloor(final
    nLay = 2,
    material = {matDOEsog, matDOEcarp}) "Floor";
Buildings.HeatTransfer.Data.OpaqueConstructions.Generic conDOEceil(final
    nLay = 4,
    material = {matDOEgyp, matDOEatticins, matDOEgyp, matDOEacoutile})
```

```
        "Ceiling";
    Buildings.HeatTransfer.Data.OpaqueConstructions.Generic conDOEroof(final
        nLay = 2,
        material = {matDOEroofmem, matDOEmetdeck}) "Roof";

    // DEFINE BUILDING GLAZING SYSTEMS (outside to roomside) ////////////
    Buildings.HeatTransfer.Data.GlazingSystems.SingleClear3 glazDOEsingle(
        UFra = 2,
        haveExteriorShade = false,
        haveInteriorShade = false) "Single Pane 3mm Fixed";
end datConstr;


model BuildingDef2_nowea_idealair "2-Zone DOE Small Office"
    import Buildings;
    extends datConstr;
    Buildings.Rooms.MixedAir z1(
        AFlo = 255,
        hRoo = 3.05,
        nConExt = 0,
        nConExtWin = 0,
        nConPar = 0,
        nConBou = 3,
        datConBou(
            layers = {conDOEfloor, conDOEceil, conDOEextwall},
            A = {255, 255, 140.8},
            til = {Buildings.HeatTransfer.Types.Tilt.Floor,
                   Buildings.HeatTransfer.Types.Tilt.Ceiling,
                   Buildings.HeatTransfer.Types.Tilt.Wall},
            T_a_start = {273.15+22, 273.15+22, 273.15+22},
            T_b_start = {273.15+22, 273.15+22, 273.15+22}),
        nSurBou = 0,
        nPorts=2,
        redeclare package Medium = Buildings.Media.IdealGases.SimpleAir,
        T_start(displayUnit="degC") = 295.15,
        lat=43);
    Buildings.Rooms.MixedAir z2(
        AFlo = 255,
        hRoo = 3.05,
        nConExt = 0,
        nConExtWin = 0,
        nConPar = 0,
        nConBou = 3,
        datConBou(
            layers = {conDOEfloor, conDOEceil, conDOEextwall},
```

```
            A = {255, 255, 140.8},
            til = {Buildings.HeatTransfer.Types.Tilt.Floor,
                   Buildings.HeatTransfer.Types.Tilt.Ceiling,
                   Buildings.HeatTransfer.Types.Tilt.Wall},
            T_a_start = {273.15+22, 273.15+22, 273.15+22},
            T_b_start = {273.15+22, 273.15+22, 273.15+22}),
        nSurBou = 0,
        nPorts=2,
        redeclare package Medium = Buildings.Media.IdealGases.SimpleAir,
        T_start=295.15,
        lat=43);
    Modelica.Blocks.Interfaces.RealInput IntLoadz1
        "Radiant, convective and latent heat input into room";
    Modelica.Blocks.Interfaces.RealInput IntLoadz2
        "Radiant, convective and latent heat input into room";
    Modelica.Thermal.HeatTransfer.Interfaces.HeatPort_a heaPorAir1
        "Heat port to air volume";
    Modelica.Thermal.HeatTransfer.Interfaces.HeatPort_a heaPorAir2
        "Heat port to air volume";
    Modelica.Fluid.Vessels.BaseClasses.VesselFluidPorts_b ports1[2](
        redeclare package Medium = Buildings.Media.IdealGases.SimpleAir)
        "Fluid inlets and outlets";
    Modelica.Fluid.Vessels.BaseClasses.VesselFluidPorts_b ports2[2](
        redeclare package Medium = Buildings.Media.IdealGases.SimpleAir)
        "Fluid inlets and outlets";
    Modelica.Blocks.Math.Gain RadSplit1(k=0);
    Modelica.Blocks.Math.Gain ConvSplit1(k=1);
    Modelica.Blocks.Math.Gain LatSplit1(k=0);
    Modelica.Blocks.Math.Gain RadSplit2(k=0);
    Modelica.Blocks.Math.Gain ConvSplit2(k=1);
    Modelica.Blocks.Math.Gain LatSplit2(k=0);
    inner Modelica.Fluid.System system(p_ambient(displayUnit="kPa"));
equation
    connect(z1.heaPorAir, heaPorAir1);
    connect(z2.heaPorAir, heaPorAir2);
    connect(z1.ports[1], ports1[1]);
    connect(z2.ports[1], ports2[1]);
    connect(z1.ports[2], ports1[2]);
    connect(z2.ports[2], ports2[2]);
    connect(IntLoadz1, RadSplit1.u);
    connect(IntLoadz1, ConvSplit1.u);
    connect(IntLoadz1, LatSplit1.u);
    connect(RadSplit1.y, z1.qGai_flow[1]);
    connect(ConvSplit1.y, z1.qGai_flow[2]);
    connect(LatSplit1.y, z1.qGai_flow[3]);
```

```
    connect(RadSplit2.y, z2.qGai_flow[1]);
    connect(ConvSplit2.y, z2.qGai_flow[2]);
    connect(LatSplit2.y, z2.qGai_flow[3]);
    connect(IntLoadz2, RadSplit2.u);
    connect(IntLoadz2, ConvSplit2.u);
    connect(IntLoadz2, LatSplit2.u);
end BuildingDef2_nowea_idealair;
```

A.12 Return Duct Splitter

```
Buildings.Fluid.FixedResistances.SplitterFixedResistanceDpM split2(
    dh={1,2,3},
    res1(m_flow(start=0)),
    res2(m_flow(start=0)),
    res3(m_flow(start=0)),
    p_start(displayUnit="Pa") = system.p_ambient,
    redeclare package Medium = Buildings.Media.IdealGases.SimpleAir,
    T_start(displayUnit="degC") = 285.93,
    m_flow_nominal={-1,0.77,0.77}*1.2,
    dp_nominal(displayUnit="kPa") = {0,0,0}) "Splitter";
```

A.13 Chilled Water Ideal Flow Source and Sink

```
Buildings.Fluid.Sources.MassFlowSource_T CHWSource(
    redeclare package Medium = Modelica.Media.Water.StandardWater,
    nPorts=1,
    use_T_in=true,
    m_flow=1.02,
    T=279.15);
```

A.14 Chilled Water Flow Splitter

```
Buildings.Fluid.FixedResistances.SplitterFixedResistanceDpM split1(
    dh={1,2,3},
    res1(m_flow(start=0)),
    res2(m_flow(start=0)),
    res3(m_flow(start=0)),
    p_start(displayUnit="Pa") = system.p_ambient,
    m_flow_nominal={1,-1,-1},
    redeclare package Medium = Modelica.Media.Water.StandardWater,
    dp_nominal(displayUnit="kPa") = {0,0,0}) "Splitter";
```

A.15 Chilled Water Modulating Valve

```
Buildings.Fluid.Actuators.Valves.ThreeWayLinear val(
    redeclare package Medium = Modelica.Media.Water.StandardWater,
    l={0.001,0.001},
    dpValve_nominal=30000,
    riseTime=60,
    m_flow_nominal=1.02);
```

A.16 Chilled Water Valve Controller

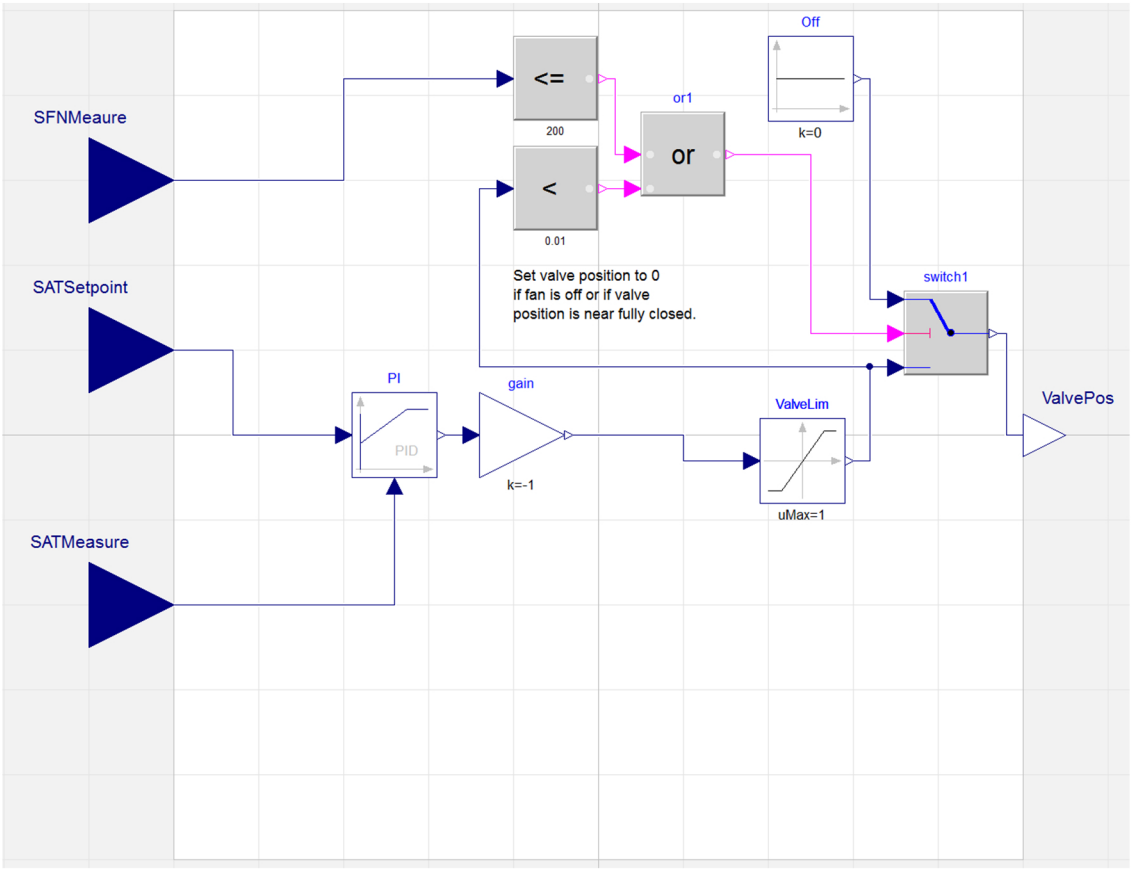

Figure A.5 – Graphical implementation of chilled water valve controller model in Dymola used for Chapter 5 simulations.

```
model CHWVController
    parameter Modelica.SIunits.MassFlowRate mw_flow_max
        "Maximum Chilled Water Flowrate";
    Modelica.Blocks.Continuous.LimPID PI(
        controllerType=Modelica.Blocks.Types.SimpleController.PI,
        yMax=0,
        yMin=-mw_flow_max,
        k=0.06,
        Ti=30);
    Modelica.Blocks.Nonlinear.Limiter ValveLim(uMin=0, uMax=1);
    Modelica.Blocks.Interfaces.RealOutput ValvePos
        "Chilled water flow valve position set";
    Modelica.Blocks.Sources.Constant Off(k=0);
    Modelica.Blocks.Logical.LessThreshold lessThreshold(threshold=0.01);
    Modelica.Blocks.Logical.Switch switch1;
    Modelica.Blocks.Logical.Or or1;
    Modelica.Blocks.Logical.LessEqualThreshold lessEqualThreshold(
        threshold=200);
    Modelica.Blocks.Interfaces.RealInput SFNMeaure;
    Modelica.Blocks.Interfaces.RealInput SATSetpoint;
    Modelica.Blocks.Interfaces.RealInput SATMeasure;
    Modelica.Blocks.Math.Gain gain(k=-1);
equation
    connect(Off.y, switch1.u1);
    connect(switch1.y, ValvePos);
    connect(lessThreshold.u, ValveLim.y);
    connect(switch1.u3, ValveLim.y);
    connect(lessThreshold.y, or1.u2);
    connect(lessEqualThreshold.y, or1.u1);
    connect(lessEqualThreshold.u, SFNMeaure);
    connect(SATMeasure, PI.u_m);
    connect(PI.y, gain.u);
    connect(or1.y, switch1.u2);
    connect(SATSetpoint, PI.u_s);
    connect(gain.y, ValveLim.u);
end CHWVController1;
```

Appendix B

Equipment Specifications and Performance

The following includes specification and catalog excerpts for the equipment selected to be used in the VAV simulation model. The supply fan specification was obtained by direct communication with a sales representative from Trane, Inc. and is not available online. A full version of the Titus Single/Dual Duct Terminal Unit performance data catalog can be found at http://www.titus-hvac.com/utility/getfile2.aspx?fileid=1163. The Titus TMR Diffuser performance data can be found at http://www.titus-hvac.com/utility/getfile2.aspx?fileid=823.

DHB AHU - Supply Fan sec [5]-1

Size 6 Horizontal Draw-Thru 10 inch FC Class 1

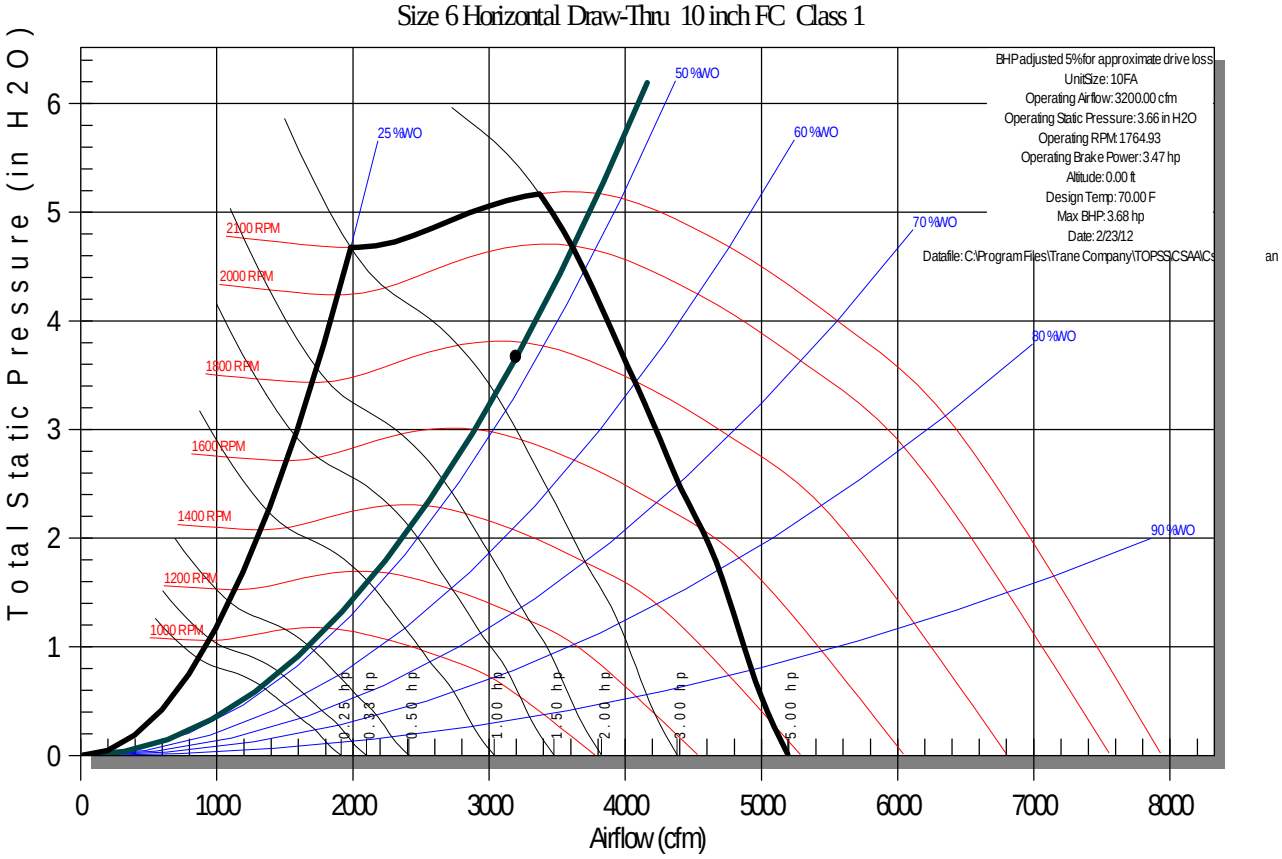

DHB AHU - Supply Fan sec [5]-1

Size 6 Horizontal Draw-Thru 10 inch FC Class 1

	63Hz	125Hz	250Hz	500Hz	1 kHz	2 kHz	4 kHz	8 kHz
Discharge	88	85	83	81	83	80	77	70
Inlet + Casing	79	77	73	60	63	62	54	41
Casing	79	74	71	68	77	57	36	28
Ducted Inlet	71	65	59	49	50	54	47	32

Performance Data

Recommended Primary Air cfm Ranges • All Terminals

Control Types:

PESV	• Pneumatic
AESV	• Analog electronic
DESV	• Digital electronic

Quick Selection Procedure

1. Select unit inlet size based upon acoustic parameters and/or maximum pressure drop requirements, using pages Q12–Q13.
2. Check inlet size selection against cfm control limits based on control type shown on this page.
3. Select accessories (multi-outlets, attenuators) as required.
4. Select reheat coil, if required. Make your selection using the actual heating flow rate, not cooling.

AESV

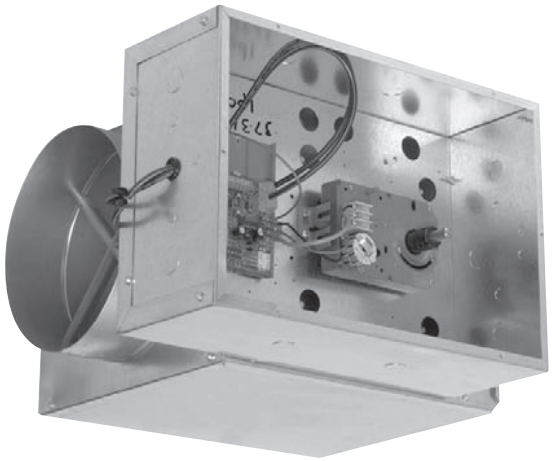

Inlet Size	Total cfm Range	cfm Ranges of Minimum and Maximum Settings							
		PESV - Pneumatic TITUS II Controller		PESV - Pneumatic TITUS I Controller		AESV - Analog Electronic TA1 Controller		DESV - Digital Typical Controller	
		Minimum	Maximum	Minimum	Maximum	Minimum	Maximum	Minimum	Maximum
4	0-225	45*-170	80-225	55*-170	80-225	45*-225	45-225	45*-225	45-225
5	0-350	65*-270	120-350	85*-270	120-350	65*-350	65-350	65*-350	65-350
6	0-500	80*-330	150-500	105*-330	150-500	80*-500	80-500	80*-500	80-500
7	0-650	105*-425	190-650	135*-425	190-650	105*-650	105-650	105*-650	105-650
8	0-900	145*-590	265-900	190*-590	265-900	145*-900	145-900	145*-900	145-900
9	0-1050	175*-700	315-1050	225*-700	315-1050	175*-1050	175-1050	175*-1050	175-1050
10	0-1400	230*-925	415-1400	300*-925	415-1400	230*-1400	230-1400	230*-1400	230-1400
12	0-2000	325*-1330	600-2000	425*-1330	600-2000	325*-2000	325-2000	325*-2000	325-2000
14	0-3000	450*-1800	810-3000	575*-1800	810-3000	450*-3000	450-3000	450*-3000	450-3000
16	0-4000	580*-2350	1100-4000	750*-2350	1100-4000	580*-4000	580-4000	580*-4000	580-4000
24x16	0-8000	1400*-5200	2600-8000	1800*-5200	2600-8000	1400*-7500	1400-7500	1400*-7500	1400-7500

*Factory cfm settings (except zero) will not be made below this range because control accuracy is reduced. On pressure dependent units, minimum cfm is always zero and there is no maximum.

Note: On controls mounted by Titus but supplied by others (FMA or Factory Mounting Authorization), these values are guidelines only. Controls mounted on an FMA basis are calibrated in the field.

Q Single/Dual Duct Terminals | Performance Data

Performance Data (continued)

PESV, AESV, DESV • Minimum Pressures

Inlet Size	cfm	Velocity Pressure VP	Basic Unit Ps	Basic + Atten. Ps	Basic + Multi-out. Ps	Basic + Round Out. Ps	Basic + 1 Row Coil Ps	Basic + 2 Row Coil Ps	Basic + 3 Row Coil Ps	Basic + 4 Row Coil Ps	Basic + Elec. Coil. Ps
4	100	0.080	0.020	0.021	0.022	0.023	0.027	0.034	0.041	0.048	0.020
	150	0.181	0.044	0.048	0.049	0.052	0.061	0.078	0.093	0.109	0.044
	200	0.322	0.078	0.084	0.088	0.092	0.108	0.138	0.165	0.193	0.078
	225	0.407	0.099	0.107	0.111	0.116	0.137	0.175	0.209	0.244	0.099
5	150	0.072	0.011	0.014	0.016	0.018	0.028	0.044	0.060	0.075	0.011
	200	0.129	0.019	0.025	0.029	0.032	0.049	0.079	0.106	0.134	0.019
	300	0.289	0.043	0.057	0.064	0.073	0.111	0.177	0.239	0.301	0.043
	350	0.394	0.059	0.077	0.088	0.099	0.151	0.241	0.325	0.410	0.059
6	200	0.059	0.033	0.038	0.044	0.060	0.063	0.092	0.120	0.147	0.033
	300	0.133	0.073	0.085	0.098	0.134	0.141	0.207	0.269	0.331	0.073
	400	0.236	0.130	0.151	0.175	0.238	0.250	0.368	0.478	0.588	0.130
	500	0.369	0.203	0.236	0.273	0.372	0.391	0.575	0.747	0.919	0.203
7	300	0.070	0.031	0.036	0.044	0.055	0.066	0.098	0.131	0.163	0.031
	400	0.125	0.055	0.064	0.079	0.098	0.118	0.175	0.232	0.290	0.055
	600	0.282	0.124	0.145	0.177	0.220	0.265	0.394	0.523	0.653	0.124
	650	0.331	0.145	0.170	0.208	0.259	0.311	0.462	0.613	0.766	0.145
8	350	0.052	0.005	0.009	0.015	0.031	0.053	0.097	0.141	0.185	0.042
	500	0.105	0.011	0.019	0.030	0.064	0.109	0.198	0.288	0.378	0.086
	700	0.207	0.021	0.038	0.059	0.126	0.213	0.388	0.564	0.741	0.169
	900	0.342	0.035	0.062	0.097	0.208	0.353	0.642	0.932	1.225	0.279
9	500	0.069	0.015	0.021	0.031	0.045	0.063	0.108	0.152	0.197	0.141
	650	0.117	0.026	0.035	0.052	0.076	0.107	0.182	0.258	0.334	0.237
	800	0.177	0.040	0.053	0.078	0.115	0.162	0.276	0.390	0.505	0.360
	1050	0.306	0.068	0.092	0.134	0.198	0.279	0.476	0.672	0.871	0.620
10	600	0.060	0.006	0.007	0.012	0.030	0.069	0.134	0.198	0.263	0.090
	800	0.107	0.011	0.012	0.022	0.054	0.124	0.238	0.352	0.467	0.160
	1100	0.203	0.021	0.023	0.041	0.102	0.234	0.449	0.665	0.883	0.303
	1400	0.328	0.035	0.035	0.066	0.165	0.378	0.728	1.077	1.430	0.491
12	900	0.064	0.012	0.006	0.014	0.033	0.080	0.150	0.222	0.292	0.101
	1200	0.113	0.021	0.011	0.025	0.058	0.142	0.266	0.394	0.519	0.180
	1500	0.177	0.032	0.016	0.039	0.091	0.222	0.416	0.616	0.811	0.281
	2000	0.314	0.057	0.029	0.070	0.162	0.395	0.740	1.095	1.441	0.500
14	1200	0.063	0.013	0.018	0.029	0.046	0.077	0.137	0.195	0.254	0.094
	1600	0.113	0.023	0.032	0.052	0.082	0.138	0.243	0.347	0.451	0.166
	2000	0.176	0.036	0.050	0.082	0.128	0.215	0.379	0.543	0.705	0.260
	3000	0.396	0.080	0.112	0.184	0.289	0.484	0.854	1.221	1.587	0.584
16	1500	0.056	0.009	0.014	0.027	0.039	0.078	0.140	0.203	0.264	0.125
	2000	0.100	0.015	0.025	0.047	0.070	0.139	0.249	0.360	0.469	0.221
	3000	0.225	0.034	0.056	0.107	0.156	0.312	0.560	0.811	1.056	0.498
	4000	0.401	0.060	0.099	0.190	0.278	0.555	0.996	1.441	1.878	0.886
24x16	2500	0.038	0.013	0.014	NA	NA	0.091	0.161	0.233	0.303	0.242
	4000	0.096	0.033	0.035	NA	NA	0.233	0.411	0.595	0.776	0.619
	6000	0.216	0.073	0.079	NA	NA	0.523	0.925	1.340	1.746	1.392
	8000	0.384	0.130	0.140	NA	NA	0.931	1.644	2.382	3.103	2.475

- Ps is the difference in static pressure across the assembly.

- To obtain total pressure (Pt), add the velocity pressure for a given cfm to the static pressure drop (DPs) of the desired ESV configuration.

  Example: Pt for a Size 8 ESV Basic Unit @ 700 cfm = 0.207 + 0.021 = 0.228

PERFORMANCE DATA

TMR, TMR-AA

	Neck Velocity	400	500	600	700	800	900	1000	1200	1400
	Velocity Pressure	0.010	0.016	0.022	0.031	0.040	0.051	0.062	0.090	0.122
	Total Pressure, Pos. 1	0.029	0.045	0.065	0.089	0.116	0.146	0.181	0.260	0.354
	Total Pressure, Pos. 2	0.047	0.074	0.106	0.145	0.189	0.239	0.295	0.425	0.578
6" Dia.	Airflow, cfm	80	100	120	140	160	180	200	235	275
	NC, Pos.1	-	-	-	14	19	23	26	32	37
	NC, Pos.2	-	12	18	22	26	29	32	38	42
	Throw feet, Pos. 1	2-2-5	2-3-6	2-4-7	3-4-8	3-5-8	4-6-9	4-6-9	5-7-10	6-7-11
	Throw feet, Pos. 2	2-3-6	2-4-7	3-4-7	3-5-8	4-6-8	4-6-9	5-7-9	6-7-10	6-8-11
8" Dia.	Airflow, cfm	140	175	210	245	280	315	350	420	490
	NC, Pos.1	-	-	12	17	21	25	28	34	39
	NC, Pos.2	-	14	19	24	28	31	34	39	44
	Throw feet, Pos. 1	2-3-7	3-4-8	3-5-9	4-6-10	4-7-11	5-7-11	5-8-12	7-9-13	8-10-14
	Throw feet, Pos. 2	3-4-8	3-5-9	4-6-9	4-7-10	5-8-11	6-8-12	6-9-12	8-9-13	8-10-14
10" Dia.	Airflow, cfm	218	273	327	382	436	491	545	654	763
	NC, Pos.1	-	-	14	19	23	27	30	36	41
	NC, Pos.2	-	15	20	25	29	32	35	41	45
	Throw feet, Pos. 1	3-4-8	3-5-10	4-6-12	5-7-12	5-8-13	6-9-14	7-10-15	8-12-16	10-12-18
	Throw feet, Pos. 2	3-5-9	4-6-11	5-7-12	5-8-13	6-9-14	7-10-14	8-11-15	9-12-17	10-13-18
12" Dia.	Airflow, cfm	315	390	470	550	630	705	785	940	1100
	NC, Pos.1	-	-	16	20	25	29	32	38	43
	NC, Pos.2	-	16	21	26	30	33	36	42	46
	Throw feet, Pos. 1	3-5-10	4-6-12	5-7-14	6-9-15	7-10-16	7-11-17	8-12-18	10-14-20	11-15-21
	Throw feet, Pos. 2	4-6-11	5-7-13	6-8-14	7-10-15	8-11-16	8-12-17	9-13 -18	11-14-20	12-15-22
14" Dia.	Airflow, cfm	425	530	635	745	850	955	1060	1270	1490
	NC, Pos.1	-	11	17	22	26	30	33	39	44
	NC, Pos.2	11	17	22	27	31	34	37	42	47
	Throw feet, Pos. 1	4-6-11	5-7-14	6-8-16	7-10-17	8-11-19	8-13-20	9-14-21	11-16-23	13-17-25
	Throw feet, Pos. 2	4-7-13	5-8-15	7-10-16	8-11-18	9-13-19	10-14-20	11-15-21	13-16-23	14-18-25
16" Dia.	Airflow, cfm	560	700	840	980	1120	1260	1400	1680	1960
	NC, Pos.1	-	12	18	23	27	31	34	40	45
	NC, Pos.2	11	18	23	28	31	35	38	43	48
	Throw feet, Pos. 1	4-7-13	5-8--16	7-10-18	8-11-20	9-13-21	10-15-23	11-16-24	13-18-26	15-20-28
	Throw feet, Pos. 2	5-8-15	6-9-17	8-11-19	9-13-20	10-15-22	11-16-23	13-17-24	15-19-27	17-20-29
18" Dia.	Airflow, cfm	710	885	1060	1240	1420	1590	1770	2120	2480
	NC, Pos.1	-	13	19	24	28	32	35	41	46
	NC, Pos.2	12	18	24	28	32	36	39	44	48
	Throw feet, Pos. 1	5-7-15	6-9-18	7-11-21	9-13-22	10-15-24	11-17- 25	12-18-27	15-21-29	17-22-32
	Throw feet, Pos. 2	6-8--17	7-11-19	8-13-21	10-15-23	11-17-25	13-18-26	14-19-27	17-21-30	19-23-32
20" Dia.	Airflow, cfm	875	1100	1310	1530	1750	1970	2190	2610	3060
	NC, Pos.1	-	14	20	25	29	33	36	42	47
	NC, Pos.2	13	19	24	29	33	36	39	45	49
	Throw feet, Pos. 1	5-8-16	7-10-21	8-12-23	10-14-25	11-16-27	12-18-28	14-20-30	16-23-33	19-25-35
	Throw feet, Pos. 2	6-9-19	8-12-22	9-14-24	11-16-25	13-19-27	14-20-29	16-22-30	19-24-33	21-25-36
24" Dia.	Airflow, cfm	1260	1570	1880	2200	2510	2820	3140	3770	4400
	NC, Pos.1	-	16	22	27	31	35	38	44	49
	NC, Pos.2	14	20	25	30	34	37	40	46	50
	Throw feet, Pos. 1	7-10-20	8-12-24	10-15-28	11-17-30	13-20-32	15-22-34	16-24-36	20-28-39	23-30-42
	Throw feet, Pos. 2	8-11-23	9-14-26	11-17-28	13-20-31	15-23-33	17-24-35	19--26-36	23-28 -40	25-31-43
30" Dia.	Airflow, cfm	1960	2450	2940	3430	3920	4410	4900	5880	6860
	NC, Pos.1	-	18	23	28	33	37	40	46	51
	NC, Pos.2	15	21	27	31	35	38	41	47	51
	Throw feet, Pos. 1	8-12-24	10-15-31	12-18-35	14-21-37	16-24-40	18-27-42	20-31-45	24-35-49	28-37-53
	Throw feet, Pos. 2	9-14-28	12-18-32	14-21-35	16-25-38	19-28-41	21-31-43	23-32-46	28-35-50	31-38-54
36" Dia.	Airflow, cfm	2820	3520	4230	4930	5630	6340	7040	8450	9850
	NC, Pos.1	12	19	25	30	34	38	41	47	52
	NC, Pos.2	16	22	28	32	36	39	43	48	52
	Throw feet, Pos. 1	10-15-29	12-18-37	15-22-41	17-26-45	19-29-48	22-33-51	24-37-53	29-41-59	34-45-63
	Throw feet, Pos. 2	11-17-34	14-21-39	17-25-42	20-29-46	22-34-49	25-37-52	28-39-55	34-42-60	37-46-65

- All pressures given are in inches of water.
- Throw values given are for terminal velocities of 150, 100 and 50 fpm and for isothermal conditions.
- To obtain static pressure, subtract the velocity pressure from the total pressure.
- If the diffuser is mounted on an exposed duct, the throw values are 70% of those listed in the table and will project downward.
- Each NC value represents the noise criteria curve which will not be exceeded by the sound pressure in any of the octave bands, 2 through 7, with a room absorption of 10 dB, re 10^{-12} watts.
- Dash (-) in space denotes an NC value of less than 10.
- Diffusers are shipped in Position 2 (cones down).
- Data obtained from tests conducted in accordance with ANSI / ASHRAE Standard 70-2006. Actual performance, with flexible duct inlet, may vary in the field. See the section, Engineering Guidelines, for additional information.
- For an explanation of catalog throw data, see the Engineering Guidelines section of this catalog.